

Diss. ETH No. 14631

# Charge injection and transport in organic semiconductors

A dissertation submitted to the  
Swiss Federal Institute of Technology  
Zürich

for the degree of  
Doctor of Natural Sciences

presented by

**Michael Kiy**

Dipl. Phys.

Technical University of Braunschweig

born July 6, 1972

citizen of Germany

accepted on the recommendation of

Prof. Dr. P. Günter, examiner

Prof. Dr. B. Batlogg, co-examiner

PD Dr. I. Biaggio, co-examiner

2002

---

# Contents

<b>Abstract</b>	<b>1</b>
<b>Zusammenfassung</b>	<b>3</b>
<b>Preface</b>	<b>5</b>
<b>1 Introduction</b>	<b>7</b>
1.1 History of Organic Electronics . . . . .	7
1.2 Conduction in organic materials . . . . .	8
1.3 Current in single carrier devices . . . . .	10
1.3.1 Injection limited currents . . . . .	10
1.3.2 Transport limited current . . . . .	12
1.3.3 Current vs. voltage curves . . . . .	14
1.4 Two carrier devices - organic light emitting diodes (OLEDs) .	15
1.5 About this work . . . . .	17
<b>2 Results</b>	<b>19</b>
2.1 About the articles . . . . .	21
2.2 Interface dependent electrical properties of organic light-emitting devices in ultrahigh vacuum . . . . .	23
2.3 Ultra-high vacuum reveals interface dependent and impurity-gas dependent charge-injection in organic light-emitting diodes	31
2.4 Impurity-gas-dependent charge injection properties at the electrode-organic interface in organic light-emitting diodes . .	43
2.5 Photoelectron spectroscopy on a running organic light-emitting diode . . . . .	51
2.6 Observation of the Mott–Gurney law in tris (8-hydroxyquinoline) aluminum films . . . . .	57
2.7 Conditions for ohmic electron injection at the Mg/Alq <sub>3</sub> interface	63
<b>3 Conclusions and Outlook</b>	<b>71</b>
3.1 Conclusions . . . . .	71
3.2 Outlook . . . . .	71

<b>A</b>	<b>Experimental</b>	<b>73</b>
A.1	Ultrahigh vacuum (UHV) . . . . .	73
A.1.1	The UHV machine . . . . .	74
A.2	Deposition . . . . .	75
A.3	Photoelectron spectroscopy . . . . .	76
A.3.1	Excitation with X-rays . . . . .	78
A.3.2	Excitation with high energy ultraviolet light . . . . .	78
A.4	Electrical characterization . . . . .	79
A.5	Impedance spectroscopy . . . . .	80
<b>B</b>	<b>Material and Interface Properties</b>	<b>83</b>
B.1	Alq <sub>3</sub> . . . . .	83
B.2	NPB . . . . .	86
B.3	ITO . . . . .	87
B.4	Magnesium . . . . .	87
B.5	Magnesium:Silver . . . . .	87
	<b>Bibliography</b>	<b>91</b>
	<b>Publications related to this work</b>	<b>105</b>
	<b>Acknowledgements</b>	<b>108</b>
	<b>Curriculum Vitae</b>	<b>110</b>

---

# Abstract

This work focuses on fundamental characterization of charge injection and transport in organic materials used in organic light emitting diodes (OLEDs). By fabrication and characterization in an ultrapure environment (here ultra-high vacuum, UHV) the intrinsic properties and their relation to material parameters could be studied. The controlled exposure to different gases allows a separate investigation of the degradation mechanisms caused by oxygen and water.

Space-charge limited (SCL) current, a well-defined squared-law dependence of the injected current on the applied voltage, is observed in tris (8-hydroxy-quinoline) aluminium ( $\text{Alq}_3$ , a widely used material in OLEDs) with magnesium (Mg) contacts. From this, one derives an electric-field-independent electron mobility of the order of  $10^{-7} \text{ cm}^2/(\text{Vs})$ , with a variation between different samples of about one order of magnitude. This is the first time, that SCL current could be observed in  $\text{Alq}_3$  thin films.

The variation of the  $\text{Alq}_3$  thickness clearly shows that the Mg/  $\text{Alq}_3$  interface forms ohmic contacts without injection barriers. Operation of the Mg/ $\text{Alq}_3$ /Mg structures in oxygen or a slightly oxidation of one contact disturbs the ohmic properties of the contacts and injection barriers dominate.

A ultraviolet photoelectron spectroscopy (UPS) characterization of a very thin (35nm) Mg cathode during operation on an OLED shows that the surface of Mg in a Mg/ $\text{Alq}_3$  structure is stable during electron injection in UHV. The creation of holes in the cathode and the degradation by black spots in the region of luminescence arises from the exposure to atmospheric gases.

UPS and X-ray photoelectron spectroscopy (XPS) are also used in this work to measure the electronic structure, injection barriers, or the element composition in all employed materials. From these results it has been determined that usual magnesium-silver cathodes do not grow homogeneous onto  $\text{Alq}_3$ . The interface to  $\text{Alq}_3$  is dominated by silver.



---

# Zusammenfassung

Diese Arbeit konzentriert sich auf die grundlegende Untersuchung von Ladungsinjektion und Ladungstransport in organischen Materialien, die in organischen Leuchtdioden (OLEDs) benutzt werden. Durch Herstellung und Charakterisierung in einer extrem sauberen Umgebung (hier Ultrahochvakuum, UHV), konnten die intrinsischen Eigenschaften und ihre Verbindung zu Materialparametern untersucht werden. Der kontrollierte Kontakt mit verschiedenen Gasen erlaubt eine getrennte Untersuchung der durch Sauerstoff und Wasser verursachten Degenerationsmechanismen.

Raumladungsbegrenzter Strom mit einer quadratischen Abhängigkeit des Injektionsstromes von der angelegten Spannung wurde in tris (8-hydroxy-quinoline) aluminium ( $\text{Alq}_3$  ist ein oft benutztes Material in OLEDs) mit Magnesium (Mg) Kontakten gemessen. Daraus konnte die Größenordnung der Elektronenbeweglichkeit (unabhängig vom elektrischen Feld) mit  $10^{-7} \text{ cm}^2/(\text{Vs})$  berechnet werden. Diese variiert um etwa eine Größenordnung für verschiedene Proben. Es ist das erste Mal, das raumladungsbegrenzter Strom in  $\text{Alq}_3$  nachgewiesen werden konnte.

Die Messung der Strom-Spannungs-Kennlinien als Funktion der  $\text{Alq}_3$ -Dicke zeigt deutlich, das an der Grenzschicht Mg/ $\text{Alq}_3$  ein Ohmscher Kontakt ohne Injektionsbarriere entsteht. Wenn Mg/ $\text{Alq}_3$ /Mg Strukturen in Sauerstoff betrieben werden oder ein Kontakt oxidiert wird, verschwinden die Ohmschen Eigenschaften der Kontakte und Injektionsbarrieren dominieren.

Messungen der elektronischen Struktur mit ultravioletter Photoelektronenspektroskopie (UPS) zeigen, das die Oberfläche einer 35 nm dicken Magnesiums Kathode in einer Mg/ $\text{Alq}_3$  Struktur stabil ist, wenn Elektronen im UHV injiziert werden. Eine an Luft beobachtbare Bildung von Löchern in der Kathode und schwarzen Flecken in der Lumineszenzregion konnte im UHV nicht nachgewiesen werden.

Mittels UPS und Röntgenstrahlen Photoelektronenspektroskopie (XPS) wurde auch die elektronische Struktur, die Injektionsbarrieren oder die Elementzusammensetzung in allen beteiligten Materialien bestimmt. Dabei wurde festgestellt, das die üblichen Magnesium-Silber-Kathoden nicht homogen auf  $\text{Alq}_3$  aufwachsen und die Grenzschicht zu  $\text{Alq}_3$  durch Silber dominiert wird.

Seite Leer /  
Blank leaf

# Preface

This thesis is based on published articles in refereed journals.

Chapter 1 gives a short overview about the history of organic electronics and introduces the reader to the fundamentals of conduction in organic materials.

Chapter 2 explains the motivation for the experiments and presents the above mentioned articles.

Appendix A gives additional details of the experimental methods of this work.

Appendix B summarizes the main properties of the materials used in this work.



Seite Leer /  
Blank leaf

---

# 1 Introduction

Organic materials play an increasing role in our everyday life. Recently, they have started being employed for electronic applications and have reached many research laboratories as interesting new electronic and photonic materials. Many new applications, *e.g.* organic light emitting diodes (OLEDs) in displays, organic transistors (OFETs), or even complete circuits have been introduced. The components for organic electronics can often be produced cheaply, because the production requires only moderately low temperatures and often no crystalline materials. As an added advantage, flexible substrates can be used which one day might allow for the construction of a TV that can be rolled up. On the other hand, there are stability problems due to the possible reactions that can take place between these materials and oxygen or moisture. Even encapsulated organic materials might be damaged by electrical currents or light.

## 1.1 History of Organic Electronics

Up to the invention of thin film Organic Light-Emitting Devices (OLEDs) using hetero-interfaces in 1987<sup>1</sup> by TANG and VAN SLYKE [1], the research on organic materials for electronic applications was infinitely small compared to research on inorganic semiconductors. In the following years more and more research groups changed their direction towards organic materials. It is not surprising that in recent years the speed of innovation increased dramatically. Both research results and commercial products have shown that organic materials have a very big potential for the future.

In general, most organic materials are electrical insulators<sup>2</sup> for electrical current. Like current conduction in vacuum tubes, the organic material becomes conducting if charge carriers are injected and transported by an electric field. The vacuum tubes were exchanged by semiconducting transistor and the knowledge of current injection and current transport in insulators fell into oblivion. Inorganic semiconductors dominated the research, and later, the world wide electronic market.

---

<sup>1</sup> The results were published 1987, the patent US 4,539,507 was filed 1983.

<sup>2</sup> Insulators, by definition, are wide band-gap materials. Low conductivity arises from low mobilities, or low free carrier densities, or both (see also section 1.2).

In recent years the field of electronic charge transport in organic insulators found a new life. Highlights in the research are

- 1963 Light generation by recombination in organic crystals [2, 3]
- 1977 Conductive polymers (NOBEL prize 2000) [4]
- 1987 Organic light-emitting diode [1]
- 1990 Polymer light-emitting diode [5]
- 2000 Fractional quantum HALL-effect in organic crystals [6]\*
- 2000 Electrical pumped laser in an organic crystal [7, 8]\*
- 2000 Induced superconductivity in an organic crystal [9]\*
- 2001 Superconductivity in a polymer [10]\*

In addition, commercial applications have been introduced by several companies [11–13]. Devices with organic displays already entered the mass market (car radios and cellular phones).

The advantages of organic electronics compared to silicon technology are low temperature processing, the possibility to produce the devices on flexible substrates and the great variety of chemistry which leads to highly optimized materials.

There are still some disadvantages which have to be minimized. First of all, the long term stability is for all organic materials a challenge and the devices have to be encapsulated for applications in such a way that no atmospheric gases can reach the device. In particular, moisture leads to strong irreversible degradation in all organic devices and is a big problem for the devices on flexible substrates. All the flexible substrates up to now are sensitive to moisture.

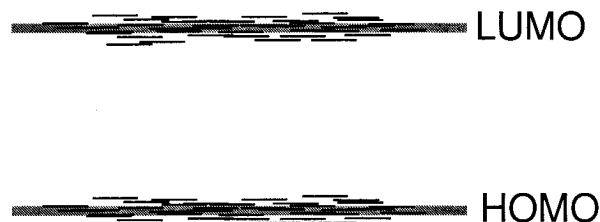
## 1.2 Conduction in organic materials

The organic materials discussed here are in principle insulators, or at least wide-band-gap semiconductors. These materials are often called “organic semiconductors” (see the title of this work) or even “organic conductors”. It is important to point out that in case of “conducting” organic materials many organic displays would not work because the separation of pixels requires isolating parts within the pixel areas.

---

\* The author wants to mention that just before the printing of this work the Bell Labs have launched inquiry into allegations of data duplication in the published articles of the here cited group (see Nature **417**, page 367 - 368 (2002))

**Figure 1.1:** Schematic of electron states of a disordered molecular system. The average of the electronic states is shown as gray line.



## How can a current flow inside an (organic) insulator?

Insulators, as everybody knows, are poor electrical conductors at room temperature. A low conductivity arises from low mobilities, or low free carrier densities, or both. However, an insulator can be made to conduct a relatively large current if the contacts permit the introduction of excess free carriers into the insulator. If the carriers enter through a surface boundary, the process is referred to as charge carrier injection.

Organic molecules can form organic crystals with a periodical arrangement and symmetries. If the molecules are randomly oriented, the materials are called amorphous. This work concentrated on amorphous organic films.

Amorphous organic materials can transport charge carriers within the molecules along conjugated bonds (alternating single/double bonds) and from molecule to molecule by hopping or tunnelling.

The electronic states in most amorphous organic materials are determined by the molecular structure because the influence from neighboring molecules is weak. As a consequence, localized electronic states with sharp energy levels are formed. Only the Lowest Unoccupied Molecular Orbital (LUMO) and the Highest Occupied Molecular Orbital (HOMO) are usually considered for describing current transport. In amorphous organic materials the electronic states can not be called “bands” as in crystalline inorganic semiconductors with band formation by periodicity.

Because of the disorder in the amorphous materials – different distances between molecules or chains, different relative orientations of the molecules or chains, or impurities – there is a characteristic spread in the energy of the levels (Fig. 1.1). This can be described by a GAUSSIAN function with variance  $\sigma$  [14]. For a simple description of the injection processes we here assume a small<sup>3</sup> value of  $\sigma$  and therefore electron states with similar energies spatially extended over the whole organic material. The LUMO can be compared to the conduction band in crystalline inorganic semiconductors and the HOMO to the valence band.

In contrast to doped inorganic semiconductors, the LUMO is empty and

<sup>3</sup> More precise theories, considering the distribution of the electronic states, are described in the literature [14–24].

the HOMO completely filled at room temperature<sup>4</sup>. Conduction becomes possible if charges are injected from a reservoir with nearly infinite charges into the organic material. The reservoirs are the electrical contacts which form the boundary of the organic device.

## 1.3 Current in single carrier devices

In the following we give an overview of the fundamental models that describe the injection and transport in organic materials for conduction dominated by one type of charge carriers. The principles are described for electron only injection and can be adapted to hole injection as well.

### 1.3.1 Injection limited currents

If the transport capability is faster than the charge injection, the current flow inside the material is determined by the injection process.

#### Large barrier heights – Fowler-Nordheim-tunnelling

If a metal and an insulator are contacted in the presence of an applied electrical field an energy barrier with a height  $\Delta$  is formed. The value of  $\Delta$  is defined by the energetic position of the LUMO relative to the FERMI-energy of the contact. In the absence of charge accumulation at the contact interface and for large barrier heights a triangular barrier is formed within the electric field  $E$ . Fig. 1.2 shows such a triangular barrier for electron injection from the electron reservoir into the LUMO. For large barrier heights the electrons can overcome the barrier by tunnelling. The tunnelling distance and thus the injection probability are strongly dependent on the electric field (an example for two different electric fields is drawn in Fig. 1.2).

From the tunnelling probability one can obtain an injected current density  $j_{FN}$  [16,25]:

$$j_{FN} = BE^2 \exp\left(\frac{-8\pi\sqrt{2m^*\Delta^3}}{3heE}\right) \quad (1.1)$$

where  $m^*$  is the effective mass of the electrons inside the dielectric,  $B$  is a constant factor with unit  $A/V^2$ ,  $h$  is PLANCKS constant, and  $e$  is the elementary charge.

---

<sup>4</sup> As an example the average HOMO-LUMO energy difference is 3.3 eV in Alq<sub>3</sub> (see section B.1) BOLTZMANN statistic gives at 300 K a ratio of  $4 \times 10^{-56}$  for the number of occupied states in the LUMO compared to the HOMO.

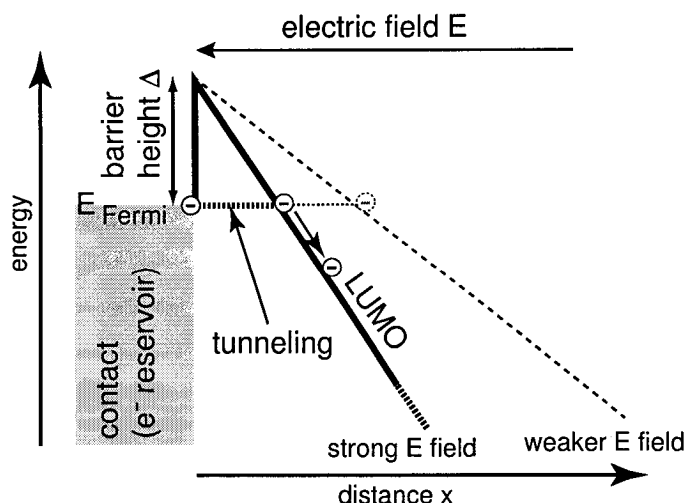


**Figure 1.2:** Tunnelling through a triangular barrier  $\Delta$ . The applied electrical field changes the tunnelling distance and therefore the tunnelling probability.

This type of electron injection is called FOWLER-NORDHEIM tunnelling. In it the image force (see section 1.3.1) and hot electron contribution to the current are neglected.

For more information about FOWLER-NORDHEIM injection in organic materials see *e.g.* Ref. 26–28.

### Low barrier height – Thermionic injection / image charge potential

The height of a triangular barrier as described above is decreased in strong electric fields by the image charge potential [16]. This potential appears when an electron at a distance  $x$  from the metal induces a positive charge (image charge) in the metal. The attractive force is

$$F(x) = -e^2/(16\pi\epsilon\epsilon_0x^2), \quad (1.2)$$

where  $e$  is the elementary charge,  $\epsilon$  the dielectric constant,  $\epsilon_0$  the permittivity of vacuum. The total potential as a function of the distance  $x$  is

$$\phi(E, x) = \Delta - e^2/(16\pi\epsilon\epsilon_0x) - eEx. \quad (1.3)$$

The resulting barrier and the barrier without the effect of the image force are shown in Fig. 1.3. The resulting barrier reduction  $\delta$  is

$$\delta = \sqrt{\frac{q^3 E}{4\pi\epsilon\epsilon_0}}, \quad (1.4)$$

and is plotted vs. the electric field in Fig. 1.4. The barrier is reduced by 0.2 eV at an electric fields of 1 MV/cm (see section 2.6).

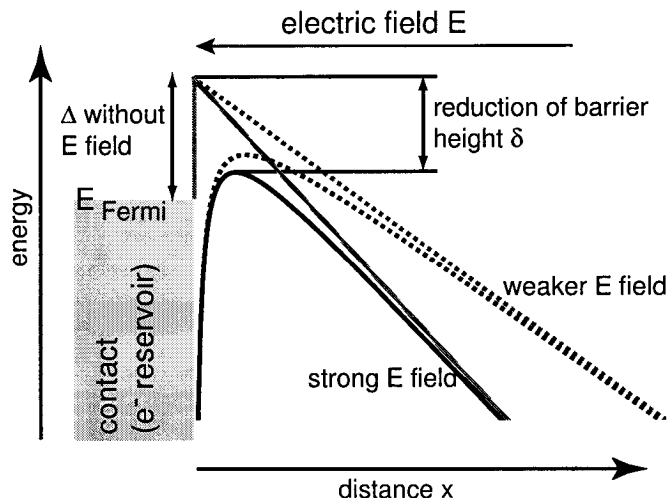


**Figure 1.3:** The image charge potential leads to a decrease of the barrier height  $\delta$ . This value  $\delta$  depends on the electric field.

The thermal energy can be sufficient to assist carrier injection from the contacts into materials with low injection barriers. The electron distribution in the metal which builds up the contacts is described by the FERMI-distribution, and therefore there are electrons with energies above the FERMI-level that enter the sample when they acquire sufficient thermal energy to cross the potential maximum. Considering a decrease of the barrier height by image charge effects, the calculation of the current-density resulting from the thermal injection (also called “thermionic injection / emission”) gives [15, 20, 25, 29]

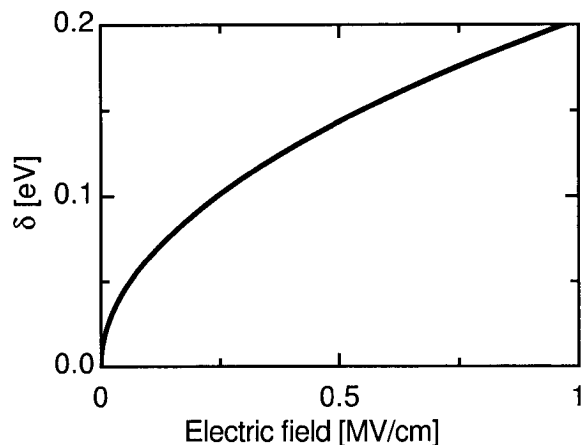
$$j(E) = CT^2 \exp\left(-\frac{\Delta - \sqrt{\frac{e^3 E}{4\pi\epsilon_0\epsilon}}}{k_B T}\right), \quad (1.5)$$

where  $C = 4\pi e k_B^2 m^* / h^3 = 120 \cdot \frac{m^*}{m_e} \text{ Acm}^2 \text{ K}^2$  is the field independent RICHARDSON-constant. This approach neglects tunnelling through the barrier and inelastic backscattering of the hot carriers before traversing the potential maximum. A more refined model considering backscattering of the hot carriers before traversing the potential is discussed in Ref. 30 and 31.

### 1.3.2 Transport limited current

In the case of “ohmic-contacts”, contacts where injection of charges carriers occurs at any voltage (without appearance of injection barriers), so that charges can be injected without any limits leads to currents limited by the transport processes in the organic insulator.

**Figure 1.4:** Reduction of barrier height  $\delta$  by the image force potential vs. the electric field for a material with  $\epsilon = 3.5$  (e.g. Alq<sub>3</sub>).



### Trap limited current

Because of impurities insulators often contain traps and this fact leads to an additional structure in the current vs. voltage characteristics. Traps are electronic structure defects with energies below the LUMO which can trap electrons for a certain time. The electrons are released from the traps by thermal excitation. In the case of current transport with trap filling the amount of carriers available for charge transport increases strongly with the injected carrier density and in the current-voltage measurement a steep increase of the current appears.

Depending on the energy distribution of the traps the resulting  $j(V)$  behavior is different. The cases of a single-level (see also section 1.3.3), exponential distribution, or a uniform distribution are described in Ref. 32.

### Space-charge limited current

The traps can be kept filled if enough current is flowing and every thermally excited trap can be refilled instantly. If the injected carriers exceed the transported carriers, space-charge effects can build up and hinder the injection of the following charge carriers. In a “parallel-plate capacitor configuration,” where the organic insulator is sandwiched between two electrodes, and at high applied voltages  $V$  the injected current density  $j$  is given by the Mott-Gurney law (also known as Child’s law in solids) [32–36]

$$j = \frac{9}{8} \mu \epsilon \epsilon_0 \frac{V^2}{d^3}, \quad (1.6)$$

where  $\mu$  and  $\epsilon$  are the mobility and the dielectric constant of the material,  $\epsilon_0$  is the permittivity of vacuum,  $d$  is the distance between the contacts, and  $V$  is the applied voltage. Eq. 1.6 is valid for a mobility  $\mu$  which is independent from the applied electric field and from the current density.



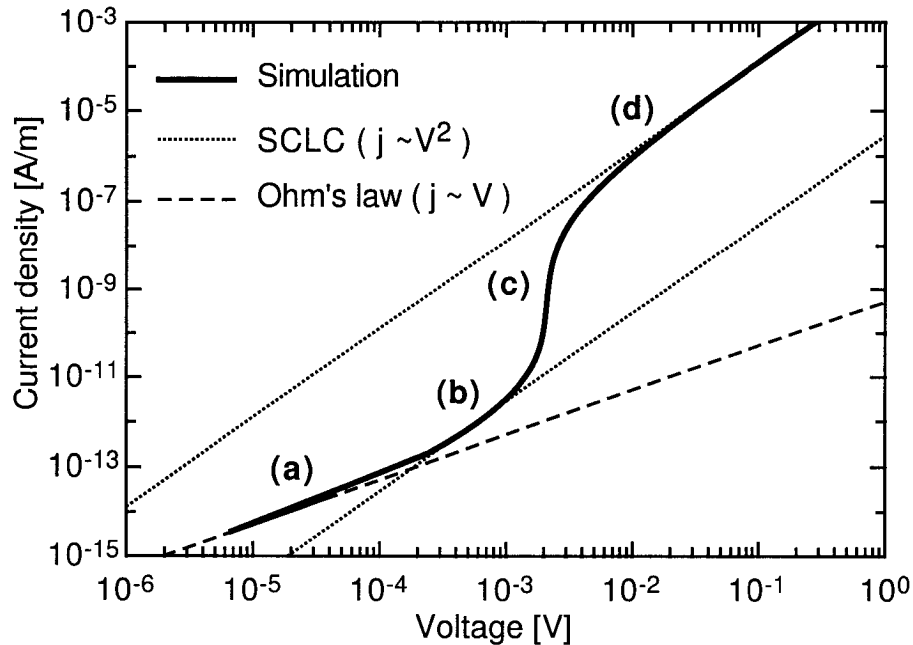


**Figure 1.5:** Calculated current vs. voltage curves of a single layer device with four characteristic regions: (a) ohmic conduction, (b) space-charge limited current (SCLC) (c) trap-filling, (d) trap-filled SCLC (courtesy of P. Losio). The parameters for the simulation are:  $n_0 = 1 \times 10^{14} \text{ m}^{-3}$  (thermal carrier density),  $N_t = 1 \times 10^{19} \text{ m}^{-3}$  (trap density),  $N_{LUMO} = 1 \times 10^{25} \text{ m}^{-3}$  (density of states in the LUMO),  $\mu = 1 \times 10^{-11} \text{ m}^2/\text{Vs}$  (intrinsic mobility),  $\Delta E_t = 0.6 \text{ eV}$  ( $\Delta E_t = E_{LUMO} - E_t$ , trap level depth)  $T = 300 \text{ K}$  (temperature),  $d = 300 \text{ nm}$  (insulator thickness),  $\epsilon = 3.5$  (dielectric constant).

### 1.3.3 Current vs. voltage curves

The application of the full theory described in Ref. 32 delivers an analytical parametric solution for the current vs. voltage curve inside a single carrier device (see Ref. 32, 37). Trap filling is described assuming a single trap level with bonding energy  $E_t$ . The related distribution of the trapped charge carriers is assumed to be

$$n_t(x) = \frac{N_t}{1 + e^{\frac{E_t - F(x)}{k_B T}}}, \quad (1.7)$$

where  $N_t$  is the trap density,  $T$  the temperature and  $F(x)$  the FERMI level. Fig. 1.5 shows an example of a calculated IV-curve. Clearly visible are four different regions with different slope of the current-voltage characteristic in the log-log plot. First, for small voltages (a), there are not enough injected charges to create the space-charge limited current and the structure behaves like an ohmic resistor. At higher voltages (b) the current is space-charge limited with a low effective mobility value corresponding to a situation when

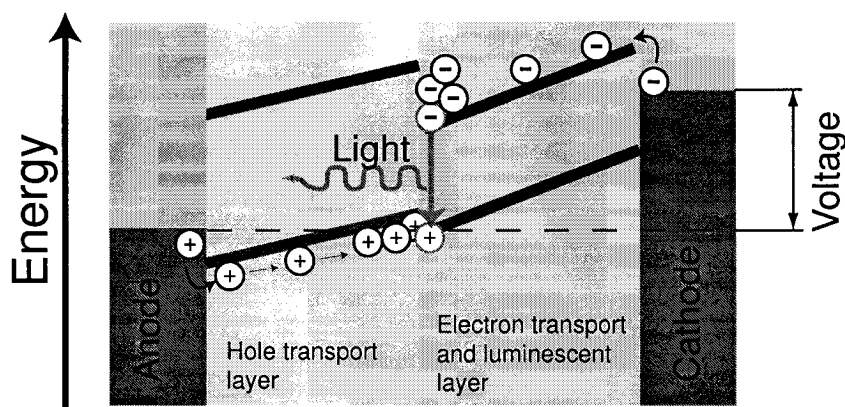


**Figure 1.6:** Basic operation of a two-layer OLED: Electrons and holes are injected from the contacts and transported towards the organic / organic interface where the charges are accumulated and recombination generates light.

most injected carriers reside in the traps. Then the traps can be filled (c) resulting in a strong increase of the current. Finally the traps are filled and the space-charge limited current (d) corresponds to trap free conduction.

Depending on the energetic distribution of the traps it is also possible to observe a current-voltage characteristic without region (b). Section 2.6 and section 2.7 give examples of this behavior.

## 1.4 Two carrier devices - organic light emitting diodes (OLEDs)

For OLED operation one needs both electron and hole injection in the organic materials. Electrons are injected from a low work function contact and holes from a high work function contact to keep the injection barriers small. At least one of the contacts has to be transparent to let the generated light out.

The basic functions of the device can be divided in three parts:

1. Injection of charge carriers (holes and electrons) from the contact reservoirs (anode and cathode) into the non occupied states (HOMO for holes and LUMO for electrons) of the organic materials,
2. Transport of the charge carriers,
3. Recombination of the charge carriers and generation of light.

Fig. 1.6 illustrates these basic operation steps for a two-layer OLED. The injection and transport processes have already been described in section 1.2. The recombination process must take place away from the contacts

for high recombination efficiency. Radiative recombination near the contacts will be quenched because the contacts hinder with their free charges the expansion of the electric field of the generated electromagnetic wave [38]. Another reason is the higher trap and defect density near the interface which can lead to many more paths for non-radiative recombination. Because of this the first experiments with electroluminescence within organic materials (see section 1.1) were not very successful and the efficiency was very low. The concept of two organic layers [1] greatly increases the efficiency. The recombination zone shifts to the organic / organic interface near the center of the OLED and far away from the contacts.

Several models have been proposed to analyze the current-voltage characteristics and device performance. For more details see *e.g.* [18, 21, 23, 39, 40].

OLEDs can be produced by vacuum deposition for small molecule materials; in the case of polymer light emitting diodes, solution technologies like spin-coating, ink-jet printing, or silk-screen printing are used.

In this work “small molecule” organic materials have been used. They are colorful powders and can be evaporated by heating the material in vacuum. Even in ultrahigh vacuum many organic (purified) materials can be heated without substantial vapor pressure.

Most of all the experiments presented in Chapter 2 require ultrapure devices. Due to atmospheric contamination (see section A.1), this requirement is very difficult to meet for OLEDs made by spin-coating polymers in air, or even by evaporating small molecules in a vacuum of the order of  $10^{-5}$  mbar. Thus, although the final aim for device production is certainly a cheap production facility for a complete physical characterization of the device-performance, a UHV system (section A.1.1) must be used for the fabrication and characterization of the OLEDs. Böhler et al. [41] showed that fabrication in UHV gives the best results for the OLED performance compared to a fabrication under worse vacuum conditions.

## 1.5 About this work

This thesis reprints a selection of papers in refereed journals in which the author of this theses was author or co-author. The articles themselves contain an introduction to their special topic, the special experimental setup, sample structures, results, discussion of the results, and conclusions. The next chapter collects six such publications selected from eight articles in reviewed journals (see page 105). They are reprinted in the style of the present work. An overview and summary of the research described in the publications is found at the beginning of the next chapter.

Seite Leer /  
Blank leaf

## 2 Results

This work initially focused on the fabrication and investigation of OLED structures (ITO/NPB/Alq<sub>3</sub>/Mg, see Appendix B for the full names and properties of the materials). Samples were produced inside an UHV system but the characterization was performed in air and the masks (see Appendix A.2) were changed during fabrication under worse than UHV conditions (in the transportation chamber with opened valve to the load-lock chamber). To characterize the devices, a first computer controlled measurement system was built, where luminescence (brightness) and current could be determined at the same time for different applied voltages.

Even if the devices were measured directly after venting the load-lock chamber, a device degradation, caused by air, strongly influenced the device performance. After several fabrications and characterizations of the devices it was clear no serious research can be performed on OLEDs without perfect encapsulation of the devices.

There are different ways to avoid the contamination from air: i) transporting the sample from the vacuum into a glove box ii) covering the sample with a protection layer, or iii) characterization of the OLED in UHV. Case i) and ii) have been often described in the literature (for case i) see [41–56], and for case ii) see [56–69]). We followed the last approach. To realize the possibility of new experiments on ultrapure samples I designed and built a new chamber especially for the characterization of OLEDs at UHV conditions, (for details, see Appendix A.4). In the early stage of the experiments no pump was attached to the chamber and no possibility to flood the chamber with gases existed (no valves).

Besides our group similar experiments in UHV have been performed by Shen et al. [70, 71] dealing with the electrical characterization of metal/organic/metal structures in UHV. To the best of our knowledge OLED operation in UHV with electrical and brightness characterization have only been published by our group up to now.

It was immediately clear that the degradation effects observed before in air vanish completely when the devices are kept in UHV.

First experiments then concentrated on the Mg/Alq<sub>3</sub> interface. It was already known from XPS [72] and UPS [73] that Mg reacts with the Alq<sub>3</sub> surface if the Mg is deposited on the Alq<sub>3</sub>. It was supposed that the Mg diffuses inside the Alq<sub>3</sub> layer (see also [65, 74]). The work of Y. Tao [72] has shown that a 1 nm thin Ag-layer can help to grow the Mg layer properly on

the Alq<sub>3</sub> layer. I was interested to know if the surface reaction of Mg on Alq<sub>3</sub> deteriorates the interface and thus the electrical properties in the ultrapure devices. Current-voltage and brightness measurements were also performed on such devices in air to compare with the ultrapure devices. The experiment and the results are described in section 2.2 on *“Interface dependent electrical properties of organic light emitting devices in ultra high vacuum”*. I have realized after several other measurements that the results of Ref. 72 can be also interpreted by a lower sticking coefficient (instead of diffusion) of Mg deposited on the Alq<sub>3</sub> surface caused by the surface reaction in the Mg/Alq<sub>3</sub> interface. There are some doubts if the Mg on the thin Ag layer has the same thickness as the Mg layer without the Ag. This might explain the large difference in lifetime of both devices in air (more details in section 2.2).

The appearance of “black spots”<sup>1</sup> in air is accompanied by the appearance of small holes in the cathode. The appearance of the holes might be an intrinsic effect which opens the cathode for the humidity, but I could show by UPS measurements (for an experimental introduction see Appendix A.3.2) on an operating OLED in UHV that the deterioration on the cathode surface is not detectable and therefore very probably an effect of the exposure to air<sup>2</sup>. This experimental setup and the results are discussed in section 2.5 *“Photoelectron Spectroscopy on a running Organic Light Emitting Diode,”* and partly in section 2.3 on *“Ultra-high vacuum reveals interface dependent and impurity-gas dependent charge-injection in organic light-emitting diodes”*.

The influence of the oxygen and air on the OLED structures were further investigated to understand the degradation mechanisms. Impedance spectroscopy measurements have also been performed to investigate the cause of the changes in the electrical properties of the devices after contamination with the gases. Section 2.4 on *“Impurity-gas-dependent charge injection properties at the electrode-organic interface in organic light-emitting diodes”* shows the resulting measurements and findings.

All the previously discussed experiments have problems with reproducibility because the work function and the roughness of the ITO are highly sensitive to the pretreatment (see section 2.2 and section 2.3). ITO was the only layer of the OLED which has not been fabricated in UHV and therefore was susceptible to uncontrolled impurities. In order to improve the reproducibility and to study more controllable systems with a better interpretation of

---

<sup>1</sup> “Black spots” are non radiative parts of the OLED and a typical type of degradation in air. More information about the degradation process can be found in the literature [53, 57, 75–79]

<sup>2</sup> An estimation of the sensitivity of these UPS measurements resulted in a limited threshold for detecting defects in the cathode. The area of the defects has to be at least the same magnitude of the sample area.

the results I resorted to an fabrication of samples without ITO where only electrons were injected. By using Mg contacts on Alq<sub>3</sub> I made the barrier for hole injection so high (3 eV, see section B.1) that only electrons contributed to the injected current.

The results are adaptable to OLED structures and the fabrication process is easier to control because of the minimized number of parameters. Measurements of IV-curves in UHV immediately after fabrication showed a region, at high voltages, where  $j \sim V^2$ . This was recognized as space-charge limited (SCL) conduction and was exploited to determine the electron mobility of Alq<sub>3</sub> in several samples. The results are discussed in section 2.6 on "*Observation of the Mott-Gurney law in tris (8-hydroxyquinoline) aluminum films*". This section presents the first observation of SCL current in Alq<sub>3</sub> and a detailed investigation of the distribution of the electron mobility values in several samples. In addition, I could show that the electron mobility is not electric field dependent up to electric fields of 1 MV/cm.

I next focused on the voltage dependence of the current-density at lower voltages where SCL current is not observed. The aim was to distinguish between two possible explanations for the observed curves – either trap filling or field dependence of electron injection through energy barriers. I could show that the first explanation applies for samples produced and operated in UHV. For voltages below the SCL region the current vs. voltage curves do not change with the Alq<sub>3</sub> thickness which proves that the Mg/Alq<sub>3</sub> contacts are indeed very ohmic, allowing electron injection by diffusion [80, 81]. Under these conditions a density of charge carriers is injected by diffusion from the metallic contacts into the organic layer [80] even without any applied voltage. To simulate oxygen barriers I operated the structures in oxygen and produced structures with artificially oxidized Mg contacts. The current in case of electron injection through the oxygen barrier can be described by FOWLER-NORDHEIM tunnelling (section 1.3.1). The results are shown in the section 2.7 on "*Conditions for ohmic electron injection at the Mg/Alq<sub>3</sub> interface*".

## 2.1 About the articles

In the following the main results of this work are presented in different sections. All these chapters have been already published in scientific journals. These papers are listed on page 105. At the beginning of every article a short abstract summarizes the results and experiments. The contents of the articles are identical to the published versions, the format was adapted to this work.



Seite Leer /  
Blank leaf

## 2.2 Interface dependent electrical properties of organic light-emitting devices in ultrahigh vacuum\*

### Abstract

We present electroluminescence and electrical measurements on organic light emitting diodes (OLEDs) which were produced and operated inside a contamination-free ultra-high vacuum (UHV) system, at a purity level corresponding to a pressure of  $10^{-9}$  mbar. We characterized devices with a simple magnesium (Mg) cathode, where Mg atoms diffuse into the 8-hydroxyquinoline aluminum ( $\text{Alq}_3$ ) layer during evaporation, and devices where a 1 nm thin silver (Ag) layer acts as a diffusion barrier between Mg and  $\text{Alq}_3$ . All OLEDs could be operated in UHV during 1 day at a brightness level of  $1000 \text{ Cd/m}^2$ , without the appearance of any "black spots". When exposed to air however, a significant degradation of the device performance was observed. The lifetime in air was a few seconds for the device with the simple Mg cathode, and a few hours for the device with the Ag layer, indicating the importance of Mg diffusion when the device is operated in air.

### INTRODUCTION

The performance of organic light emitting diodes (OLEDs) is critically sensitive to fabrication parameters and environmental parameters. A controlled characterization of the fabrication parameters, such as different cathode materials, is only possible if the influence of environmental parameters, such as water and reactive gases like oxygen, can be excluded.

Because of atmospheric contamination, this requirement is very difficult to meet for OLEDs made by spin-coating polymers in air, or even by evaporating small molecules in a vacuum of the order of  $10^{-5}$  mbar. Thus, although the final aim for device production is certainly a cheap production facility, for a complete physical characterization of the device-performance and its origin, we resorted to a ultra-high vacuum (UHV) system developed for molecular beam epitaxy.

Since uncontrolled environmental parameters can be present both during device fabrication and during device operation, we operate and characterize test devices in the same UHV system where they are fabricated. We use a

---

\* The results of this section have been published in Synthetic Metals Vol. 111-112, page 307-310 in the year 2000.

UHV system that contains dedicated chambers for molecular beam deposition of organic molecules, for deposition of metallic layers, and for surface characterization by ultraviolet photoelectron spectroscopy (UPS) and X-ray photoelectron spectroscopy (XPS). The system was expanded by adding a dedicated chamber equipped with electrical and optical connections for the measurement of electroluminescence and current-voltage characteristics.

Thanks to this system, we are able to deposit different cathode structures, measure their work function, use them in the assembly of an Organic Light Emitting Device, and characterize the device performance, while at all times maintaining the device in a vacuum of the order of  $10^{-9}$  mbar. The fact of avoiding atmospheric contamination in an extremely clean UHV system during both fabrication and characterization of OLEDs, opens a new dimension of purity for the study of the physics of organic light emitting devices.

The cathode material and preparation is one of the main issues influencing the performance of OLEDs. It has recently been found [72–74] that some metals including Mg exhibit partial condensation at the  $\text{Alq}_3$  surface and diffuse into the organic layer during evaporation of the electrode. An ultra-thin Ag layer can be used to block this kind of diffusion when Mg as cathode material is used. [72].

In the present work, we produced multilayer OLEDs with an indium tin oxide (ITO) anode, the hole transport layer NPB (N,N'-bis-{1-naphthyl}-N,N'-diphenyl-1,1'-biphenyl-4,4'-diamine) and  $\text{Alq}_3$  (tris {8-hydroxyquinoline aluminium}) as an electroluminescent layer, and with two different cathodes, one consisting of pure Mg, and the other with a 1 nm thick Ag layer separating the Mg from the organic  $\text{Alq}_3$  layer.

The two types of OLEDs were then operated in the same UHV system where they were grown, without any contact with the atmosphere prior to and during operation. The data we obtained is presented below, together with a discussion of how the OLED properties change when they are exposed to atmospheric contamination. This is, to our best knowledge, the first time OLEDs have been produced and characterized in a contamination-free UHV system, at a purity level corresponding to the pressure of  $10^{-9}$  mbar.

## SAMPLE PREPARATION

For every device we used a glass substrate with photolithographically patterned, 160 nm thick, ITO anodes. The ITO is patterned in such a way that we get 12 devices, each with  $18\text{mm}^2$  surface area, on one substrate. The substrate was cleaned by ultrasound using acetone and ethanol and then rinsed in purified water.

To exclude the influence of short-circuits between the ITO and the metal

layer near the device edges we used quite thick organic layers. On top of the patterned ITO we evaporated a 80 nm thick NPB layer as hole transport layer and a 100 nm thick Alq<sub>3</sub> layer as electron transport and light emitting layer (substrate temperature 25° C). The deposition of the organic materials took place in a special UHV chamber (base pressure  $\leq 4 \times 10^{-9}$  mbar) for organic materials. The thickness was controlled by a temperature stabilized quartz micro balance. A metal mask protected part of the ITO on the sample, to be used for electrical contacts.

After the organic deposition, and with the sample always remaining in the UHV system, we changed the mask and moved the sample to another UHV chamber where the cathodes were deposited (base pressure  $\leq 1 \times 10^{-9}$  mbar, substrate at room temperature).

We used two types of cathodes, which we identify symbolically with “Mg-52” and “Ag-1/Mg-57”. Mg-52 is a cathode consisting of pure Mg, 52 nm thick. Ag-1/Mg-57 is a cathode consisting of an ultrathin 1 nm Ag layer in contact with Alq<sub>3</sub>, followed by a 57 nm thick Mg layer. The deposited layer thicknesses were also controlled by a temperature stabilized quartz microbalance in this chamber.

## RESULTS AND DISCUSSION

### Work functions of the cathodes

The work functions for electron extraction from the Mg-52 and Ag-1/Mg-57 cathodes were measured by evaporating separately the same structures on a silicon substrate and measuring the work function by Ultraviolet Photoelectron Spectroscopy. As photon source we used a Helium gas discharge lamp with a photon energy of 21.2 eV and the electron analyzer was a hemispheric one. During the measurement the sample was biased by -5 Volts.

The work function of Mg-52 was found to be 3.8 eV. The work function of Ag-1/Mg-57 was measured to be of the order of 4.0 eV, still 0.6 eV smaller than the work function of pure Ag. The structure with the thin Ag layer is not expected to be better than pure Mg from the point-of-view of electron-injection efficiency alone. However, the thin Ag layer has the advantage that it blocks the diffusion of Mg [72], and we will show below that the Ag layer can efficiently act as a protective layer during device operation in air.

### Electrical and electroluminescent properties

First we characterized the devices in UHV. We removed the masks used during cathode deposition and connected the substrate to electrical contacts

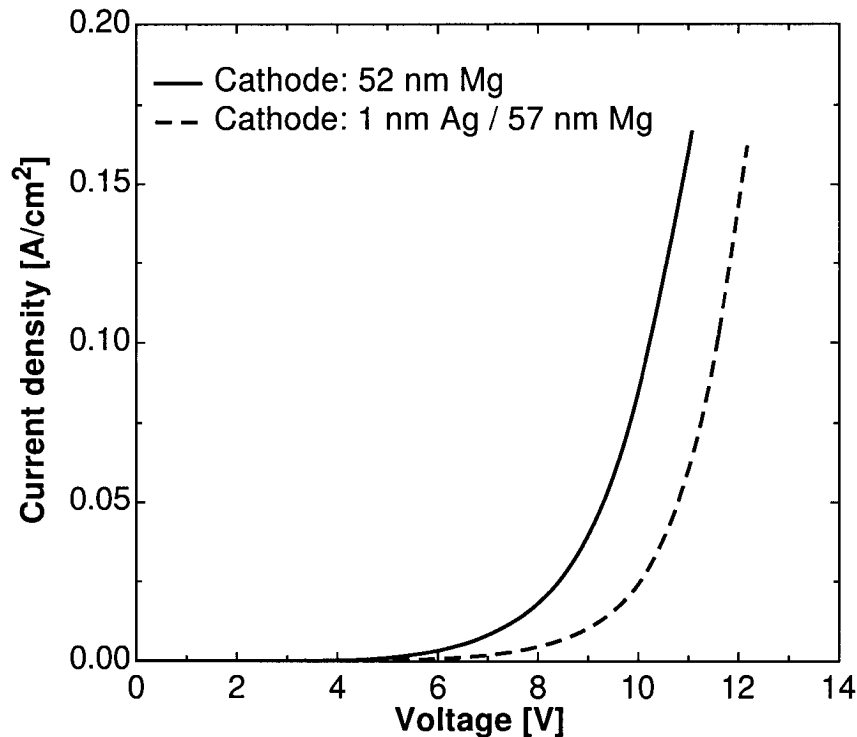


**Figure 2.1:** Current-density vs. voltage characteristic for OLEDs fabricated and operated in UHV. The solid curve corresponds to the Mg-52 cathode, the dashed curve to the Ag-1/Mg-57 cathode.

in a specially designed UHV chamber. The light leaving the OLED was reflected by an aluminium mirror, exited the UHV system through a glass window, and was measured by a Minolta LS100 luminance meter. The losses caused by mirror and glass windows are estimated to be of the order of 15%. We multiplied the brightness measured with this system with 1.15 to compare it with brightness measured in air. The voltage and current were measured by a computer controlled Fluke-45 multimeter.

The current-voltage and the luminescence-current characteristics obtained with the two cathodes Mg-52 and Ag-1/Mg-57 are shown in Figs. 2.1 and 2.2. As expected from the difference in work functions (the height of the injection-barrier for the Mg-52 cathode is lower), the device with the Mg-52 cathode works with a voltage-threshold which is approximately 1.4 V lower when compared with the device with the Ag-1/Mg-57 cathode (see Fig. 2.1). The effect of the cathode work function is also seen in Fig. 2.2, which shows that the device with the Mg-52 cathode has a 20% better efficiency ( $360 \text{ cd/m}^2$  instead of  $300 \text{ cd/m}^2$  at a current density of  $0.02 \text{ A/cm}^2$ ).

The diffusion of Mg into the  $\text{Alq}_3$  does not strongly influence the device performance when the device is not exposed to the atmosphere. Both devices were operated continuously for at least one day and no black spots were

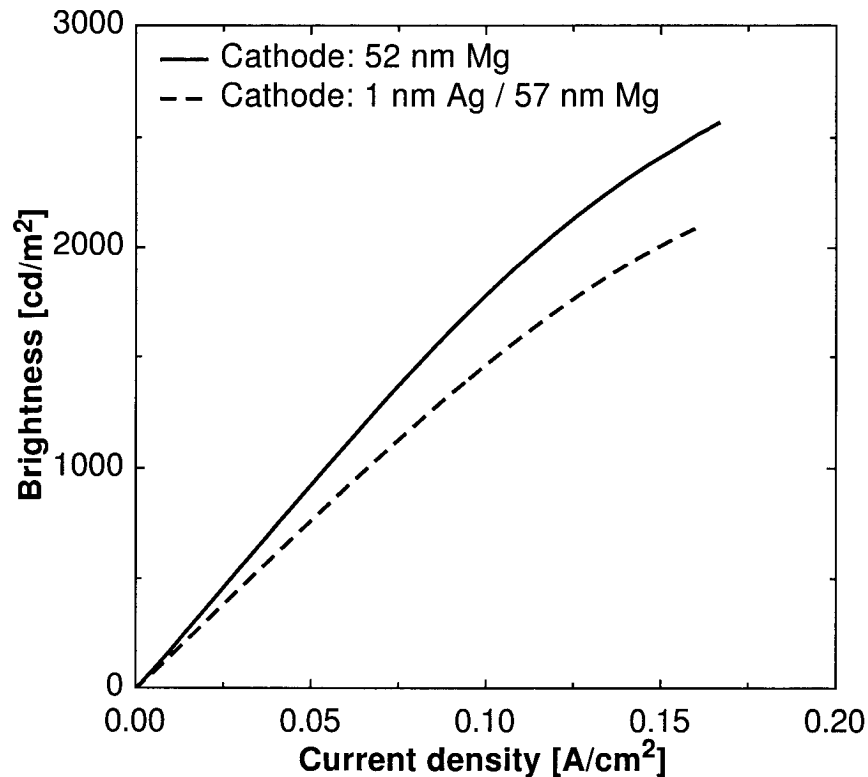


**Figure 2.2:** Brightness vs. current-density characteristic for OLEDs fabricated and operated in UHV. The solid curve corresponds to the Mg-52 cathode, the dashed curve to the Ag-1/Mg-57 cathode.

observed. This behavior must be contrasted with what we observed when operating the devices outside of the UHV system, at atmospheric pressure.

In air, the Mg-52 device could be operated only during a few seconds before its performance degraded irreversibly. Because of the short life time it was not possible to measure current-voltage and brightness-current characteristics.

One reason for this very short lifetime can be the small thickness of the Mg-cathode, which allows for rapid oxidation of the whole cathode in air, but a much more important role is probably played by the Mg that diffused inside the Alq<sub>3</sub> during evaporation of the electrode. In fact, the Ag-1/Mg-57 device, with the thin Ag protection layer between Alq<sub>3</sub> and Mg, could operate in air for a much longer time (more than 5 hours). This allowed a systematic study of the influence of the atmosphere in the device Ag-1/Mg-57.

Fig. 2.3 shows current-voltage characteristics of OLEDs with an Ag-1/Mg-57 cathode. Data are given for a device in UHV, for a device that was exposed to air during 1 hour and than again operated in UHV, and for a device that was operated in air.

Contact with air increases the threshold voltage by about 1.4 V for LED

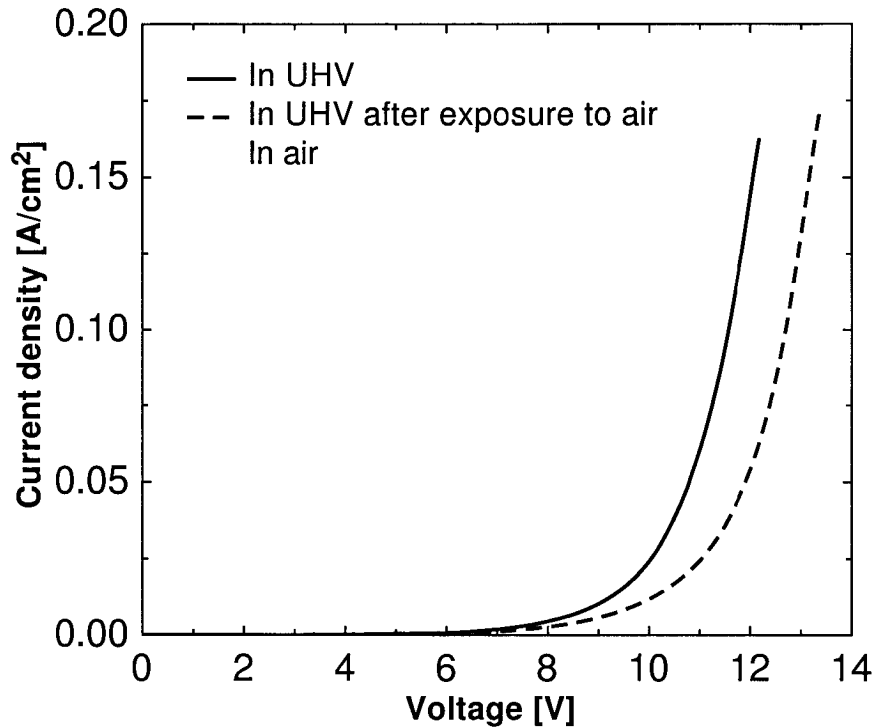


**Figure 2.3:** Current-density vs. voltage characteristic of the OLED with the diffusion protection layer when operated in UHV (solid curve), in UHV after about 1 hour exposure to air (dashed curve), and in air (dotted curve).

operation. The brightness-current characteristic (Fig. 2.4), on the other hand, shows that the efficiency of the device is nearly twice as large when it is operated in air. For the device that has been only briefly exposed to air before operation in UHV, the efficiency does not change significantly.

Lifetime measurements in air on the Ag-1/Mg-57 device showed that black spots reached a size of the order of  $1 \text{ mm}^2$  in about 30 minutes. This is to be contrasted with the behavior of the same device in UHV, where it could be operated for more than 24 hours without any appearance of black spots.

The difference in the lifetime of the devices with Mg-52 cathode and with Ag-1/Mg-57 cathode is a strong indication that the Mg atoms which diffused inside the  $\text{Alq}_3$  layer react with atmospheric gases to rapidly deteriorate the device during operation.

Although further experiments are needed to pinpoint the exact deterioration mechanism induced by the intimate contact between Mg atoms and  $\text{Alq}_3$  [82], we can already say that the degradation mechanism is assisted by the presence of atmospheric gases (most probably oxygen) and water.

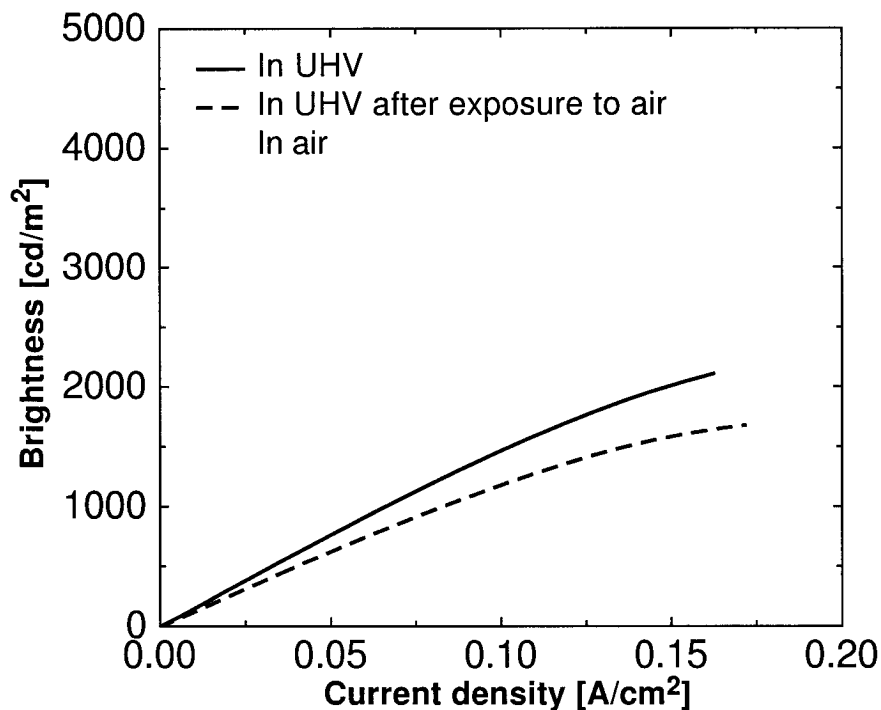


**Figure 2.4:** Brightness vs. current-density characteristic of the OLED with the diffusion protection layer when operated in UHV (solid curve), in UHV after about 1 hour exposure to air (dashed curve), and in air (dotted curve).

## CONCLUSIONS

We presented data on the performance of organic light emitting devices grown and operated in a contamination-free UHV system. We were able to show that atmospheric influence has a dramatic effect on the efficiency of the devices, on their lifetime, and on the mechanism of their degradation. We confirmed that Mg diffusion into Alq<sub>3</sub> is detrimental to the performance of an OLED, but observed that this is only the case when the device is operated in air, indicating that chemical reaction with atmospheric gases plays an important role in the degradation mechanism. No black spots were observed when the devices were operated at a pressure of the order of  $10^{-9}$  mbar.



Seite Leer  
Blank leaf

## 2.3 Ultra-high vacuum reveals interface dependent and impurity-gas dependent charge-injection in organic light-emitting diodes\*

### Abstract

We present a complete characterization of Organic Light Emitting Diode (OLED) structures performed in an ultra-pure Ultra High Vacuum (UHV) environment and under controlled influence of oxygen and atmospheric gases. We fabricated **and** characterized standard NPB/Alq<sub>3</sub> devices with an Indium Tin Oxide (ITO) anode and a magnesium cathode in an UHV system. With this system we are able to study the injection properties of very clean, controllable interfaces in the absence of any impurity gas. We found that the threshold voltage for OLED operation always increased after exposure to any atmospheric gas, an indication of deteriorated injection properties. However, the luminescence efficiency can become higher after exposure to impurity gases. Without contact to air the OLED do not degrade with appearance of so called "black spots".

To investigate the intrinsic stability of the OLEDs in ultra-high vacuum we performed a real time observation on the surface of a 35 nm thin magnesium cathode with Ultraviolet Photoelectron Spectroscopy (UPS). We found that even with a 35 nm thin magnesium-cathode, the underlying organic layer never appeared at the surface also after hours of operation in the ultra-pure conditions. The only sign of deterioration at the cathode is a slow oxidation of the magnesium surface. Thus, OLEDs with semitransparent cathodes are stable if the are operated under ultra-high vacuum conditions.

### INTRODUCTION

Organic Light-Emitting Diodes (OLEDs) have been optimized for use in several applications, and efficient devices with longtime stability have been demonstrated. However, this results should not conceal the fact that many physical mechanisms and parameters determining the performance of the OLEDs are not well known yet.

In non encapsulated OLEDs operated in air for some time, dark spots appear and become larger and larger with time. Atmospheric water seems to

---

\* The results of this section have been published in Proceedings of Int. Soc. Opt. Eng. (SPIE) Volume 4105: "Organic Light-Emitting Materials and Devices IV", page 299-306 in the year 2001.

be responsible for this effect [75,76,83,84]. In the present work, we investigate the behavior and degradation mechanisms of devices without any influence from gases or humidity.

For this investigations we used the cleanest available environment - an Ultra-High Vacuum (UHV) system. The gas pressure in an UHV system is below  $10^{-8}$  mbar. The common pressure in our system varies from  $2 \cdot 10^{-10}$  mbar to  $7 \cdot 10^{-9}$  mbar. In this pressure range several hours are needed to adsorb a monolayer of gases on the surface of the sample. There are several advantages for using such a pure environment for fabrication and characterization of OLEDs:

- One can measure the injection properties of very clean interfaces, allowing better comparison to theoretical models based on intrinsic material parameters.
- A comparison of the injection under clean conditions and after contamination with impurity gases can be done.
- Thin semi-transparent cathodes can be used.
- The appearance of “black spots” can be totally avoided [83, 84]. This allows an investigation of the degradation process in the absence “black spots”.
- Surface analysis tools can be used (UPS, XPS, AES).

In the following we will introduce our ultra-high vacuum system and will show two examples of the new characterization possibilities which are suggested in the above list.

The first example shows how the oxygen and air influences the injection properties and electroluminescence of an OLED. The second example uses the fact that the OLED never comes into contact with impurity gases and that very sensitive surface analysis tools (*e.g.* Ultraviolet Photoelectron Spectroscopy (UPS), which requires UHV conditions) can be used to study surface changes of the OLED. This can give important information about the stability of the cathode without influence of gases.

## EXPERIMENTAL

For fabrication of the OLEDs we use an UHV system constructed for Molecular Beam Epitaxy (MBE). Fig. 2.5 shows a schematic view of the system. It consists of a deposition chamber for organic materials (6 effusion cells), one metallization chamber (2 effusion cells, 2 electron beam evaporators), a

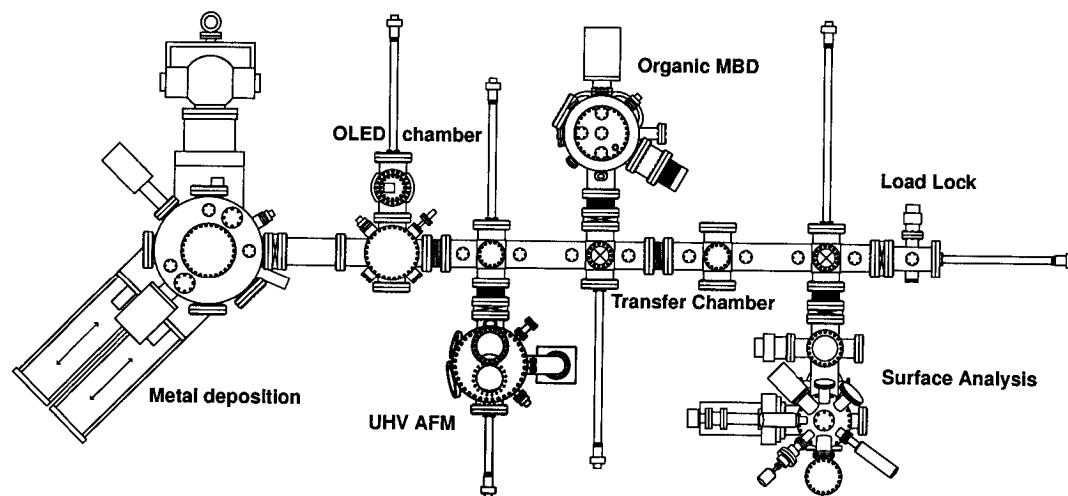


**Figure 2.5:** Schematic drawing of the Ultra-High Vacuum (UHV) system which we use for fabrication and characterization of OLEDs. The system consists of one organic Molecular Beam Deposition (MBD) chamber, a metal deposition chamber, a surface analysis chamber, an Atomic Force Microscope (AFM) chamber, and a special chamber for electrical characterization of OLEDs in ultra-high vacuum. All the chambers are connected by a transfer system. A load-lock chamber serves as a gateway to the atmospheric pressure.

surface analysis chamber (Ultraviolet Photoelectron Spectroscopy (UPS), X-ray Photoelectron Spectroscopy (XPS)) and a special chamber with electrical contacts to operate the OLED inside the UHV environment. Additionally, there is a chamber with a Atomic Force Microscope (AFM) and a load-lock chamber to bring the samples in and out of the UHV. All the chambers are connected by a transport system. The samples can be moved from chamber to chamber without breaking the vacuum.

The sample size in our UHV system can be up to 3inch in diameter, which is optimal for research with OLEDs. As substrate we used  $40 \times 40 \text{ mm}^2$  glass substrates with 30 nm Indium Tin Oxide (ITO). They were cleaned in an ultrasonic bath with acetone and ethanol and after that rinsed in water.

The current-voltage-brightness characteristics can be measured directly after fabrication of the OLED without breaking the ultra-high vacuum. This allows a characterization of OLED with very clean interfaces, which can be useful for comparison with theoretical models.

Fig. 2.7 gives a view inside the chamber for OLED characterization. The luminescence light is reflected by an aluminum mirror, exits the UHV system through a glass window, and is measured by a Minolta LS100 luminance meter. The losses caused by mirror and glass windows are estimated to be of the order of 15%. But all measurements shown here have been performed using the same system and they have therefore the same loss, which can therefore be neglected when comparing the results. The voltage and current

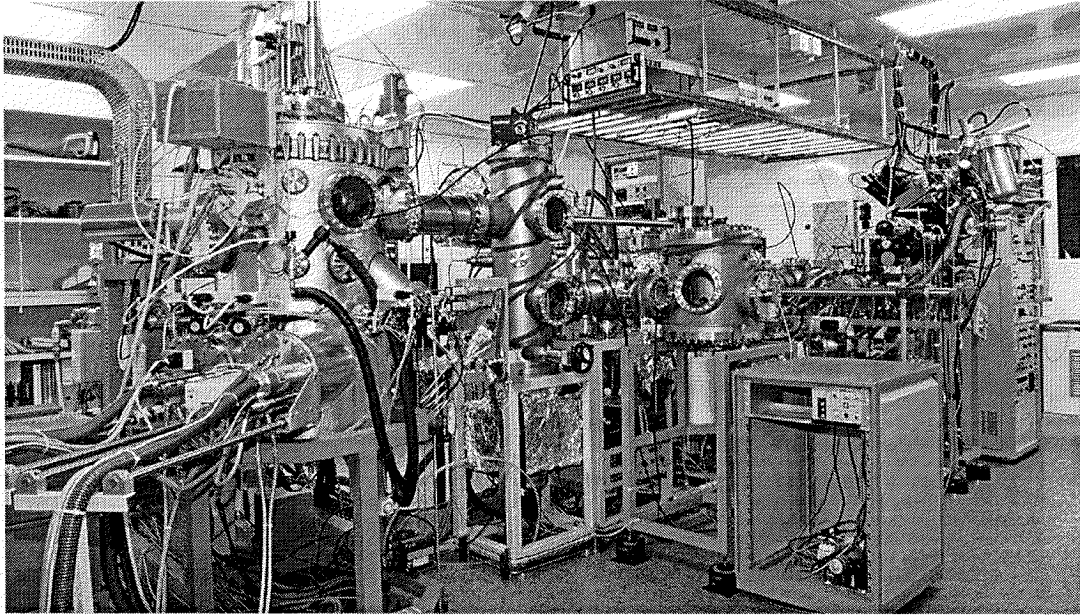


**Figure 2.6:** Picture of the UHV system which was used for fabrication and characterization of OLEDs under ultra-pure conditions. The machine stands in a clean room.

were measured by a computer controlled Fluke-45 multimeter.

## GAS DEPENDENT INJECTION PROPERTIES

### Introduction

By fabricating the devices in UHV we can produce well defined interfaces, which are known to strongly influence the device performance. As an example, in Ref. 31, page 410, it is shown that 0.3 nm silver on the interface to the organic layer determines alone the device performance, even with different metals on top of that layer. Especially for low work function metals, which are often used as cathode materials, it is very important to evaporate them under ultra-high vacuum conditions if precise interfaces are needed for, *e.g.*, comparison with theoretical models. The injection properties are then mainly influenced by the energy barrier in the interfaces. This barrier height is influenced by the work function of the metal and the ionization potential of the organic layers. The work function of a surface can be investigated by UPS or by the Kelvin method. The latter gives more an average of the bulk work function, while UPS is more surface sensitive.

The following example should explain the problem. Fig. 2.8 shows an UPS measurement on the surface of a magnesium layer directly after deposition. The photoelectron intensity is approximately proportional to the density of occupied electron states in the material. In a metal the electron states

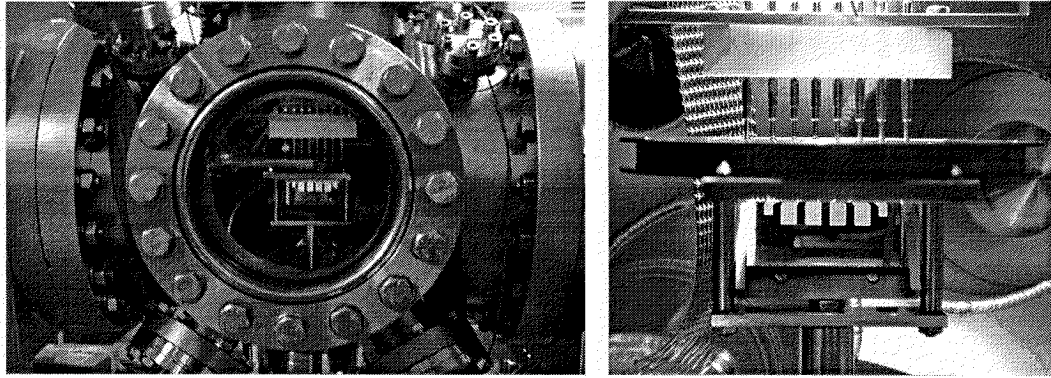


**Figure 2.7:** Picture of an operating OLED inside our UHV chamber. There are two small and four big devices. The big devices were used for the electrical characterization. The area of the larger devices is about  $18\text{mm}^2$ . The picture on the right side shows a close up view. One can see the cable, the contacts, the sample holder and the electroluminescence light of the OLED through a mirror. The sample itself is perpendicular to the contacts and is not visible in this view. The glass side of the device is at the bottom of the device and the light is reflected out of the UHV window by an aluminium mirror.

are filled up to the Fermi energy. The abrupt change from occupied to unoccupied can be identified by a edge in the UPS measurement, which can be clearly seen at the right of Fig. 2.8. This feature identifies a metal surface. The work function corresponding to the observed Fermi edge is about  $3.8\text{ eV}$ . After two days of storing under ultra-high vacuum conditions a second measurement was performed. Even in our ultrapure environment (pressure in the UPS chamber  $7 \cdot 10^{-10}\text{ mbar}$ ) the magnesium was oxidized on the surface. No Fermi edge is observed anymore and one can see the valence band of magnesium oxide at  $-4.4\text{ eV}$  in binding energy. The inset shows the results of the UPS measurement in a simple band structure diagram. Of course the oxidation is only at the surface (the escape depth of the electrons in UPS is less than  $1\text{ nm}$ ), But Y. Mori [31] showed that an interface layer as thin as  $0.3\text{ nm}$  can already determine the performance of an OLED if it is placed at the interface between organic material and electrode.

If magnesium is deposited in non ultra-high vacuum system it is not possible to obtain a pure magnesium interface. Therefore the simple band model using work functions measured in the literature (under UHV conditions) cannot be used anymore to analyze the performance of the device. Oxidation introduces another, more complicated interface structure.

This does not mean that a pure interface is better for device performance. However, a controllable interface is certainly a prerequisite for research on the intrinsic properties that determine charge injection in an OLED.

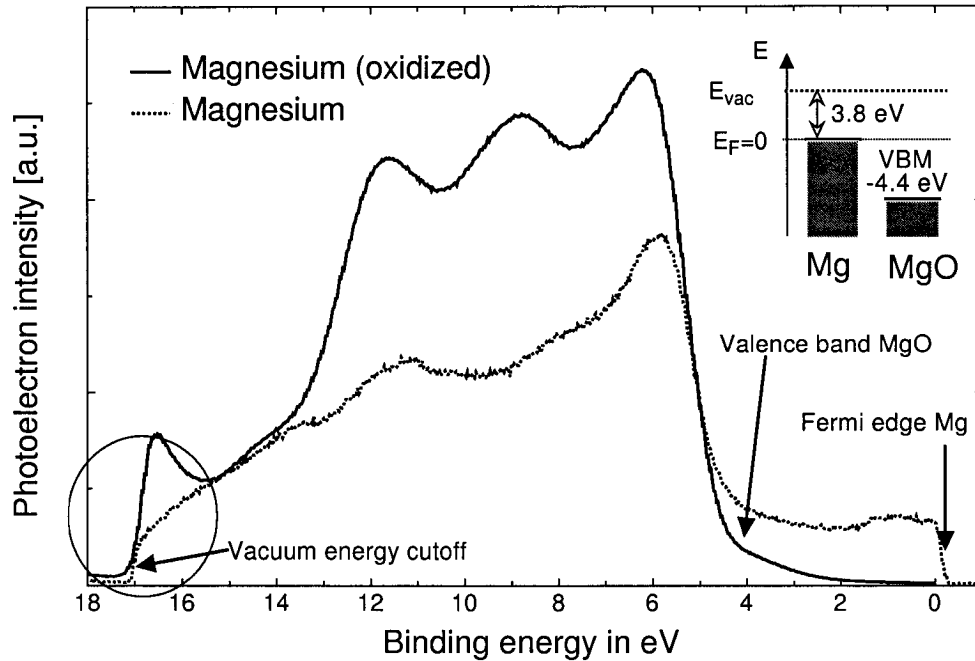


**Figure 2.8:** UPS measurement of a magnesium layer directly after deposition and two days storing in UHV. The surface is changing from a metal (magnesium) with a Fermi edge to an insulator (magnesium oxide) with a valence band edge of  $-4.4$  eV binding energy. For clarity, the photoelectron intensity of the curves was normalized.

## Results and discussion

The first electroluminescence data of an OLED fabricated **and** operated inside an UHV system [83] demonstrated that the OLEDs operating in air shows a higher brightness at the same current-density, but black spots become visible, while in UHV no black spots appear and the luminescence efficiency was lower.

To prove which gas is responsible for the enhancement in the efficiency we made new measurements with OLEDs in UHV, and after contamination with air and pure oxygen. To exclude variations caused by different measurement conditions, we measured all the OLEDs inside the UHV chamber, exposed them for 17 hours to air or oxygen, and measured again the changes inside the UHV chamber. To be sure that our measurement is not influencing the results, we measured at low currents and repeated the measurement three times, confirming that the properties of the device were not modified by the measurement at the low currents we used.

We fabricated two devices consisting of a 30 nm ITO anode, 40 nm NPB (N,N'-bis-{1-naphthyl}-N,N'-diphenyl-1,1'-biphenyl-4,4'-diamine), 65 nm Alq<sub>3</sub> (tris {8-hydroxyquinoline aluminium}), and a 200 nm magnesium

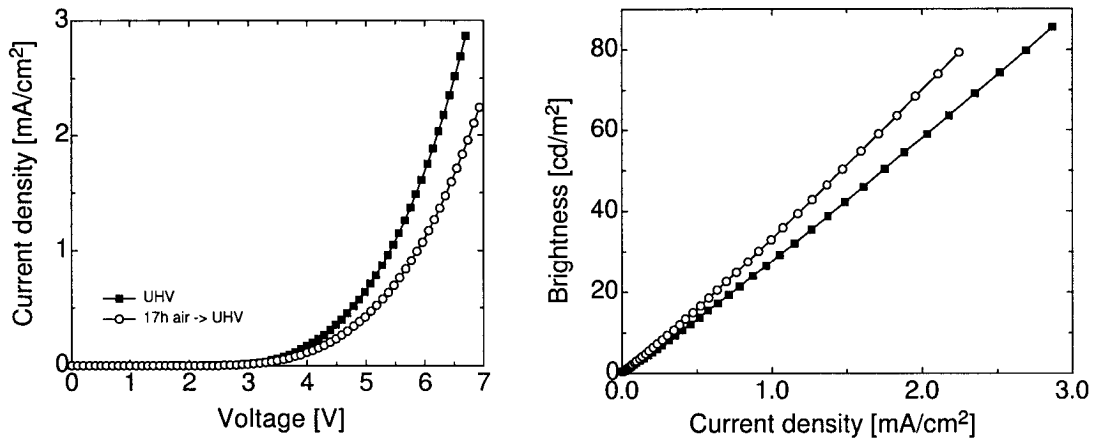


**Figure 2.9:** **Left:** Current-density vs. voltage characteristic of an OLED which was first characterized directly after production in UHV (filled squares) and successively came in contact with air for 17 hours (open circles). **Right:** Brightness vs. current-density characteristic of the devices described in the left part.

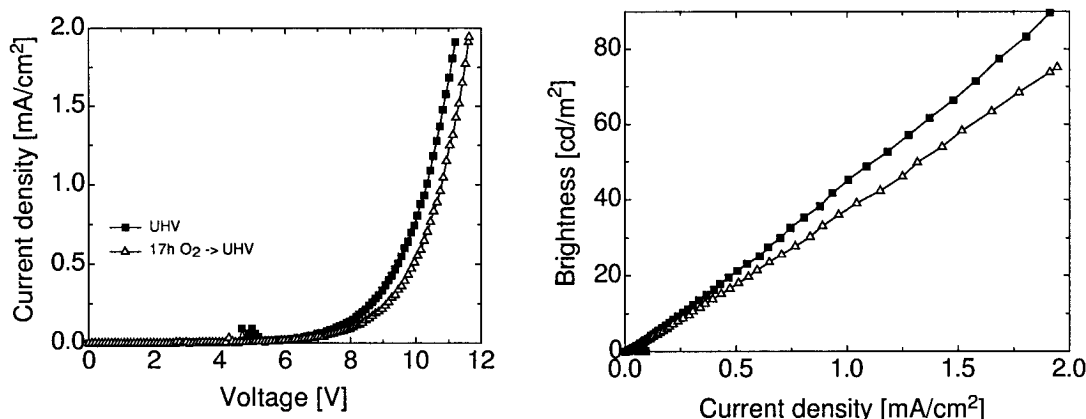
cathode. Both devices were characterized after fabrication inside the ultra-high vacuum to get the “intrinsic” characteristic. By comparing the curves marked “UHV” (filled squares) in Fig. 2.9 and 2.10 one can see easily that there are different threshold voltages and different proportionalities between the brightness and the current density (*i.e.* the efficiency). These differences are probably due to our ITO anodes, which without special treatments are not very reproducible, but do not influence our measurements. Here we are interested in changes caused by impurity gases and the results are the same for all the devices, even if their characteristics was different at the beginning.

Fig. 2.9 shows the current-density vs. voltage and brightness vs. current-density characteristic of a device before and after contamination for 17 hours in air. In the current-density vs. voltage characteristic one can see that the turn-on voltage increases, and in the brightness vs. current-density characteristic an enhancement of the efficiency caused by exposure to the air is visible. The exposure to air also initiated the appearance of black spots.

If we do the same experiment using pure oxygen, we get a different result. Fig. 2.10 shows the current-density vs. voltage and brightness vs. current-density characteristic of the device before and after 17 hours exposure to oxygen. The turn-on voltage also increases, but the efficiency does not. Moreover, exposure to pure oxygen did not induce the appearance of any black spot.

There is thus an enhancement of efficiency if the OLED comes for long time in contact with air, and a decrease in efficiency if the device comes for a long time in contact with oxygen. In both cases the turn-on voltage increases





**Figure 2.10:** **Left:** Current-density vs. voltage characteristic of an OLED which was first characterized directly after production in UHV (filled squares) and successively came into contact with pure oxygen for 17 hours (open triangles). **Right:** Brightness vs. current-density characteristic of the devices described in the left part.

after contamination. The enhancement is accompanied by the appearance of black spots when the device is exposed to air.

During this kind of measurements the contact resistance can increase (due to oxidation of the cathode). But this effect does not influence the brightness vs. current-density characteristic because the current is not affected by the contact resistance, and a voltage-drop on the contact resistance can only effect the current-density vs. voltage characteristic by changing the effective voltage applied to the device.

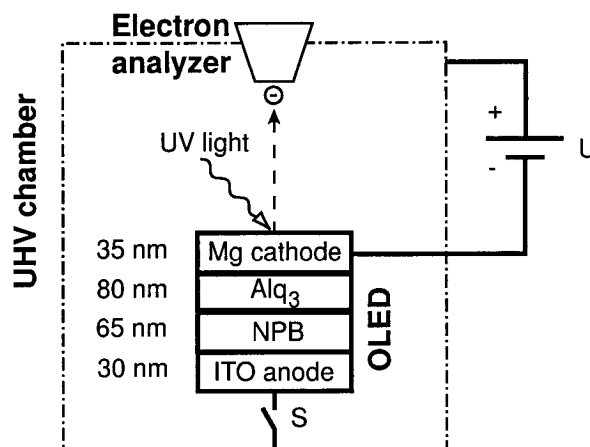
From these facts we conclude that both the black spots and the enhancement of efficiency are related to gaseous water in air, while the increase in threshold voltage is related to oxygen, and is probably caused by an oxidation which can reach the Alq<sub>3</sub>/ magnesium interface.

## UPS OBSERVATION AT THE SURFACE OF AN OPERATING OLED

When studying the degradation of OLEDs it is very important to know if it is due to external influences (gases) or if there are also internal destruction mechanisms. It is a known fact that the cathode is not stable in air [75, 76]. In order to investigate the intrinsic stability of the cathode and the cathode / organic interface in the absence of any uncontrollable impurity gases, we produced a very thin cathode and observed the surface of the operating OLED with Ultraviolet Photoelectron Spectroscopy (UPS).

As before, the devices were fabricated in an UHV deposition chamber

**Figure 2.11:** Schematic drawing of the arrangement inside the UHV chamber. If the switch S is open the arrangement corresponds to a normal UPS measurement with bias voltage. To run the OLED the switch S is closed, but this does not have any influence on the UPS measurement, which can then be used to directly study the cathode degradation.



(base pressure  $3 \cdot 10^{-10}$  mbar) using masks for the device structure. After fabrication the sample was moved without breaking the UHV to a special surface analysis chamber equipped with a He discharge lamp, and a hemispherical electron analyzer (base pressure  $5 \cdot 10^{-10}$  mbar).

A schematic drawing of the experimental set-up and of the electrical connections used to operate the OLED inside the surface analysis chamber is shown in Fig. 2.11. An electrical connection for applying a bias voltage to the sample during UPS measurements was used to contact the cathode of the device. The OLED anode can be contacted with the walls of the vacuum chamber, which are grounded. Using these two contacts we can apply a voltage to the OLED, and inject a current to induce the electroluminescence, while at the same time measuring the UPS Energy Distribution Curve (EDC). By moving the sample holder slightly, one can remove the electrical connection of the device anode to the ground, which allows an UPS measurement on the cathode of the inactive device, without electroluminescence.

For the UPS measurement we used the Helium I line (photon energy 21.2 eV) to measure the photoelectron spectrum of the magnesium cathode on top of the device. We confirmed that Ultraviolet Photoelectron Spectroscopy (UPS) does not induce any change in the brightness of the electroluminescence. This means that the 21.2 eV photons we use do not lead to rapid photodegradation of the organic layers in our OLEDs. The diameter of the UV spot on the cathode was about 2 mm, while the device size was  $4 \times 4$  mm. Since the electroluminescence was visible through our thin magnesium cathode, we could check the position of the beam while the OLED was running, confirming that the electroluminescence was always visible under the UV beam spot. The small surface area illuminated by the UV light in the middle of the cathode guarantees that all collected photoelectrons come from the cathode of the device. The electron analyzer position is perpendicular to the sample surface.

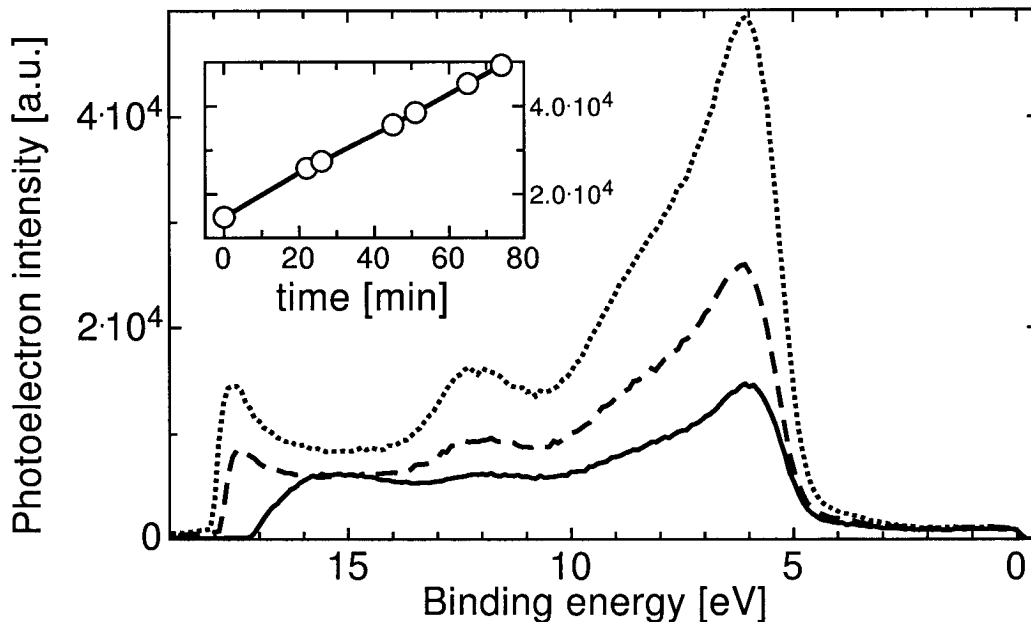


**Figure 2.12:** UPS measurement on the cathode surface of a device before it was operated for the first time (0 min, solid), after 22 min of operation at a bias voltage of 8 V (dashed), and after 74 min of operation at 8 V bias voltage (dotted). The inset shows the photoelectron intensity at the binding energy 6.1 eV versus time.

In the case where the anode has no contact to the chamber the arrangement does not differ from a standard UPS measurement: the surface of the cathode (the material to be analyzed by UPS) is negatively charged, relative to the electron analyzer, by the applied bias voltage. This is the usual technique used to overcome the analyzer work function. For the UPS measurement alone, no change is expected if the anode of the OLED is grounded, because the charge on the cathode is the same. The only difference is that, with the electrical connection between anode and ground in place, a current flows inside the OLED, inducing the electroluminescence.

Fig. 2.12 shows a UPS measurement on the cathode surface of an OLED before it was operated for the first time (solid curve). After application of a 8 Volts bias voltage to the device, bright green light was visible on the whole cathode area. After 22 minutes we measured again the UPS signal, and this time obtained the dashed line in Fig. 2.12. The current which was flowing through the  $18 \text{ mm}^2$  area of the device at this time was 3.9 mA. We made several measurements later. The curve after 74 min is shown as a dotted curve in Fig. 2.12. The intensity of the UPS signal is increasing with time. The inset in Fig. 2.12 shows the photoelectron intensity of the peak at 6.1 eV binding energy versus time. The line connecting the points corresponds to a linear relation.

We interpret the increase in the intensity of the UPS spectrum as the effect of the slow oxidation [85] of the magnesium layer that takes place even in UHV because of the very reactive magnesium. UPS is so sensitive that even a part of a monolayer of oxidized magnesium at the surface already affects the photoelectron spectrum.

After half a day the Fermi edge is not anymore visible in the UPS spectra and the cathode surface turns completely into magnesium oxide (an insulator).

However, no sharp peak in the UPS spectrum, which could be related to organic molecules at the surface of the cathode, was observed. If Alq<sub>3</sub> molecules could reach the surface of the magnesium layer the signal would be drastically changed. But we did not find any new peak even after a longer time.

This means the magnesium cathode of an OLED is not destroyed by an intrinsic mechanism like, *e.g.*, diffusion of magnesium into Alq<sub>3</sub>. The thin cathodes we used would be very sensitive to any changes which occur from the interface and grow towards the surface. From these experiments we can conclude that any interfacial changes taking place at the Mg/Alq<sub>3</sub> interface will be very localized, with a maximum extension lower than 35 nm, the thickness of the cathodes we used.

## CONCLUSIONS

By producing ultra-pure OLEDs and also characterizing them in an UHV system, we can investigate the influence of impurity gases on the device performance.

We found that air can enhance the efficiency of the OLEDs compared to the efficiency in UHV, but that this effect is accompanied by appearance of black spots. Exposure to pure oxygen can only decrease the efficiency but black spots does not appear. By comparison of the results in air and pure oxygen we can say that water is the cause of the enhancement of efficiency and of the appearance of black spots.

We could perform a real time UPS observation of an operating OLED cathode surface, and we found that no intrinsic degradation mechanisms can affect the surface even of a 35 nm thin magnesium cathode. If there were an effect of the OLED operation on the Mg/Alq<sub>3</sub> interface, this interfacial changes would be limited to a thickness of less than 35 nm from the interface.

## **ACKNOWLEDGEMENTS**

This work was supported by the Swiss Federal Institute of Technology (ETH) Zürich. I want to thank my colleagues A. Tapponnier and Dr. R. Ono for discussions.

## 2.4 Impurity-gas-dependent charge injection properties at the electrode-organic interface in organic light-emitting diodes\*

### Abstract

We determine how impurity gases, such as oxygen and water, influence the performance, stability, and electronic properties of organic light-emitting diodes (OLEDs). We fabricate and operate the devices in a controlled ultrahigh-vacuum (UHV; pressure below  $10^{-9}$  mbar) environment. The UHV system allows complete control of the exposure to impurity gases, and the measurement of current-voltage characteristics, electroluminescence, and impedance spectroscopy before and after exposure to oxygen or air. These measurements showed that both pure oxygen and air increase the threshold voltage for light emission. Exposure to air leads to a higher efficiency and to a degradation of the devices with the appearance of black spots. This is not the case for oxygen. Additional impedance spectroscopy measurements also confirm that exposure to air has a large influence on the stability of the electrode interfaces, with the appearance of an additional capacitance in the equivalent circuit for a device with an Mg cathode exposed to air, a fact that could be connected to the effect of atmospheric gases such as oxygen and water on the Alq<sub>3</sub>/Mg system.

### INTRODUCTION

Organic materials are interesting candidates for novel electronic devices, because they can have good physical and chemical stability, can be compatible with large field applications, and can in principle lead to low-cost devices. Organic light emitting diodes (OLEDs) are one of the most promising applications, with some products already starting to appear on the market, and the promise of delivering full colour, large-area, flat panel displays with further development of the technology. Although OLEDs have been optimized for use in several applications, and efficient devices with long-term stability have been demonstrated, many physical mechanisms and parameters determining the performance of the OLEDs are not well known yet.

In the present study, we investigate the behaviour and degradation mechanisms of devices in the absence of any impurity gases, or under the controlled influence of pure oxygen or air. To do this, we use the cleanest available envi-

---

\* The results of this section have been published in *Materials Science and Engineering B85*, page 144-148 in the year 2001.

ronment an ultrahigh vacuum (UHV) system with an impurity gas pressure ranging from  $2 \times 10^{-10}$  to  $7 \times 10^{-9}$  mbar. For the purpose of fundamental characterization of intrinsic device properties, the best attempts at encapsulation cannot beat what can be done with both fabricating and operating a device in such a UHV system [83].

The first electroluminescence data of an OLED fabricated and operated inside a UHV system demonstrated that OLEDs operating in air have a higher brightness at the same current density, but that black spots become visible, whereas in UHV no black spots appear and the luminescence efficiency is lower [83].

To prove which gas is responsible for the enhancement in the efficiency we made new measurements with OLEDs in UHV, and after contamination with air and pure oxygen.

## EXPERIMENTAL

To characterize the devices, we measured the voltage-current and brightness-current characteristics of the devices, as well as the complex impedance versus frequency, in a special UHV chamber provided with the necessary electrical contacts and optical windows. Measurements were performed on ultraclean devices fabricated in the same UHV system and moved to the characterization chamber without breaking the vacuum, and on devices that had been exposed for a controlled amount of time to selected impurity gases. Additionally, we also show what is obtained when the same measurements are performed in air.

To exclude variations caused by different measurement conditions, we measured all the OLEDs inside the UHV chamber, exposed them for 17 h to air or oxygen, and again measured the changes inside the UHV chamber. To be sure that our measurement was not influencing the results, we measured at low currents and repeated the measurement three times, confirming that the properties of the device were not modified by the measurement.

We fabricated two devices consisting of a 30 nm ITO anode, 40 nm NPB, 65 nm Alq<sub>3</sub>, and a 200 nm magnesium cathode. Both devices were characterized after fabrication inside the UHV to obtain the intrinsic characteristics.

## RESULTS

Fig. 2.13 shows the current-density versus voltage and brightness versus current-density characteristics of a device before and after contamination for 17 h in air. One can observe an increase of the threshold voltage, and an enhancement of the efficiency after the device has been exposed to air. The

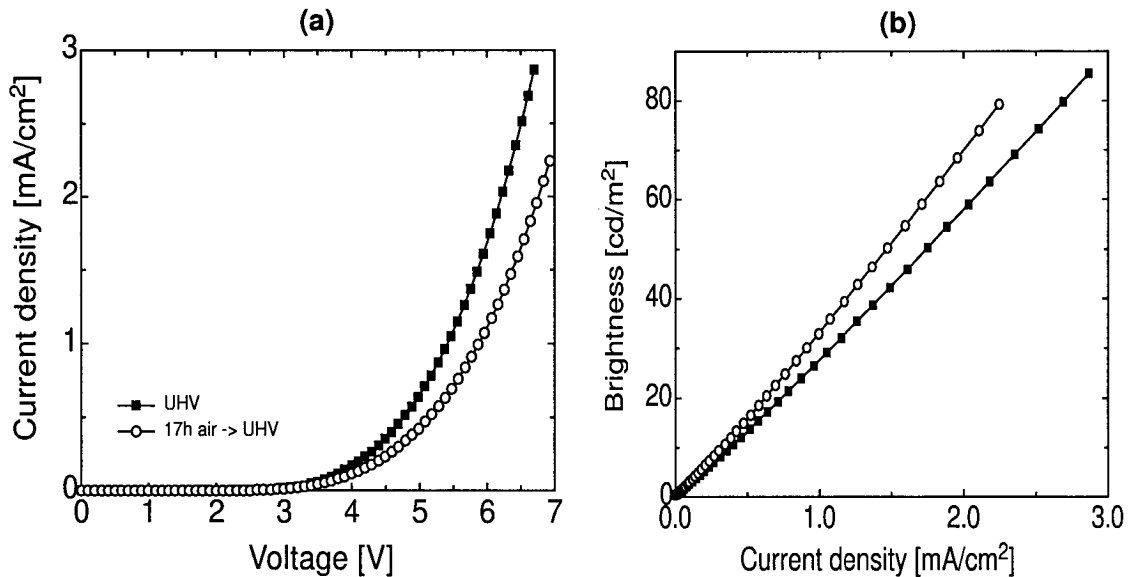


**Figure 2.13:** (a) Current-density versus voltage characteristic and (b) brightness versus current-density characteristic of a double-layer OLED fabricated in UHV and before (black squares) and after (open circles) a 17 h exposure to air.

exposure to air also initiated the appearance of black spots. Fig. 2.14 shows the data for a device before and after 17 h exposure to oxygen. The threshold voltage also increases, but the efficiency does not. Moreover, exposure to pure oxygen did not induce the appearance of black spots.

By comparing the curves marked UHV (filled squares) in Fig. 2.13 and Fig. 2.14, one can see easily that there are different threshold voltages and different proportionalities between the brightness and the current density (i.e. the efficiency). These differences are probably due to our ITO anodes, which without special treatments are not very reproducible; however, this does not influence our measurements. Here we are interested in changes caused by impurity gases, and the results are the same for all the devices, even if their characteristics were different at the beginning. Note also that in these kinds of measurement the contact resistance can increase (due to oxidation of the cathode). However, this effect does not influence the brightness versus current-density characteristic because the current is not affected by the contact resistance, and a voltage drop on the contact resistance can only affect the current-density versus voltage characteristic by changing the effective voltage applied to the device.

From the above facts we conclude that both the black spots and the enhancement of efficiency are related to gaseous water in air, whereas the increase in threshold voltage is related to oxygen, and is probably caused by an oxidation that can reach the Alq<sub>3</sub> magnesium interface.



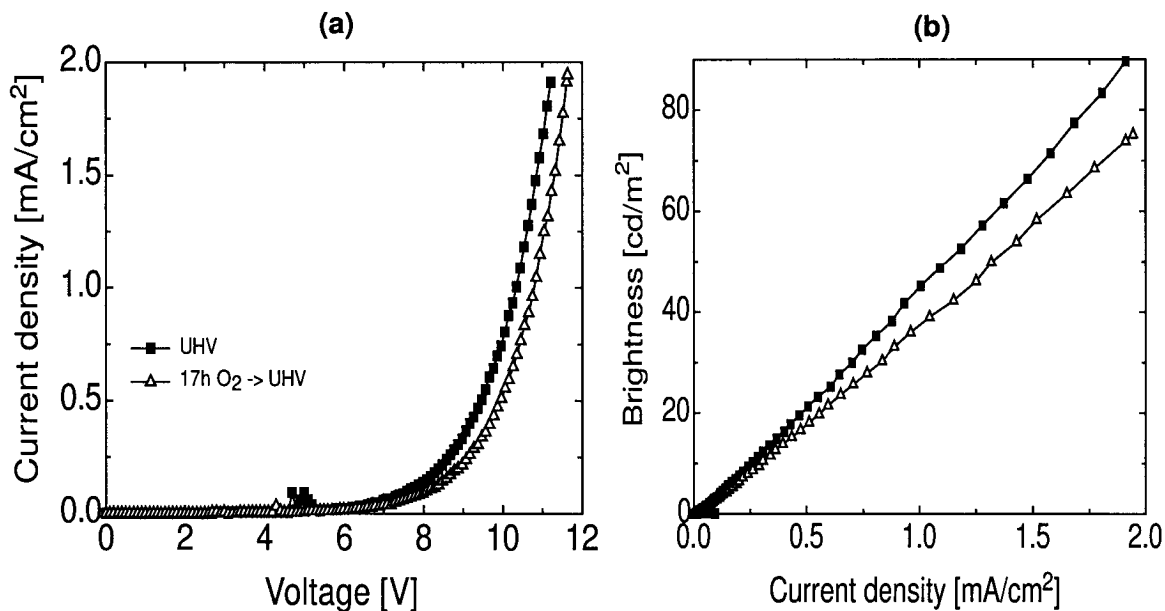


**Figure 2.14:** (a) Current-density versus voltage characteristic and (b) brightness versus current-density characteristic of a double-layer OLED fabricated in UHV and before (black squares) and after (open triangles) a 17 h exposure to pure oxygen.

To investigate the cathode-organic interface further and reduce the number of parameters involved in the description of an OLED, we fabricated single-layer ITO/Alq<sub>3</sub>/Mg devices, and characterized them by impedance spectroscopy. We used a programmable impedance analyser (Hewlett-Packard, HP 4129A) and applied an AC voltage with a root-mean-square amplitude of 0.1 V in the frequency range between 10 Hz and 10 MHz.

Fig. 2.15 shows the impedance spectroscopy data of an ultrapure device measured in UHV. The dots represent the experimental data, and the lines are a fit with the equivalent circuit shown in the inset of Fig. 2.15(a). As expected, the real part of the impedance at low frequency decreases for increasing bias voltages. However, at low bias voltage a peculiar frequency dependence of the real part of the impedance is observed. Oscillations in the impedance data are generally observed at low frequencies and voltage ( $f < 1$  kHz,  $U < 8$  V), and at high frequencies ( $f > 100$  kHz), and are typical for a device fabricated and measured in UHV. Note that 8 V corresponds roughly to the threshold voltage for LED operation. Fig. 2.15(b) displays the Cole–Cole plots (real part of the impedance versus imaginary part) of the same device, in a double logarithmic plot. The minimum  $\text{Re}(Z)$  value observed at high frequencies corresponds to a resistance  $R_s$  in series with the OLED (probably mostly due to the bulk resistance of the ITO anode). In this device,  $R_s$  is about 310  $\Omega$ . The maximum  $\text{Re}(Z)$  value at low frequencies

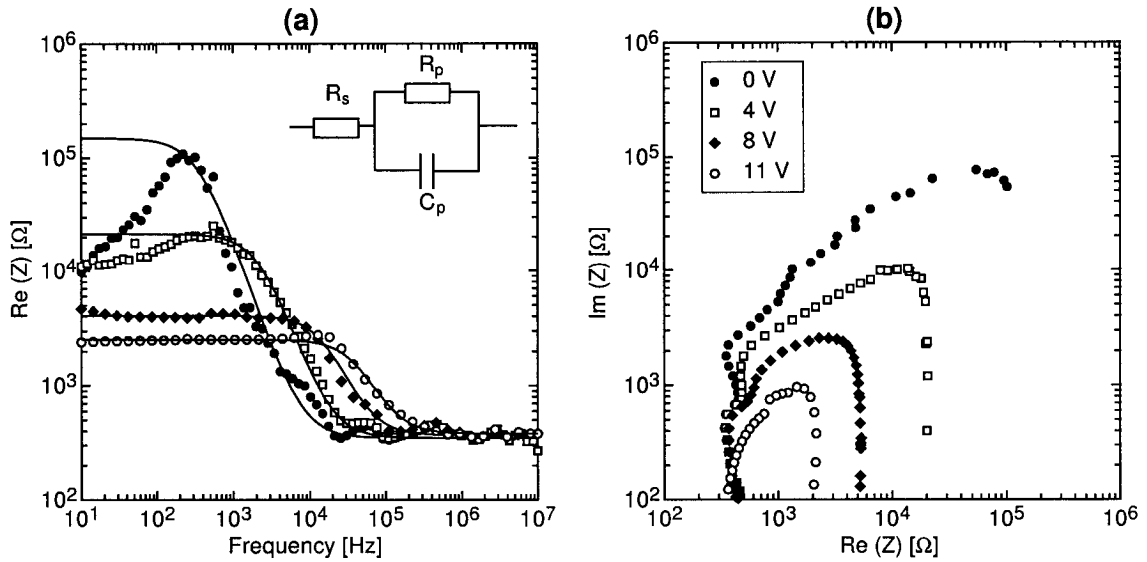


**Figure 2.15:** (a) Real part  $\text{Re}(Z)$  and (b) Cole–Cole plot of the complex impedance  $Z$  of a single-layer OLED at different bias voltages in UHV. The dots represent the measurement results; the solid curves were obtained by a least-squares fit using the equivalent circuit shown in the inset.

corresponds to the sum of  $R_s$  and the OLED resistance  $R_p$ , which is strongly bias dependent. The Cole–Cole plot basically displays only one semicircle for this UHV measurement, corresponding to the single capacitance/resistance equivalent circuit in the inset of Fig. 2.15(a).

Fig. 2.16 shows the impedance spectroscopy data for the same ITO/Alq<sub>3</sub>/Mg device after it had been removed from the UHV system. The data were gathered in air. Some characteristic differences with the results in UHV can be noticed immediately. The oscillations in the complex impedance observed in UHV disappear. In particular, the unexpected frequency dependence of  $\text{Re}(Z)$  observed at low voltages and frequencies in UHV is removed, and is replaced by a frequency dependence that can be associated with a second circuit in series, as displayed in the inset of Fig. 2.16(a). The same observation can be made from the Cole–Cole plot, where a second semicircle is observed at bias voltages below 8 V.

It is interesting to note that the peculiar frequency dependence of the real part of the impedance observed at low voltages in UHV is replaced, in the same voltage range, by a frequency dependence that can be simply modelled by a second circuit in series in the presence of air. As the bias voltage increases above 8 V the threshold voltage for LED operation is passed, and both the simple current-voltage characteristics and the impedance spectroscopy data in Fig. 2.15 and Fig. 2.16 approach those typical of an ideal diode; the current and brightness increase drastically with increasing bias,

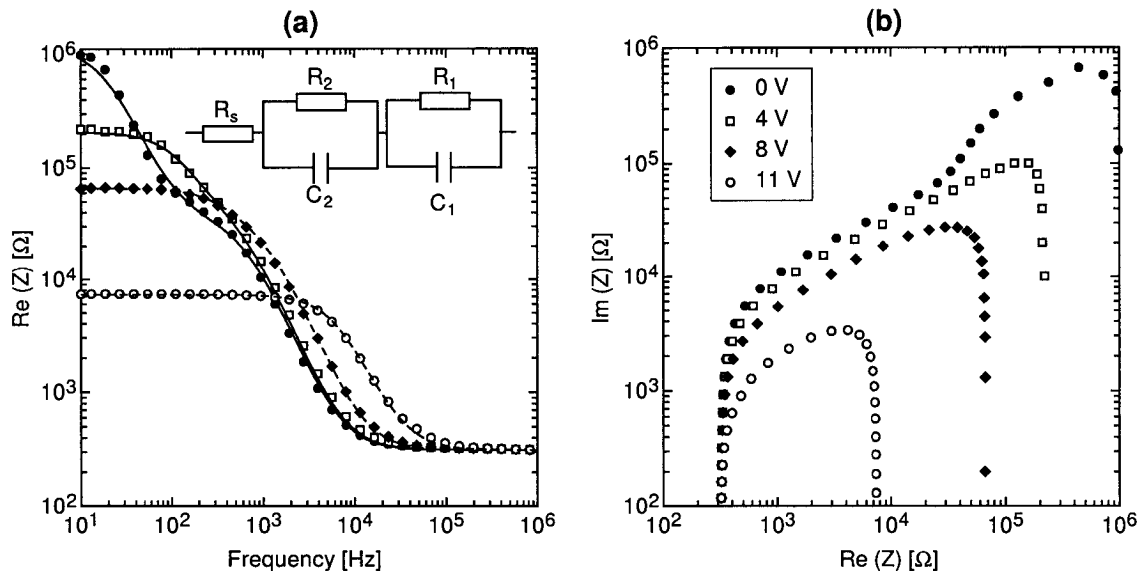


**Figure 2.16:** (a) Real part  $\text{Re}(Z)$  and (b) Cole–Cole plot of the complex impedance  $Z$  of a single-layer OLED at different bias voltages in air. The dots represent the measurement results; the solid curves were obtained by a least-squares fit using the equivalent circuit shown in the inset. At high bias, the single circuit of Fig. 2.16 fits the data very well (broken curves).

and the impedance spectroscopy data can be modelled by a simple equivalent circuit with a capacitor and a resistance in parallel.

The exact origin of the peculiar impedance spectroscopy data obtained in UHV is not clear yet. However, current instabilities are also typically observed below the threshold voltage when measuring current–voltage characteristics in UHV. It could be that this behaviour is caused by a poor, inhomogeneous, and unstable contact between the organic layer and the electrodes, and that these contacting problems are enhanced in UHV. The fact that these instabilities disappear in the presence of air means that atmospheric gases play a role in stabilizing the electrical contacts with the organic layer. If we assume that in UHV the interface between electrode and organic layer is inhomogeneous, then at some spatial points the contact will be better than at other points, causing for example electric field spikes, which would be the main points of injection at low voltage, leading to a localization and a spatial inhomogeneity of the current. When the threshold voltage for LED operation is reached, the current injection at the electrodes increases and becomes more homogeneous. At bias voltages below the threshold voltage, the interface plays a more important role in the carrier accumulation and localized carrier injection, whereas at higher voltages the importance of these effects decreases.

The above results confirm that the presence of atmospheric gases has a

strong influence on the interface and charge-injection properties in an OLED. Atmospheric gases such as oxygen and water may diffuse through the OLED layers and affect the electrode interfaces, with the end effect of stabilizing and making more homogeneous the contacts at the electrodes and the carrier injection.

When the measurement is performed in air, the results of impedance spectroscopy below 8 V are consistent with a model circuit containing two circuits in series, each with a resistance and a capacitance in parallel, plus a single resistance in series, as displayed in the inset of Fig. 2.16(a). It is important to note that the second circuit is only observed when (1) an Mg electrode in contact with Alq<sub>3</sub> is used and (2) the device is exposed to air. If a thin layer of Ag (5 nm) is inserted between the Mg electrode and Alq<sub>3</sub> layer, no second circuit is observed [86]. Thus the second circuit observed in Fig. 2.16 can be related to an additional interfacial capacitance connected with the reaction of Mg and Alq<sub>3</sub> in the presence of air [86]. It may be that Mg is able to diffuse inside the Alq<sub>3</sub> layer [72, 73], thus increasing its effect on the electrical properties of the device. Although further investigations are needed to understand better the points made above, we can already conclude that air has a decisive influence on the Mg/ Alq<sub>3</sub> interface, an influence that is also clearly seen when measuring current-voltage and brightness-current characteristics.

## CONCLUSION

We found that controlled exposure to impurity gases from UHV to atmospheric conditions is an important tool for the characterization and differentiation of the intrinsic and extrinsic properties of OLED structures.

We found that air can enhance the efficiency of the OLEDs compared with the efficiency in UHV, but that this effect is accompanied by the appearance of black spots. Exposure to pure oxygen only decreases the efficiency, and the black spots do not appear. By comparison with the results in air and pure oxygen we can say that water is the cause of the enhancement of efficiency and of the appearance of black spots.

Impedance spectroscopy has demonstrated the strong effect that atmospheric gases have on the electrode-organic interfaces and on charge carrier injection. An additional contribution to the device impedance could be related to the effect of atmospheric gases on the Mg/Alq<sub>3</sub> system.

Seite Leer /  
Blank leaf

## 2.5 Photoelectron spectroscopy on a running organic light-emitting Diode\*

### Abstract

The Mg cathode surface of a simple ITO / NPB / Alq<sub>3</sub> / Mg Organic Light Emitting Device (OLED) was observed by Ultraviolet Photoelectron Spectroscopy (UPS) during operation of the device in ultra-high-vacuum (UHV). We found that even with a 35 nm thin Mg-cathode, the underlying organic layer never appeared at the surface also after hours of operation in the ultra-pure conditions typical of UHV. The only signs of deterioration at the cathode are a slow oxidation of the Mg-surface. We could show that OLEDs with semitransparent cathodes are stable if they are operated under ultra-high-vacuum conditions.

### INTRODUCTION

The stability of the metal-organic interface at the cathode of an Organic Light Emitting Device (OLED) is an important parameter that can impose a limit on the lifetime of the device. In order to allow an optimization of the devices towards such applications as wide area displays, it is important to better characterize and understand the intrinsic degradation mechanisms that can take place at the cathode interface even in encapsulated devices. In this work we examined the cathode surface of a running, "encapsulated" OLED, by operating it in Ultra-High-Vacuum (UHV) and using Ultraviolet Photoelectron Spectroscopy (UPS). UPS is a very sensitive tool to detect surface changes. Since the device was fabricated and operated in UHV, we can exclude the effects of impurities, and the isolation of the device from the environment is better than any encapsulation technique.

Any intrinsic deterioration mechanism that affects the Mg-cathode would be visible as a change of the electronic states at the surface of thin Mg cathodes. As an example, one might expect that the Mg further diffuses inside the organic material underneath during operation of the device, and that after a while the electronic states belonging to the organic material start being detected at the surface by UPS.

In order to be able to use a thin Mg cathode, and in order to be able to perform this kind of surface-sensitive measurements, a Ultra-High-Vacuum (UHV) is required.

---

\* The results of this section have been published in *Nonlinear Optics*, Vol. 25, page 461-466 in the year 2001.

## EXPERIMENTAL

We produced very simple bilayer device structures on a glass substrate coated with an Indium Tin Oxide (ITO) anode ( $\sim 30$  nm thick), the hole transport layer NPB (N,N'-bis-(1-naphthyl)-N,N'-diphenyl-1,1'-biphenyl-4,4'-diamine,  $\sim 65$  nm thick) and Alq<sub>3</sub> (tris (8-hydroxyquinoline aluminium),  $\sim 80$  nm thick) as an electroluminescent layer, and with Mg ( $\sim 35$  nm) as cathode material. The thicknesses were measured using a calibrated quartz microbalance. Exact thickness measurements of the organic and Mg layer by Rutherford Backscattering Spectroscopy (RBS) were used to calibrate the quartz microbalance (RBS measurements on organic layers are discussed, *e.g.*, in Ref. [87]).

The devices were fabricated in an UHV deposition chamber (base pressure  $3 \cdot 10^{-10}$  mbar) using masks for the device structure. After fabrication the sample was moved without breaking the UHV to a special surface analysis chamber equipped with a He discharge lamp, and a hemispherical electron analyzer (base pressure  $5 \cdot 10^{-10}$  mbar).

An existing electrical connection for applying a bias voltage to the sample during UPS measurements was used to contact the cathode of the device. The OLED anode can be contacted with the walls of the vacuum chamber, which are grounded. Using these two contacts we can apply a voltage to the OLED, and inject a current to induce the electroluminescence, while at the same time measuring the UPS energy distribution curve (EDC). By moving the sample holder slightly, one can remove the electrical connection of the device anode to the ground, which allows an UPS measurement of the cathode of the inactive device, without electroluminescence.

## ULTRAVIOLET PHOTOELECTRON SPECTROSCOPY

For the UPS measurement we used the He I line (photon energy 21.2 eV) to measure the photoelectron spectrum of the Mg cathode on top of the device. We confirmed that Ultraviolet Photoelectron Spectroscopy (UPS) does not induce any change in the brightness of the electroluminescence. This means that the 21.2 eV photons we use do not lead to rapid photodegradation of the organic layers in our OLEDs. The diameter of the UV spot on the cathode was about 2 mm, while the device size was  $4 \times 4$  mm. Since the electroluminescence was visible through our thin Mg cathode, we could check the position of the beam while the OLED was running, confirming that the electroluminescence was always visible under the UV beam spot. The small surface area illuminated by the UV light in the middle of the cathode guarantees that all collected photoelectrons come from the cathode of the device.

The electron analyzer position is perpendicular to the sample surface.

In the case where the anode has no contact to the chamber the arrangement does not differ from a standard UPS measurement: the surface of the cathode (the material to be analyzed by UPS) is negatively charged, relative to the electron analyzer, by the applied bias voltage. This is the usual technique used to avoid slow electrons which otherwise can not be well detected. For the UPS measurement alone, no change is expected if the anode of the OLED is grounded, because the charge on the cathode is the same. The only difference is that, with the electrical connection between anode and ground in place, a current flows inside the OLED, inducing the electroluminescence.

## RESULTS AND DISCUSSION

Figure 2.17 shows a UPS measurement on the cathode surface of an OLED before it was operated for the first time (solid curve). After application of a 8 Volts bias voltage to the device, bright green light was visible on the whole cathode area. After 22 minutes we measured again the UPS signal, and this time obtained the dashed line in Figure 2.17. The current which was flowing through the  $18 \text{ mm}^2$  area of the device at this time was 3.9 mA. We made several measurements later. The curve after 74 min is shown as a dotted curve in Figure 2.17. The intensity of the UPS signal is increasing with time. The inset in Figure 2.17 shows the photoelectron intensity of the peak at 6.1 eV binding energy versus time. The line connecting the points corresponds to a linear relation.

We interpret the increase in the intensity of the UPS spectrum as the effect of the slow oxidation of the Mg layer that takes place even in UHV because of the very reactive Mg. UPS is so sensitive that even a part of a monolayer of oxidized Mg at the surface already affects the photoelectron spectrum.

After a half day the Fermi edge is not anymore visible in the UPS spectra and the cathode surface turns completely into MgO (an insulator).

No sharp peak in the UPS spectrum, which could be related to organic molecules at the surface of the cathode, was observed. If Alq<sub>3</sub> molecules could reach the surface of the Mg layer the signal would be drastically changed. But we did not found any new peak or changes even after longer time.

This means the Mg cathode of an OLED is not be destroyed by an intrinsic mechanism like diffusion of Mg into Alq<sub>3</sub>. The thin cathodes we used would be very sensitive to any changes which occur from the interface and grow towards the surface. From these experiments we can conclude that any interfacial changes taking place at the Mg/Alq<sub>3</sub> interface will be very localized, with a maximum extension lower than 35 nm, the thickness of the



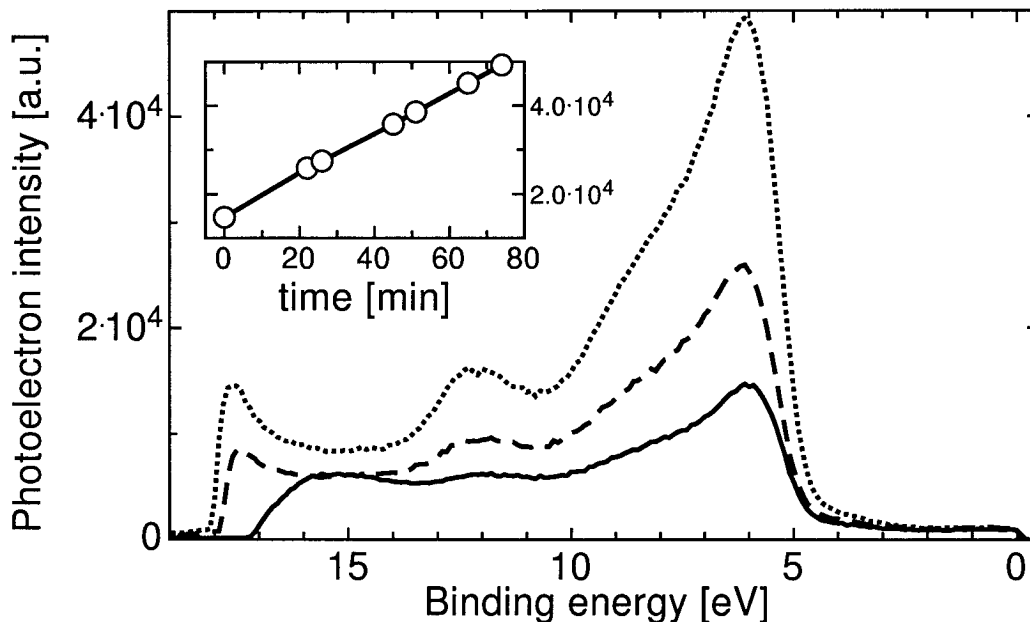


**Figure 2.17:** UPS measurement on the cathode surface of a device before it was operated for the first time (0 min, solid), after 22 min of operation at a bias voltage of 8 V (dashed), and after 74 min of operation at 8 V bias voltage (dotted). The inset shows the photoelectron intensity at the binding energy 6.1 eV versus time.

cathodes we used.

An additional feature that we observed in the UPS spectrum is a shift of the left edge of the spectrum, related to the slow electrons, when the device is running. While the oxidation of the Mg-cathode is still visible by UPS when the OLED is switched off, this shift in the spectrum only appears when the device is being operated. The left edge becomes sharper and moves by about 1 eV to the left if the current is flowing through the device.

The reason for this behavior is not clear yet. We propose two tentative explanations: (1) Because of the relative arrangement of cathode and ITO-anode on our sample, a deformation of the electric field of the negatively charged cathode can take place when the anode is on ground potential. This involves an higher UPS signal at the slow electron edge and shifts the position of the UPS spectrum to the left, depending on where on the cathode the photoelectrons are emitted from. (2) A non-homogenous conduction at the cathode surface could lead to spatially inhomogeneous voltage drops over the cathode surface, which would lower the acceleration of photoelectrons, also producing a shift of the left edge of the UPS spectrum.

## CONCLUSIONS

In conclusion, we could observe, for the first time to our knowledge, the changes in the UPS spectrum of the thin Mg cathode of a running OLED.

We found that no intrinsic degradation mechanisms can destroy even a 35 nm thin Mg-cathode. If there is an effect of the OLED operation on the Mg/Alq<sub>3</sub> interface, that this interfacial changes are limited to a thickness of less than 35 nm from the interface.

## ACKNOWLEDGEMENTS

This work was supported by the Swiss Federal Institute of Technology (ETH) Zürich. The authors would like to thank Dr. Max Doebli for the thickness measurements using Rutherford Backscattering Spectroscopy.

Seite Leer /  
Blank leaf

## 2.6 Observation of the Mott–Gurney law in tris (8-hydroxyquinoline) aluminum films\*

### Abstract

We show that tris (8-hydroxyquinoline) aluminum (Alq<sub>3</sub>) thin films produced and characterized under ultrahigh vacuum conditions present a well-defined squared-law dependence of the injected current on the applied voltage at applied electric fields of the order of 0.25 – 1 MV/cm. From this, one derives an electric-field-independent electron mobility of the order of 10<sup>-7</sup> cm<sup>2</sup>/(Vs), with a variation between different samples of about one order of magnitude. Observations of current–voltage characteristics with clear indications of trap-filling and space-charge-limited conduction at high fields in Alq<sub>3</sub> excludes the existence of traps with an exponential distribution of trap energies, as is commonly assumed in amorphous materials.

### Article

An electric current can be driven through an insulator by injecting charge carriers from electrical contacts. When energy barriers at the contacts become negligible, and when trapping of injected carriers at localized energy levels does not depend on the current, then it is possible to reach a limit where one observes a space charge limited (SCL) current [32]. In this limit the only material parameters determining the current are the carrier mobility  $\mu$  and the dielectric constant  $\epsilon$ , leading to a simple method to determine intrinsic charge-carrier mobilities in insulators [32, 88, 89]. In a “parallel-plate capacitor configuration,” where the insulator is sandwiched between two electrodes, and at high applied voltages  $V$ , where charge-carrier diffusion and injection barriers can be neglected, the injected current density  $j$  is given by the Mott-Gurney law (also known as Child’s law in solids) [32–36]

$$j = \frac{9}{8} \mu \epsilon \epsilon_0 \frac{V^2}{d^3} \quad (2.1)$$

where  $\mu$  and  $\epsilon$  are mobility and dielectric constant of the material,  $\epsilon_0$  is the permittivity of vacuum,  $d$  is the distance between the contacts, and  $V$  is the applied voltage. Eq. 2.1 is valid for a mobility  $\mu$  which is independent of the applied electric field and of the current density.

\* The results of this section have been published in Applied Physics Letters Vol. 80 (7), page 1198-1200 in the year 2002.

Organic insulators have been increasingly studied in recent years for device applications such as field effect transistors and light emitting diodes, and the basic functionality of the devices is almost always obtained by injecting charge carriers into the organic materials by high applied electric fields. A characterization and understanding of the injection process as well as the bulk conductivity process is important in order to further optimize and develop new organic systems for electronics and photonics applications.

Among such systems, thin films of tris (8-hydroxyquinoline) aluminum ( $\text{Alq}_3$ ) molecules currently enjoy widespread use as the electron-conductor and the photoemissive material in organic light emitting diodes. But despite this popularity, electron injection and transport in  $\text{Alq}_3$  are still relatively poorly understood. Several authors, (*e.g.*, [90–98]) measured current–voltage characteristics in  $\text{Alq}_3$  systems, but none succeeded in observing a clear square-law dependence as expected from Eq. 2.1. In addition, there is some controversy [90, 92–95, 99] about the separate influence of injection barriers, impurity levels that act as electron traps, and electric-field dependent mobility, all processes that can explain the fact that no square-law current–voltage dependence has been observed to date.

In this letter we show that it is possible to achieve SCL conductivity in  $\text{Alq}_3$  thin films — with a clear proportionality between current density and the square of the applied voltage — by optimizing the fabrication and characterization conditions of an  $\text{Alq}_3$  layer sandwiched between magnesium contacts. This entails (1) the use of ultrapure magnesium contacts deposited in ultrahigh vacuum (UHV) at an impurity gas pressure of less than  $10^{-9}$  mbar; and (2) the measurement of current–voltage characteristics in the same UHV environment within a few hours after deposition of the  $\text{Mg}/\text{Alq}_3/\text{Mg}$  system. The data obtained in such a way highlights the intrinsic properties of  $\text{Alq}_3$  as an electron conductor and can be useful to describe the properties of devices under conditions of perfect encapsulation [83, 84, 100].

Under the above mentioned UHV conditions, the choice of magnesium as the contact material leads to a relatively low energy barrier for electron injection in  $\text{Alq}_3$ , and ensures that the current is dominated by electrons. In our experiments no light emission from the sample, indicative of bipolar injection, could be observed. The use of magnesium requires UHV because of its high susceptibility to oxidation [70]. Even in UHV, an oxide layer thicker than 2nm appears on the magnesium surface in about two days [84, 100]. Such an oxide layer at the  $\text{Alq}_3/\text{Mg}$  interface could lead to an additional energy barrier that would not allow ohmic contacts in the experimentally accessible range of applied electric fields. To minimize these effects the devices were characterized directly after the deposition.

$\text{Mg}/\text{Alq}_3/\text{Mg}$  samples were prepared by molecular beam deposition on

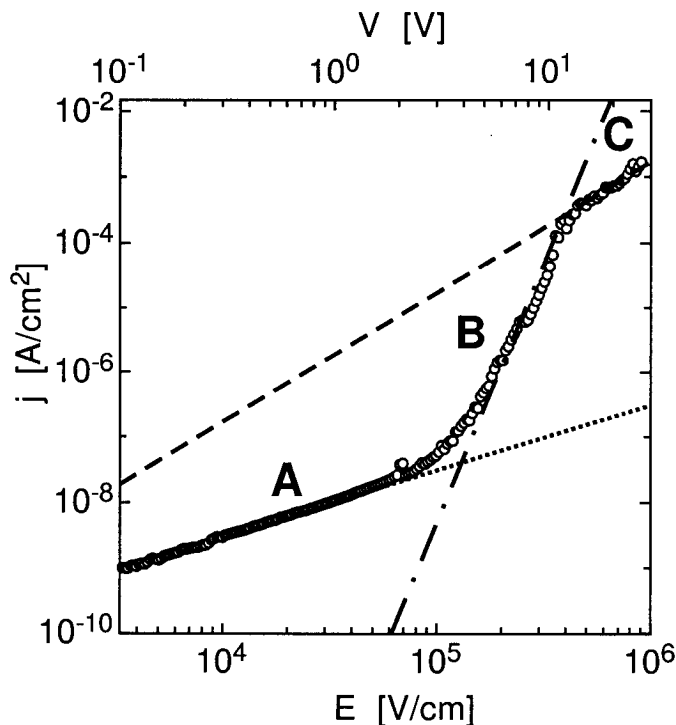


**Figure 2.18:** Current-density vs average applied field  $E = V/d$  for a Mg/Alq<sub>3</sub>/Mg electron-only injection device with a  $d = 300$  nm-thick-Alq<sub>3</sub> layer (open circles). The dashed line corresponds to a  $j \sim V^2$  dependence. The dotted line shows a linear proportionality  $j \sim V$ .

a glass substrate in an UHV chamber at a base pressure of less than  $4 \times 10^{-10}$  mbar. During deposition of the first magnesium contact and of the Alq<sub>3</sub> layer the substrate was heated to  $100^\circ\text{C}$ . For the second magnesium contact on Alq<sub>3</sub> the substrate was held at  $-50^\circ\text{C}$  to get a better sticking of magnesium on Alq<sub>3</sub>. The thickness of the magnesium contacts was between 40 and 100 nm. The thickness of the Alq<sub>3</sub> layer was varied between 230 and 550 nm, and was measured for each device using a Tencor Alpha-Step 500 surface profilometer. The surface area of the devices was 1, 6, and 9 mm<sup>2</sup>. We purified our Alq<sub>3</sub> by one vacuum sublimation step.

After fabrication each substrate, holding 12 separate Mg/Alq<sub>3</sub>/Mg devices, was moved without leaving the UHV environment to an electrical characterization chamber at a base pressure of less than  $3 \times 10^{-9}$  mbar. The current–voltage characteristics were measured in darkness with a computer controlled Sourcemeter (Keithley 6430).

In about 100 samples we measured current densities between  $10^{-10}$  and  $10^{-2}$  A/cm<sup>2</sup> for applied fields between 1 kV/cm and 1 MV/cm. In about 80% of these samples we observed at least one voltage region where  $j \sim V^2$ , and more than 50% showed a clear transition from an Ohmic-type conductivity to a space-charge limited conductivity that can be exemplified by the curve

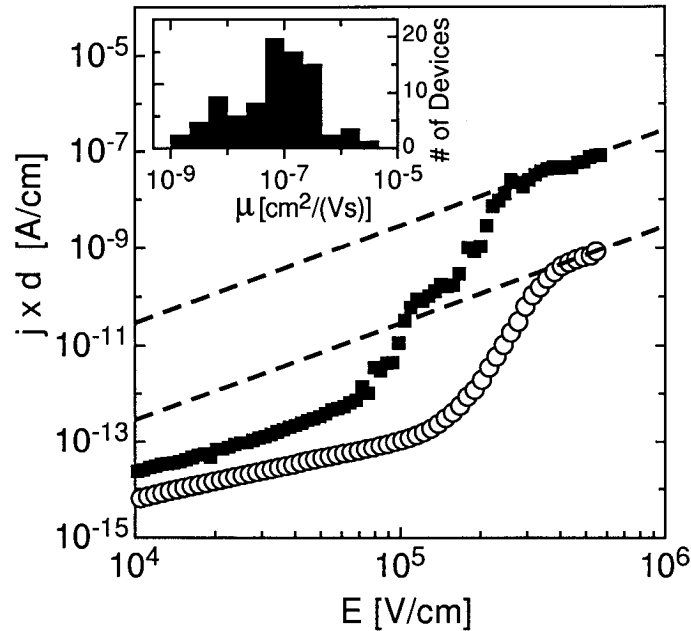


**Figure 2.19:** Examples of measurements in two different Alq<sub>3</sub> samples which showed different mobility values  $\mu$ . For better comparison  $j \times d$  is plotted as a function of  $E = V/d$ . Most of the current–voltage characteristics we measured were distributed between these two curves. The inset shows a histogram with the measured distribution of the electron mobilities.

in Fig. 2.18. For electric fields up to 80 kV/cm (region A) the current is proportional to the applied voltage (dotted line), corresponding to impurity dominated conduction of the organic material. Between 80 and 400 kV/cm (region B) the current increases strongly and becomes proportional to about  $V^8$  (dashed dotted line), which can be explained by the onset of carrier injection and trap filling. Finally, starting from 400 kV/cm (region C) the current follows the  $V^2$  dependence predicted by Eq. 2.1 for SCL current injection into an insulator (dashed line). A change in the polarity of the applied voltage did not influence these observations. The data in Fig. 2.18 indicate that the electron mobility in this example is field independent for applied electric fields between 0.4 and 1 MV/cm. The samples are destroyed by electric breakdown at applied fields higher than about 1 MV/cm.

The electron mobility derived from region C varies by roughly one order of magnitude between different devices with different thickness and different time intervals between fabrication and characterization. Fig. 2.19 shows as an example two measurements with two distinctive low and high mobilities  $\mu$  in a  $j \times d$  vs  $E$  plot.

We also observed that the region of steep current increase (region B) moves toward larger electric fields when the time interval between fabrication and characterization of the device increases, a fact that hints at an increase

of the trap concentration with time.

The inset in Fig. 2.19 shows as a histogram the distribution of electron mobility values from all measurements with  $j \sim V^2$  regions. About 60% of the measurements are within the mobility range from  $5 \times 10^{-8}$  to  $5 \times 10^{-7}$  cm<sup>2</sup>/(Vs). These mobilities were derived from Eq. 2.1 using  $\epsilon = 3.5$  [90].

The relatively large range of mobilities derived from region C could be due to the fact that the SCL conduction we observed corresponds to a trap-limited mobility which is still influenced by a density of shallow traps which varies from sample to sample.

The electron mobility we obtain is of the order of  $10^{-7}$  cm<sup>2</sup>/(Vs) and is electric-field independent up to an applied field of 1 MV/cm. This is below the range of mobility values (from  $1 \times 10^{-6}$  to  $2 \times 10^{-5}$  cm<sup>2</sup>/(Vs)) at 0.4 MV/cm [69, 90, 101, 102]) reported so far and obtained with time of flight methods [69, 101, 102] or transient electroluminescence [69, 90]. The reason for this lower value is not completely clear yet, although dynamics of trap filling and sensitivity to trap-limited mobilities is different for the different methods.

It must be noted that the very fact of observing a well-defined trap-filling transition and the current predicted by Eq. 2.1 in Alq<sub>3</sub> implies that the levels responsible for electron trapping cannot have an exponential energy distribution, as is commonly assumed in amorphous materials. A possible reason for this might be connected with nanocrystals formed during deposition of the thin films. SCL currents in amorphous organic thin films have also been observed in Refs. 103 and 104

A number of other groups measured current–voltage characteristics in electron-only Alq<sub>3</sub> devices, but a clear squared law dependence ( $j \sim E^2$ ) at high electric fields could not be observed up to now. Current–voltage characteristics in Mg/Alq<sub>3</sub>/LiF/Al devices have been measured in Ref. 92 and the data were described using a SCL current model with an electric field dependent mobility (for electric fields of the order of 1 MV/cm).

References 90, 95 interpreted its current–voltage characteristic data as given by trap filling of an exponential trap distribution, with a current  $j \sim V^{l+1}$  ( $l+1$  between 3.4 and 4.4), while at the same time observing a thickness and temperature dependence in agreement with trap-free SCL current.

By comparing our experimental conditions to those presented in the literature we conclude that the reason why the squared-law dependence predicted by Eq. 2.1 was never clearly observed in Alq<sub>3</sub> thin films is related to the effects of impurity gases. Atmospheric gases influence the barrier for electron injection and the density of impurity levels in the Alq<sub>3</sub> layers. Therefore, a current–voltage characteristic steeper than  $j \sim V^2$  can be due to injec-



tion barriers, trap filling, or both. Ultrapure conditions appear to be a requirement for establishing the conditions that allow space-charge-limited conduction in the Mg/Alq<sub>3</sub> system. We showed that even small traces of atmospheric gases lead to the disappearance of SCL conduction: the SCL current could not be observed anymore after venting our UHV chamber with nitrogen gas (to simulate a good glove box), or after leaving a sample in UHV for 2 days. Compared to our experimental setup, all previous measurements were performed under relatively bad isolation from atmospheric gases.

In conclusion, we observed SCL conduction with a clearly visible trap-filling transition to a  $j \sim V^2$  dependence in Alq<sub>3</sub> films grown and characterized in UHV. From this it follows that electron trapping centers have a relatively well-defined energy, an unexpected result in an amorphous material, and that the electron mobility is independent of the electric field for applied fields below 1 MV/cm.

This work was supported by a research grant of the Swiss Federal Institute of Technology (ETH) Zürich. M. Koehler would like to thank CNPq for a research fellowship.

## 2.7 Conditions for ohmic electron injection at the Mg/Alq<sub>3</sub> interface\*

### Abstract

We show that the contacts formed by magnesium on tris (8-hydroxyquinoline) aluminium (Alq<sub>3</sub>) are intrinsically ohmic when they are fabricated and operated in ultrahigh vacuum. Under the same conditions, the injected current shows a steep increase approximately proportional to the 7th power of the applied voltage that we assign to trap-filling. Only a subsequent contact with oxygen leads to an injection-limited behavior, where the observed steep current increase is caused by potential barriers at the contacts. In addition, we observe that electron injection in oxidized structures can be very well described by Fowler-Nordheim tunneling in the case when electrons are injected from the Mg contact evaporated onto Alq<sub>3</sub>.

### Article

The injection of charge carriers from a metal contact into an organic material is of fundamental importance for any application or device involving polymers or small molecule materials. Technologically relevant examples are organic light emitting devices (OLEDs) and organic field effect transistors (OFETs). A better knowledge and control of the effects determining the efficiency of charge-carrier-injection from a metal contact is important for a better theoretical understanding as well as for optimizing device performance. Moreover, the controlled study of the effects of oxygen exposure is interesting because up to now most organic devices had to be encapsulated and protected from atmospheric gases. To control degradation effects in future devices it is important to understand the influence of oxygen.

Here we focus on electron injection from magnesium contacts into tris (8-hydroxyquinoline) aluminium (Alq<sub>3</sub>), a widely used electron transport and luminescence material in OLEDs. Current-voltage (IV) measurements in Alq<sub>3</sub> structures with electron injecting contacts are characterized by a low-voltage ohmic region where the current density  $j$  is proportional to the voltage  $V$ , followed by a steep current increase where  $j \sim V^x$ ,  $x \approx 7$ . This feature has been reported in several publications [24, 25, 90–92, 94–99] and was variously explained as caused by injection processes [24, 25, 99], space-charge limited (SCL) current with exponential trap distribution [92, 94] or SCL current with field dependent mobility [90, 95].

---

\* The results of this section have been published in Applied Physics Letters Vol. 80 (23) page 4366-4368 in the year 2002.

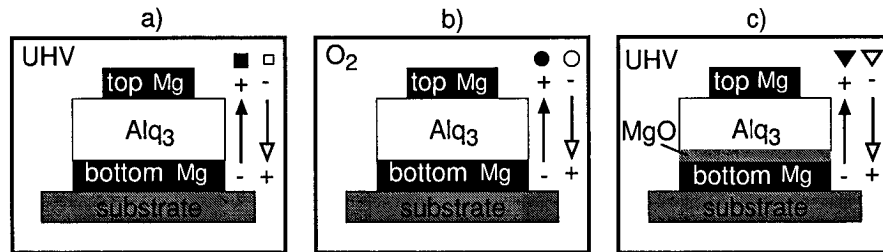


**Figure 2.20:** The three structures investigated in this work. a) Mg/Alq<sub>3</sub>/Mg structure operated in UHV, b) the same structure operated in pure oxygen at atmospheric pressure, and c) a Mg/MgO/Alq<sub>3</sub>/Mg fabricated by exposing to bottom Mg contact for 2 hours to 99.998% pure oxygen at partial pressure of  $1 \times 10^{-5}$  mbar (measured with a vacuum gauge calibrated for nitrogen gas) and operated in UHV. The arrows and the symbols above them indicate the electron drift direction and the corresponding shape of the data points in Figs. 2-4, respectively.

In the present work we show, by characterization of the structures in UHV and under the controlled influence of oxygen, that in the Mg / Alq<sub>3</sub> / Mg system the steep current increase can be determined both by injection barriers or by trap filling processes with charge diffusion from ohmic contacts, depending on the purity of the materials and of the characterization environment. Injection barriers are only observed in samples that have been exposed to oxygen.

Mg / Alq<sub>3</sub> / Mg samples were prepared by molecular beam deposition on a glass substrate in an UHV chamber [100]. The fabrication details are described in Ref. 105. The thickness of the Alq<sub>3</sub> layer was varied between 340 and 650 nm, and was measured for each structure using a Tencor Alpha-Step 500 surface profilometer. The surface area of the top magnesium contact was 1 mm<sup>2</sup>. The electrical characterization was performed by a computer controlled sub-femtoampere source meter Keithley 6430. The samples were discharged for 2 min at  $\pm 0.1$  V before the measurements.

The 3 sample structures studied in this work are shown in Fig. 2.20. We define as “positive” the voltage for which electrons are injected from the bottom contact (as indicated by filled arrows in Fig. 2.20).

IV-characteristics of Mg / Alq<sub>3</sub> / Mg structures fabricated and characterized in ultrahigh vacuum (UHV) show an Ohmic-conduction region at low applied voltages ( $j \sim V$ ), a steep current increase at intermediate voltages ( $j \sim V^x$  with  $x \approx 7$ ), and a space-charge-limited (SCL) current described by the Mott -Gurney law ( $j \sim V^2$ ) at higher voltages [105]. In this work we increased the voltage only up to a value which allowed us to observe the steep current increase, thus avoiding the larger voltages required to observe space charge limited currents [105], and minimizing possible degradation effects

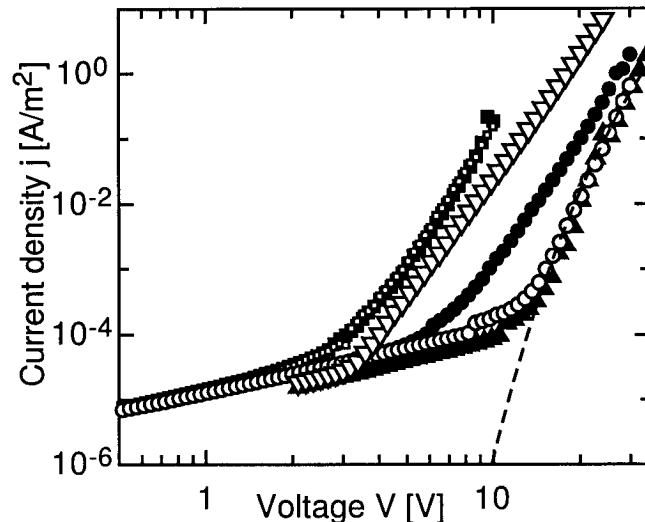


**Figure 2.21:** Current-density vs. absolute voltage for the structures and experimental conditions described in Fig. 2.20 with Alq<sub>3</sub> thickness 340 nm. The dashed curve is a plot of Eq. 2.23 (Fowler-Nordheim injection) with  $B = 5.16 \times 10^8 \text{ A}/(\text{Vm})$  and  $\Delta = 0.19 \text{ eV}$ .

that would be induced at higher voltages.

Figure 2.21 (squares) shows the IV-curve of structure (a) in Fig. 2.20, which was fabricated and operated in UHV. The IV-curve does not depend from the direction of the injection, as is expected for identical contacts. The same observation has been reported in Ref. 71 for a Mg/Alq<sub>3</sub>/Mg structure with a 120 nm thick Alq<sub>3</sub> film. The IV-data reported in Ref. 71 coincide very well with our measurements for voltages higher than 2 V, despite the fact that the Alq<sub>3</sub> thickness differs by a factor of two. This fact already indicates, as will be discussed below, that the MgAlq<sub>3</sub> contacts are ohmic, allowing electron injection by diffusion [80,81].

To study the influence of oxygen we flooded the UHV chamber with 99.995% pure oxygen at atmospheric pressure and again measured the IV-characteristic in the same structure. The resulting IV-curves are shown as circles in Figure 2.21. Oxidation leads to IV-curves which are asymmetric with respect to the sign of the applied voltage and which show a higher “threshold” voltage for the onset of the steep increase in current. For 340 nm and 380 nm thick Alq<sub>3</sub> layers, the highest threshold voltages were observed for negative voltages (electron injection from the the top contact). We will show below that this is not the case for structures with a larger Alq<sub>3</sub> thickness. The asymmetry of the IV-curve with respect to the injection direction is an indication that the increase in the threshold voltage cannot only be caused by an increase in the trap density in the Alq<sub>3</sub> bulk upon oxidation, but must depend on the oxidation state of the metal/organic interfaces.

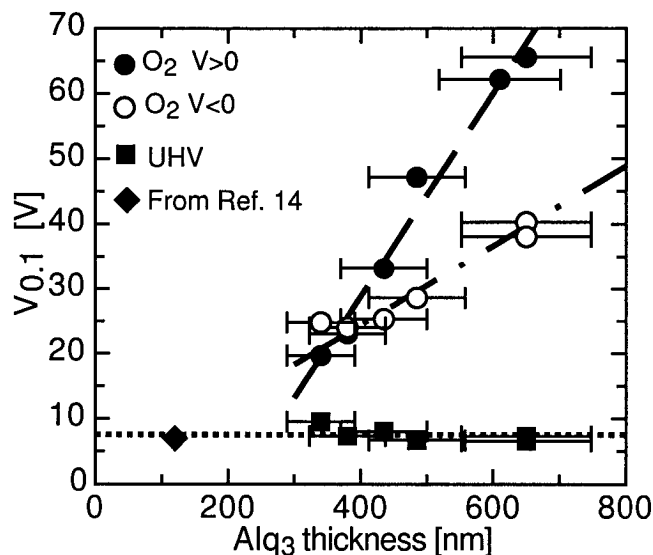


**Figure 2.22:** The voltage  $V_{0.1}$  for a current-density of  $0.1 \text{ A/m}^2$  is plotted vs. the thickness of  $\text{Alq}_3$  films for the structures and experimental conditions described in Fig. 2.20. The filled diamond represents a UHV measurement reported in Ref. 71. The lines are guides to the eye.

A first confirmation that it is the oxidation at the interfaces that leads to this asymmetry is found in the IV-curves of a structure where an oxide barrier was artificially produced at one of the magnesium contacts (Fig.2.20c). A magnesium oxide layer between bottom contacts and  $\text{Alq}_3$  is the only difference between this structure and the one discussed above. An  $\text{Alq}_3$  layer of the same thickness and the top Mg contact were evaporated in UHV, where also the characterization took place. Therefore, we do not expect any change in the parameters of the remaining layers, such as the trap density in  $\text{Alq}_3$ . The resulting IV-curves are shown as triangles in Fig. 2.21. The threshold voltage for a cathode with an oxide barrier is as high as for injection through the top contact in the originally non oxidized structure that was subsequently exposed to oxygen. For electron injection from the other side, however, the threshold voltage is only slightly increased compared to the structure (a) in Fig. 2.20. The potential barrier has obviously a much smaller influence when it is positioned at the anode.

An additional confirmation of the importance of oxide barriers at the metal/organic interface is found in the dependence of the position of the steep current increase from the  $\text{Alq}_3$  thickness. Since the concept of “threshold” voltage used above depends on the density of free charges responsible for the Ohmic part of the IV-curve, it is not suitable for a general quantitative evaluation. We therefore arbitrarily define an “injection” voltage as the voltage required to inject a current density of  $0.1 \text{ A/m}^2$  and we plot it as a function of

the Alq<sub>3</sub> layer thickness in Fig. 2.22. The corresponding measurement from Ref. 71 is also plotted, as a black triangle.

One observes that in all structures that have been fabricated and operated in UHV the injection voltage is practically constant at about 7 V and is independent from Alq<sub>3</sub> thickness in the range between 120 [71] and 650 nm. From this observation we argue that the steep current increase is caused by trap filling in a situation where charge carriers are injected from perfect ohmic contacts. Under these conditions a significant charge carrier density enters the organic layer by diffusion from the metallic contacts even without any applied voltage [80]. The presence of these charges can explain the ohmic conduction region at low applied voltages observed in Fig. 2.21 and the independence of the onset of trap filling from the Alq<sub>3</sub> thickness (Fig. 2.22) [81]. The similarity with the current voltage curves of Ref. 71 hints at a similar trap density as in our Alq<sub>3</sub> films.

On the other hand, the data for the structures operated in oxygen has a clear thickness dependence. For injection from the top contact the thickness dependence is close to linear and for injection from the bottom contact the thickness dependence is stronger. For Alq<sub>3</sub> thicknesses of 340 and 380 nm the injection voltage for injection by the bottom contact is lower compared to the injection from the top contact, while it is higher for all other thicker structures.

These observations lead to the following conclusions:

(1) The injection voltage does not depend on the Alq<sub>3</sub> thickness for structures operated in UHV because the injected current is determined by ohmic contacts, by electron diffusion, and by trap filling.

(2) The thickness-dependence of the injection voltage in structures operated in oxygen atmosphere and the asymmetry of the IV-curves with respect to injection direction indicate that injection barriers have been built up by the oxygen treatment.

Additional information on this second point is found when the data of Fig. 2.21 are plotted in a Fowler-Nordheim plot. The result is shown in Fig. 2.23. In this plot a straight line corresponds to a current density that has the following electric-field dependence [16, 25]

$$j_{FN} = BE^2 \exp(-b/E), \quad (2.2)$$

where  $B$  is a constant factor,  $E$  is the average electric field  $V/d$ ,  $b = 4\sqrt{(2m^*)\Delta^3}/(3\hbar e)$ ,  $m^*$  is the effective electron mass (here assumed to be equal to the free electron mass),  $\Delta$  is the barrier height, and  $e$  is the unit charge. We observe that the injection through the artificial oxide barrier at the bottom contact as well as the injection through the top contact in

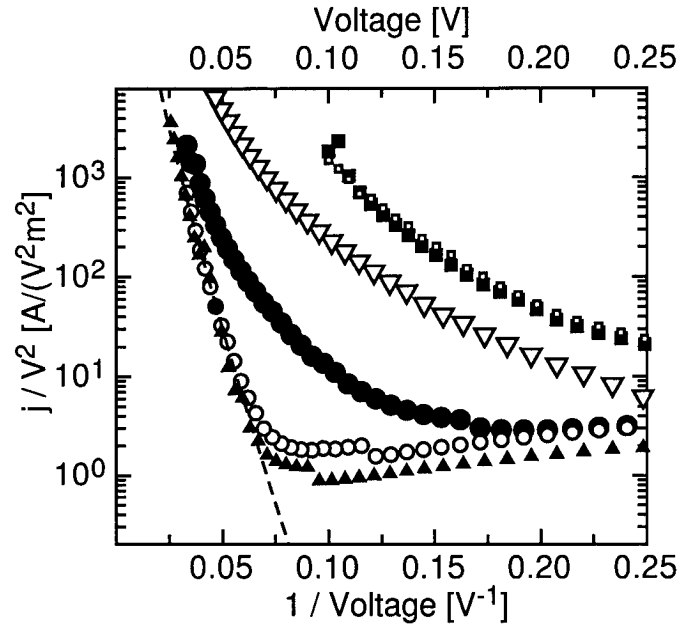


**Figure 2.23:** Fowler-Nordheim-Plot of the data in Fig. 2.21.

the structure operated in oxygen atmosphere can be very well described by Eq. 2.23. The current density for voltages exceeding 13 V can be well fitted over 4 decades in current using the parameters  $\Delta = 0.19$  eV and  $B = 5.16 \times 10^8$  A/(Vm). The corresponding current density is plotted as a dashed curve in Fig. 2.23 and Fig. 2.21.

It is not clear why the IV-curve of structure b) in Fig. 2.20 follows the Fowler-Nordheim law only for one injection direction. An explanation is not possible at this stage, because of the limited knowledge that is available on the behavior of the oxidized Mg / Alq<sub>3</sub> interface. The asymmetry of the IV-curves for the oxidized structures must be caused by a different oxidation behavior of the two morphologically different Mg / Alq<sub>3</sub> interfaces (one where Alq<sub>3</sub> was deposited on flat Mg, one where hot Mg was deposited on Alq<sub>3</sub>). However, the difference in morphology does not influence the IV-measurements for the structure of Fig. 2.20a) in UHV, where both interfaces lead to ohmic contacts.

In conclusion, we showed that a pure Mg/Alq<sub>3</sub> interface fabricated and operated in UHV forms an ohmic contact leading to a transport limited current that is only influenced by the trap density. An additional confirmation of the presence of ohmic contacts in such non oxidized structures has been reported earlier by the direct measurement of the Mott-Gurney law in similar structures [105]. Oxidation at the Mg contacts leads to a potential barrier for electron injection which strongly influences the IV-curves. Intrinsically, Mg/Alq<sub>3</sub> structures are thus capable of supporting very efficient charge car-

rier injection, with the possibility of achieving high currents at low voltages.

## **Acknowledgement**

This work was supported by a grant from the Swiss Federal Institute of Technology (ETH) Zürich. We thank A. Rashid for the excellent cleaning of the Alq<sub>3</sub> molecules. M. Koehler gratefully acknowledges the Conselho Nacional de Desenvolvimento Científico e Tecnológico (CNPq) for his research fellowship.



Seite Leer /  
Blank leaf

---

## 3 Conclusions and Outlook

### 3.1 Conclusions

We show that a proper characterization of charge injection, transport and radiative recombination in Mg / Alq<sub>3</sub> structures is only possible if the fabrication and characterization take place in an ultrapure environment. This was demonstrated in this work by combining organic molecular beam deposition and electrical / optical characterization in the same UHV system.

I could show that the surface of a 35 nm thick Mg cathode in a ITO/NPB/Alq<sub>3</sub>/Mg device is stable if the device is operated in UHV.

Space-charge limited conduction with a clearly visible trap-filling transition to a  $j \sim V^2$  dependence in Alq<sub>3</sub> films grown and characterized in UHV has been observed for the first time. From this it follows that electron trapping centers have a relatively well-defined energy, an unexpected result in an amorphous material, and that the electron mobility is independent of the electric field for applied fields below 1 MV/cm. The value of electron mobility in Alq<sub>3</sub> thin films has been determined.

Moreover, it could be shown that the Mg/Alq<sub>3</sub> interface always forms ohmic contacts under ultrapure conditions, while operation in oxygen deteriorates the ohmic contact and leads to a potential barrier for electron injection which can be described by Fowler-Nordheim tunneling when Mg is deposited on Alq<sub>3</sub> to form the contact. Intrinsically, the Mg/Alq<sub>3</sub> is thus capable of supporting very efficient charge carrier injection.

### 3.2 Outlook

This work showed that it is possible to inject carriers into the organic material without any injection barrier. This result can help to produce optimized organic devices for applications, as organic electrical pumped lasers or organic transistors.

Seite Leer /  
Blank leaf

# A Experimental

In this work several physical techniques were applied to identify the mechanisms of OLED operation, current transport, injection and degradation. This chapter presents an introduction to the experimental methods that have been used in this work, namely an introduction to ultra-high vacuum technology, thin film deposition, X-ray Photoelectron Spectroscopy (XPS), Ultraviolet Photoelectron spectroscopy (UPS), electrical characterization, and impedance spectroscopy.

## A.1 Ultrahigh vacuum (UHV)

The mass of our earth attracts, fortunately for mankind, our atmosphere. As a consequence the whole environment is influenced by atmospheric gases such as oxygen. For example, the metallic mineral resources are mostly oxides. The oxygen can be displaced by heating and melting of the material, but even if the material is cooled, the surface will remain oxidized. Only heating in sufficient vacuum can keep the surface clean. The necessary vacuum level depends on the requirements of surface purity. Of course, for bulk measurements there is no need for vacuum, but for measurements where the first atomic layers play a role, a very good vacuum is required to exclude contamination from atmospheric gases. The contamination of the surface can be described by the formation time of one monolayer of adsorbed gas molecules. One can calculate this time  $t_{mono}$  from the kinetic theory of gases and the MAXWELL-BOLTZMANN distribution .

The number of particles which reach the surface per time and area [106] is given by

$$n = \frac{1}{4} \frac{N}{V} \bar{v}, \quad (\text{A.1})$$

where  $N$  is the number of gas particles,  $V$  is the volume and  $\bar{v}$  the average speed of the gas particles. From MAXWELL statistics one gets

$$\bar{v} = \sqrt{\frac{8k_B T}{\pi \cdot m}}, \quad (\text{A.2})$$

and from the ideal gas equation

$$\frac{N}{V} = \frac{p}{k_B T}. \quad (\text{A.3})$$

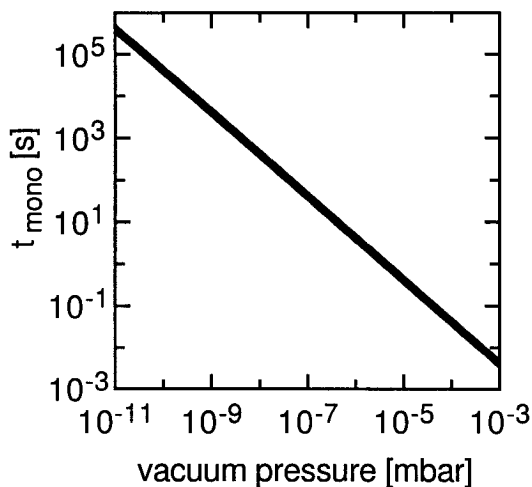


**Figure A.1:** Adsorption time of one monolayer of oxygen on the sample surface at different gas partial pressures. Only the pressure range below  $10^{-8}$  mbar allows a contamination free measurement in reasonable time.

By combining Eq. A.1, Eq. A.2, Eq. A.3 and the relation  $t_{mono} = (n \cdot d^2)^{-1}$  where  $d$  is the molecular distance of the adsorbed particles, one gets

$$t_{mono} = \frac{\sqrt{2\pi m k_B T}}{pd^2}. \quad (\text{A.4})$$

Usually not all gas particles which reach with the surface remain on the surface. Eq. A.4 corresponds to the worst case scenario, where all particles, that hit the surface stick to it.

As an example, the mass of  $O_2$  is about  $m = 32 \cdot m_{proton} = 5.3 \times 10^{-26}$  kg, the molecular distance can be estimated by  $d = 4 \times 10^{-10}$  m and the temperature is assumed to be  $T = 300K$ . Fig. A.1 shows the result of the calculation. Only for partial pressures below  $1 \times 10^{-8}$  mbar, the sample can remain atomically clean during the usual experiment time of several minutes.

This vacuum pressure range below  $1 \times 10^{-8}$  mbar is called Ultrahigh Vacuum (UHV).

### A.1.1 The UHV machine

In this work, a complex UHV system was used to observe the properties of clean OLEDs. The pressure during sample fabrication was usually below  $5 \times 10^{-10}$  mbar, during surface analysis measurements (XPS, UPS) below  $1 \times 10^{-9}$  mbar, and during transportation below  $3 \times 10^{-8}$  mbar.

This UHV system was the base for several measurements which could never be successful under vacuum conditions worse than a pressure of  $10^{-8}$  mbar. Fig. 2.5 in the experimental part of section 2.3 on page 33 shows a schematic view of the UHV system.

It consists of

- a deposition chamber for organic materials (6 effusion cells)
- one metallization chamber (2 effusion cells, 2 electron beam evaporators)
- a surface analysis chamber (UPS, XPS)
- a special chamber with electrical contacts to operate the OLED inside the UHV environment (attached to the existing system during this work, called “OLED chamber” in Fig. 2.5)

Additionally, there is a chamber with an Atomic Force Microscope (AFM) and a load-lock chamber to bring the samples in and out of the UHV. All the chambers are connected by a transfer system. The samples can be moved from chamber to chamber without breaking the vacuum.

The system was designed as a Molecular Beam Epitaxy (MBE) system for 3 inch wafers and later extended to an organic / metal deposition machine [107, 108].

## A.2 Deposition

Thin film fabrication was carried out in the organic deposition chamber and in the metallization chamber. The materials were heated in effusion cells (also called KNUDSEN cells, see Ref. [109–111]). The properties of the materials employed are described in Appendix B.

Both chambers are equipped with a liquid nitrogen cooling shroud. During the deposition the shrouds were cooled and the achieved vacuum pressure was about  $5 \times 10^{-9}$  mbar in the metallization chamber and  $2 \times 10^{-10}$  mbar in the organic chamber. The sample holder can be heated and cooled by liquid nitrogen.

The thickness was monitored by a quartz micro balance, which was calibrated with RUTHERFORD Back Scattering (RBS) measurements [87], optical transmission spectroscopy, and a Tencor Alpha-Step 500 surface profilometer.

The substrates were held in special copper sample holders. The substrates were prepared by pre-cleaning them in acetone and ethanol in an ultrasonic water bath. Then the substrate was rinsed with water. The water was blown away to dry the sample. For magnesium deposition this procedure was not sufficient because magnesium reacted on the sample surface and became transparent. To avoid that reaction the samples were heated over night in the vacuum chamber at 130 degree.

Metal masks define the area of deposition on the substrate. The masks were stored inside the transfer chamber all the time and the mask change was realized inside UHV in the transfer chamber. Usually two or three masks were used for an OLED fabrication.

The sample holder in the organic chamber can not be rotated. This leads to problems during the deposition. A shadow can appear because of the oblique incidence (approximately 25 degree to the sample normal) of the molecular beam. This small area without material can cause a short circuit in the device. This problem was solved by moving the sample to the electrical chamber, which is equipped with a rotatable plate, and back. Later the shadow effect was minimized by a new device concept with a large area flat contact on the glass and large area organic film followed by a small area second contact on top of the organic film.

The number of effusion cells in the organic deposition chamber have been doubled during the course of this work (from three to six).

### A.3 Photoelectron spectroscopy

Photoelectron spectroscopy is based on the inner photoelectric effect (discovered by HALLWACHS [112] and explained by EINSTEIN [113]). If a material is illuminated with high energy light<sup>1</sup> electrons can escape the surface.

The momentum of the photons is so small, that there is almost no momentum transfer to the electron. Energy conservation gives

$$h\nu = \Phi + E_{bind} + E_{kin} \quad (\text{A.5})$$

with  $h\nu$  the photon energy,  $\Phi$  the work function,  $E_{bind}$  the binding energy of the electron and  $E_{kin}$  the kinetic energy of the emitted electron. At a fixed photon energy, different bonded electrons have different kinetic energies in the vacuum.

By irradiating the sample with monochromatic light and by measuring the amount of electrons per kinetic energy interval the so called Energy Distribution Curve (EDC) can be obtained. The electron density of states inside the material at a given binding energy approximately agrees with the measured electron density at the corresponding kinetic energy. This fact is used to determine the binding energy dependent electron density of states inside the investigated sample.

The electron escape process can be described by the three step model illustrated in Fig. A.2.

---

<sup>1</sup> The energy of light has to be higher than the ionization energy for electrons (work function for metals, ionization potential for insulators).

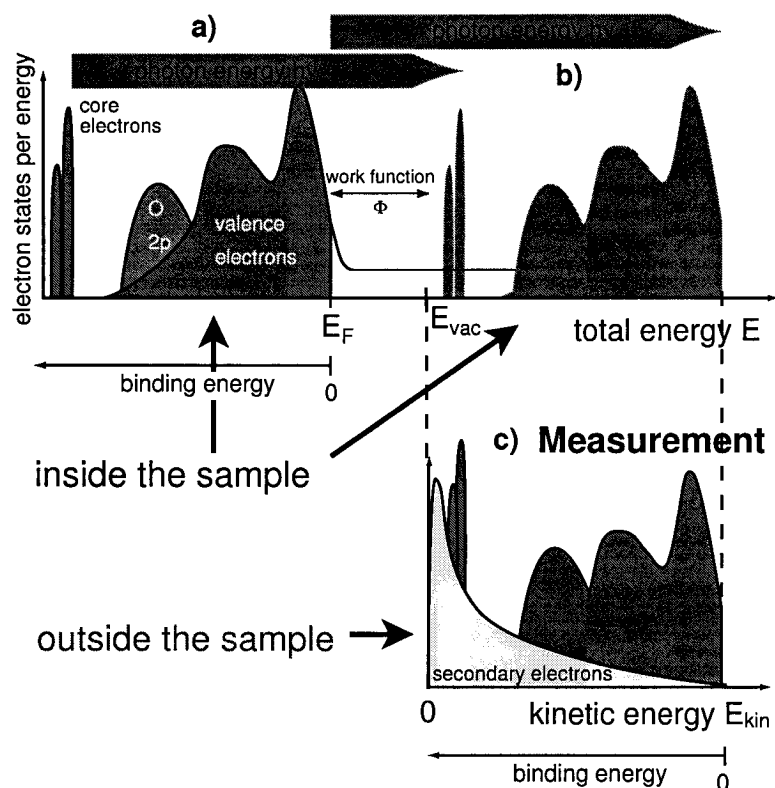


**Figure A.2:** Schematic UPS principle: (a) The electronic structure of a metal with adsorbed oxygen atoms as example. (b) The light increases the energy of the electrons by  $h\nu$ . Electrons with energy higher than the vacuum energy  $E_{vac}$  can escape the sample. (c) Some electrons are scattered and visible as a characteristic distribution superposing the measurement.

1. Optical excitation of the electrons to energies above the vacuum level  $E_{vac}$  with the photon energy  $h\nu$ .
2. Traveling of the electrons to the sample surface (with the possibility of scattering).
3. Escape of the electrons into the vacuum.

The inelastic electron scattering deteriorates the information on the energetic origin of the electrons and gives a characteristic distribution of electrons at low kinetic energies. Because of the high scattering probability only electrons from the surface can leave the sample. The average mean free path length for electrons in almost all materials is 0.5 nm (UPS) to 2 nm (XPS) [114]. This means that photoelectron spectroscopy is a very surface sensitive method and that UHV is required to avoid contamination of the sample.

In this work a hemispherical electron analyzer (VG clam II) was used to detect the electrons.



Depending on the photon energy, the accessible energetic depth of the excited electrons can be varied. The result and interpretation of measurements observed with the different photon energies of UV-light and X-rays are so different, that they will be described in the following two separate subsections.

### A.3.1 Excitation with X-rays

If X-rays are used to excite the electrons in photoelectron spectroscopy, strongly bonded electrons can escape the sample. This type of measurements is called X-ray Photoelectron Spectroscopy (XPS) or Electron Spectroscopy for Chemical Analysis (ESCA). In this work, a X-ray gun with 1253.6 eV (Mg  $K_{\alpha}$ ) and 1486.6 eV (Al  $K_{\alpha}$ ) photons acted as photon source for the XPS measurements.

The electrons with deep binding energy (more than 15 eV) interact only weakly with the electrons of other atoms. They are very localized and their electronic states are comparable to the free atom. Only sharp energy levels, mainly influenced by the atomic structure, are allowed. This sharp energetic levels give a fingerprint of the atoms and can be only shifted slightly by the surrounding atoms. This fact can be used for the identification of elements on sample surfaces. Not only a qualitative identification of the elements can be made, also quantitative results can be obtained by XPS. In particular, the ratio of elements in alloys can be easily measured with a calibration measurement on a sample with a known ratio.

In XPS measurements secondary electrons play a minor role, because of the high kinetic energy of the unscattered electrons.

### A.3.2 Excitation with high energy ultraviolet light

If ultraviolet ((UV)) light excites the electrons, the method is called Ultraviolet Photoelectron Spectroscopy (UPS). In this work a helium discharge lamp generated photons from the helium  $1s2p \rightarrow 1s^2$  transition with 21.22 eV ( $\lambda = 58$  nm) and from  $2p \rightarrow 2s$  light with 40.8 eV ( $\lambda = 30$  nm). Here, only relatively weakly bound electrons can escape the sample. The transition can be described as a transition from bound electrons to free electrons.

Due to the high resolution of electron spectroscopy at lower kinetic energies, values like the work function for metals or the ionization potential for excitation from the Highest Occupied Molecular Orbital (HOMO) in organic materials can be obtained. These values are important to understand the injection mechanisms in OLEDs (see section 1.3.1). Unfortunately, unoccupied states like the Lowest Unoccupied Molecular Orbital (LUMO) can not

be measured by this method.

The sample is electrically contacted and a bias voltage can be applied in relation to the electron analyzer. This bias voltage is needed to overcome the electron analyzer work function and to accelerate the slow electrons from states with higher binding energy to higher kinetic energies, where the electron analyzer is more sensitive. Eq. A.5 has to be extended by adding a term that accounts for the energy added by the bias voltage  $V_{bias}$  (this is a negative voltage value).

$$h\nu = \Phi + E_{bind} + E_{kin} + e \cdot V_{bias} \quad (\text{A.6})$$

The energy of the vacuum cut-off edge<sup>2</sup> and the FERMI-level or LUMO, together with the photon energy  $h\nu$  can be extracted from the EDC-curves to derive the work function or the ionization potential.

The UPS measurements shown in this work use the binding energy as energy axis. All the corrections by bias voltage, work function and photon energy are considered.

For further information about photoelectron spectroscopy please refer to [114,115].

## A.4 Electrical characterization

The materials investigated in this work (*e.g.* magnesium, Alq<sub>3</sub> and NPB) are very sensitive to atmospheric gases. Therefore a contamination-free measurement of the electrical properties was performed.

A small UHV chamber was built to characterize the OLEDs inside the UHV. This chamber was attached to the transfer system of the existing apparatus.

The chamber is equipped with a turbo molecular pump, a pressure gauge, a leak valve, a mechanical linear / rotation feedthrough, 8 contacts wired to an electrical feedthrough, and two viewports. The whole chamber can be separated from the transfer chamber with a valve. It can be individually flooded with air or with other gases. Fig. 2.7 in section 2.3 on page 35 (left) shows a viewport with an operating OLED sample inside the chamber and a close-up view with the sample on the sample holder (right). The light leaving the OLED is reflected by an aluminium mirror, exits the UHV system through a glass window, and can be measured by a Minolta LS100 luminance meter. The losses caused by the mirror and the glass windows are estimated to be of the order of 15%.

<sup>2</sup> The vacuum cut-off edge corresponds to the electrons with  $E_{kin} = 0$ .

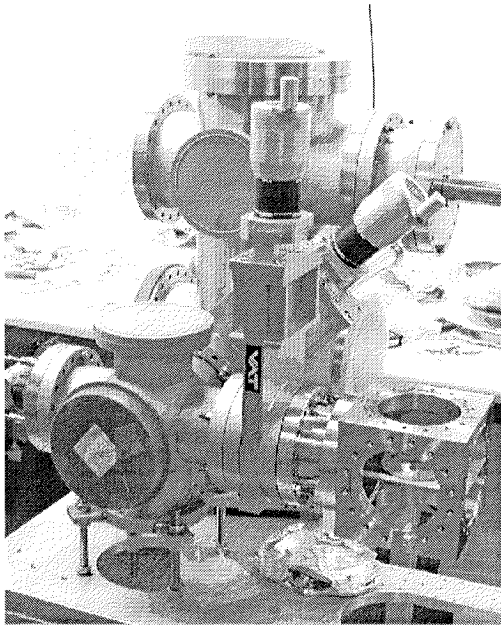


**Figure A.3:** Picture of the transportable chamber during assembling. It consists of a portable part (cube (size:  $(15\text{ cm})^3$ ), right below, here without vacuum flanges), two vacuum valves (VAT) and a sample storage lift in the back. The cube can be equipped either with viewports or electrical feedthroughs or both. The sample lift can store five samples. The whole extension is now connected to the transfer system of the UHV system.

The electrical measurements in the were initially obtained by a self made measurement device consisting of a computer controlled digital to analog converter and an analog-to-digital converter. It was later improved by a FLUKE-45 multimeter and afterwards by a Keithley 6430 sub-femtoamp source meter.

A portable UHV chamber with a load-lock system and a sample storage elevator was also designed and successfully built during this work for future measurements on samples in UHV in labs outside the UHV apparatus (Fig. A.3). It is now attached to the transfer system of the UHV system.

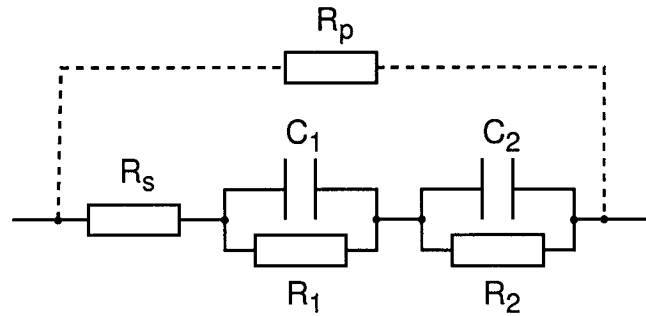
## A.5 Impedance spectroscopy

A dielectric material within two contacts acts as a capacitor. Therefore the OLED can be described by a capacity  $C = \epsilon\epsilon_0 A/d$  where  $\epsilon$  is the dielectric constant of the dielectric material,  $\epsilon_0$  is the permittivity of vacuum,  $A$  is the area of the OLED, and  $d$  is the thickness of the organic layers. Due to the injection properties of the contacts the device can not be described by the capacity alone. A resistance parallel to the capacitance improves the electrical model of an OLED. For the thin film contacts, there are contact resistances as well and a serial resistance completes the circuit.

If there is more than one organic material, the different dielectric constants, conductivities or charge accumulation on the interfaces can divide the device in more than one capacitance and resistance. For two layer devices the circuit shown in Fig. A.4 was used.

The complex impedance of such a system is

**Figure A.4:** For high frequency measurements a two-layer OLED can be described by a pair of parallel resistance and capacitance ( $R_1, C_1, R_2, C_2$ ) and a contact resistance  $R_s$ . The parallel resistance  $R_p$  can be used to limit the entire real impedance.



$$\mathcal{Z} = R_s + \left( \frac{1}{R_1} - i\omega C_1 \right)^{-1} + \left( \frac{1}{R_2} - i\omega C_2 \right)^{-1} \quad (\text{A.7})$$

This complex impedance was measured by a HP4192A impedance analyzer. The measurements can be fitted with the function above to get the values for  $R_1, R_2, C_1, C_2, R_s$ . Especially the value of  $R_s$  is very easy to investigate. At high frequencies the impedance of the capacities becomes zero and the measured impedance is equal to the resistance  $R_s$ . The measurement range of the HP4192A is limited to max. 1.13 M $\Omega$ , but the resistances  $R_1, R_2$  are usually higher ( $> 10$  M $\Omega$ ). In order to measure more points at low frequencies, an additional, well known resistance  $R_p$  can be used to reduce the maximum real impedance (dotted connections in Fig. A.4). The fit-function has to be extended:

$$\mathcal{Z}' = \left( \left( R_s + \left( \frac{1}{R_1} - i\omega C_1 \right)^{-1} + \left( \frac{1}{R_2} - i\omega C_2 \right)^{-1} \right)^{-1} + \frac{1}{R_p} \right)^{-1} \quad (\text{A.8})$$

At low frequency the resistance is now dominated by the value of  $R_p$ , but if the real part of the value  $\mathcal{Z}(\omega)$  comes close to  $4 \cdot R_p$  the resulting impedance change can be detected. The range of measurement has been extended to about 4 M $\Omega$  without dramatic loss of resolution.

Seite Leer /  
Blank leaf

# B Material and Interface Properties

The first published organic light-emitting thin film device [1] was produced with the organic molecular material  $\text{Alq}_3$  and a diamine as the hole transport material. Up to now,  $\text{Alq}_3$  is one of the most widely used materials for green emitting devices. It was the aim of this work to study the fundamental properties of widely used organic materials. Most of the experiments are adaptable to other organic materials. All the samples shown in this work were fabricated with  $\text{Alq}_3$ , NPB, (organic materials) and Mg, Ag, ITO (inorganic materials).

## B.1 $\text{Alq}_3$

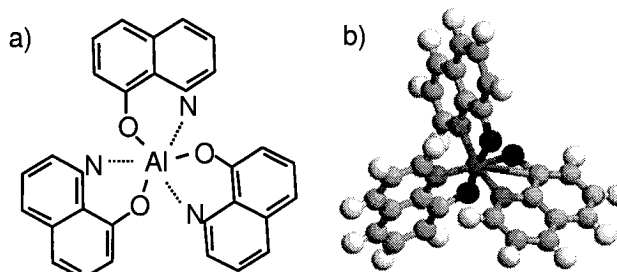
Tris (8-hydroxy-quinoline) aluminium ( $\text{Alq}_3$ ) (Fig. B.1) is a so called “electron transport” material. The electron mobility ( $\mu_{\text{electron}} \approx 1 \cdot 10^{-7} \text{ cm}^2/\text{Vs}$  see section 2.6) and ionization potential<sup>1</sup> ( $E_{\text{IP}} = 6.0 \text{ eV}$ ) have been measured in this work.

From the UPS measurement shown in Fig. B.2 the energetic position of the HOMO relative to the vacuum energy and FERMI-level<sup>2</sup> can be obtained. Thin films of  $\text{Alq}_3$  on Mg substrates lead to strongly bound electrons in the HOMO ( $E_{\text{HOMO}} = 3.0 \pm 0.1 \text{ eV}$  from Fig. B.2). Therefore,

<sup>1</sup> The ionization potential is defined by the difference of the HOMO energy and the vacuum energy. It is similar to the work function in metals and gives the minimum photon energy for photoexcited electrons in an insulator.

<sup>2</sup> The position of the substrate (here Mg) FERMI-Level gives the origin of the binding energy. I use here positive values for the binding energy of occupied states and negative for unoccupied states.

**Figure B.1:** (a) Chemical structure formula and (b) 3D-visualization of tris (8-hydroxyquinoline) aluminium ( $\text{Alq}_3$ ).



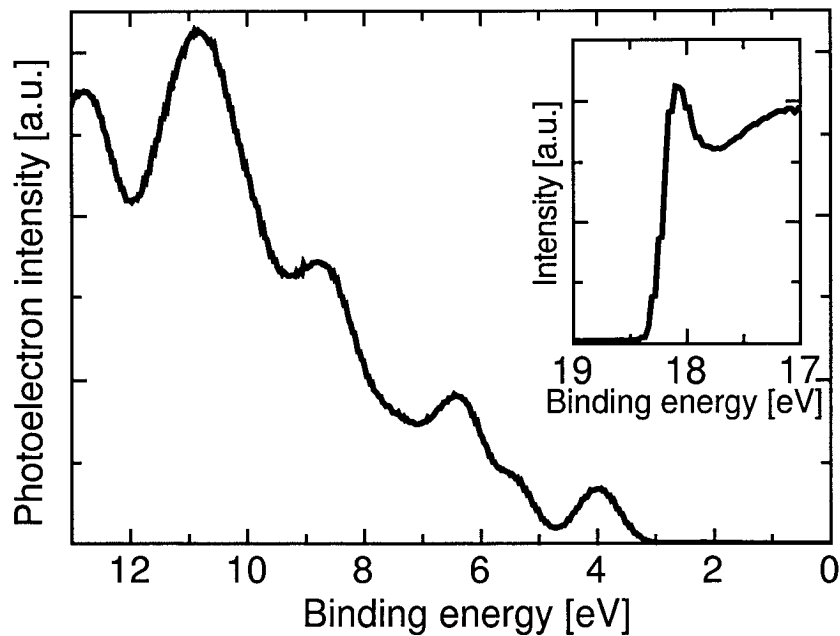


**Figure B.2:** UPS-spectra of Alq<sub>3</sub>. The HOMO starts at 3.0 eV binding energy and the inset shows the vacuum energy cutoff edge. With the knowledge of the photon energy ( $h\nu = 21.2$  eV) the ionization potential  $E_{IP} = 6.0$  eV can be derived.

considering the difference  $E_{HOMO} - E_{LUMO} = 3.3 \pm 0.16$  eV obtained with tunnel-spectroscopy [116], the LUMO has to be  $0.3 \pm 0.26$  eV above the Mg FERMI-level and ohmic contacts without injection barriers (see section 2.6 and section 2.7) might be formed by barrier reduction due to image charge effect (up to 0.2eV, see section 1.3.1). Direct measurements of the LUMO position of Alq<sub>3</sub> have been performed by tunnel-spectroscopy experiments [116] on gold and silver substrates and give a minimum injection threshold for electron injection of 0.8eV. Almost all values for the LUMO positions of Alq<sub>3</sub> on magnesium substrates in the literature are estimated from the HOMO position measured by UPS combined with the optical gap (see below) and obtain values between  $E_{LUMO} = -0.1$  eV and  $E_{LUMO} = -0.6$  eV [73, 117–120] in binding energy. Moreover the sequence of deposition changes the interfacial electronic structure, Alq<sub>3</sub> on Mg gives different UPS measurements compared to Mg on Alq<sub>3</sub> [73]. Other direct measurements using internal photoemission experiments are reported in Ref. 91 and Ref. 121. They give a value of  $E_{LUMO} = -0.6$  eV. The fact that I could show ohmic contact formation in the Mg/Alq<sub>3</sub> interface (section 2.6 and section 2.7), hints at a very small injection barrier for electrons and therefore a small binding energy for  $E_{LUMO}$ . The most direct measurement was presented in Ref. 116 and gives the most reasonable value (see above)  $E_{LUMO} = 0.3 \pm 0.26$  eV.

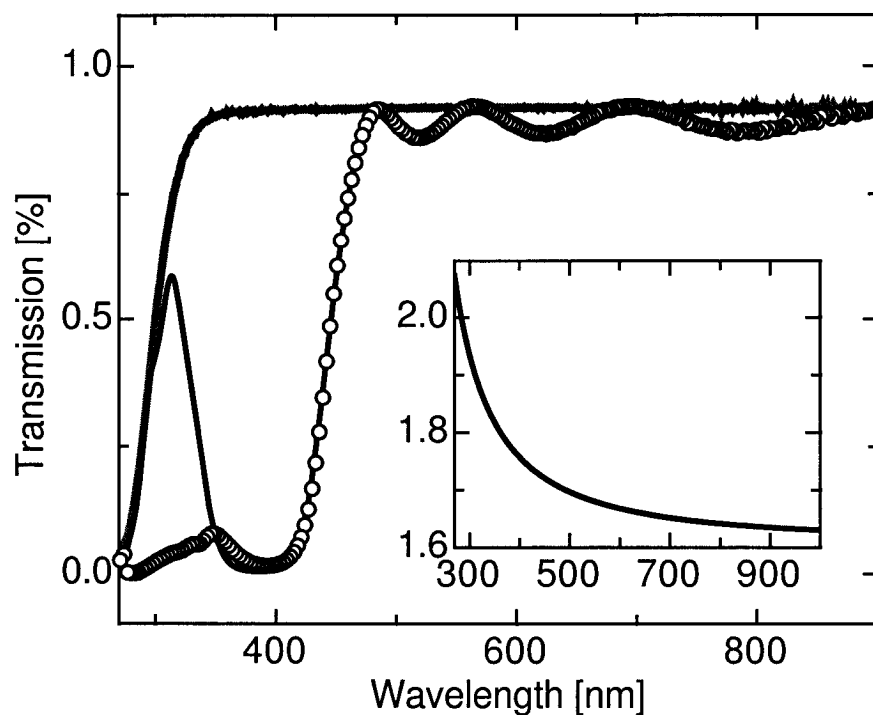


**Figure B.3:** Optical transmission spectra of Alq<sub>3</sub> (open circles) on glass and glass alone (gray curve). To obtain the thickness of the Alq<sub>3</sub> film the data were fitted (black curve) taking into account multiple reflections, a gaussian absorption peak and refractive index dispersion (courtesy of A. Tapponnier). The inset shows the dispersion of the refractive index over the wavelength as it was used for the theoretical model.

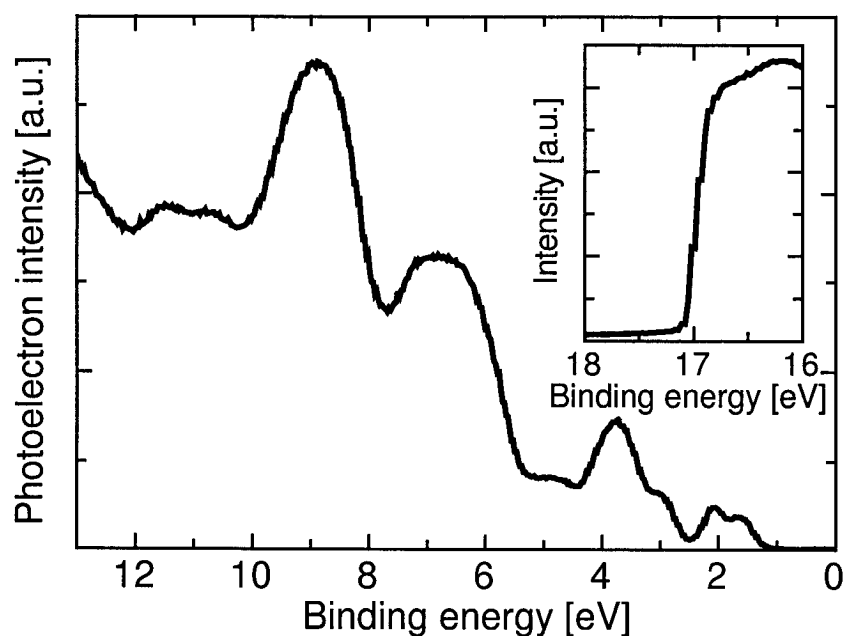


**Figure B.4:** UPS-spectra of NPB. The HOMO starts at 1.3 eV binding energy and the inset shows the vacuum energy cutoff edge. The resulting ionization potential is  $E_{IP} = 5.5$  eV



Fig. B.3 (open circles) shows an optical transmission spectra of a Alq<sub>3</sub> film on a glass substrate<sup>3</sup>. The transmission oscillation within 500 nm and 900 nm is caused by multiple reflections inside the Alq<sub>3</sub> film. By fitting the data with a model taking into account multiple reflections with a gaussian absorption peak and a refractive index dispersion (black line in Fig. B.3), the real thickness of the Alq<sub>3</sub> films have been measured. Fig. B.3 shows the best-fit curve achieved for 850 nm film thickness. These measurements were used to compare with the results from other thickness measurement methods:  $\alpha$ -step, quartz microbalance and RUTHERFORD-backscattering.

From the measurement in Fig. B.3 the optical gap energy  $E_{\text{gap}} = 2.66$  eV can be determined by the beginning of the absorption edge of Alq<sub>3</sub> (465 nm) and is comparable to the reported value 2.7 eV [73, 122]. Other groups published different values for the optical gap energy, *e.g.* 2.8 eV [64, 123] or 3.17 eV [124]. The difference might result from different definitions of the optical gap energy. I define the lowest energy, where absorption starts to appear, as optical gap energy. The maximum of the light emission generated by photoluminescence or electroluminescence is at 531 nm (2.33 eV) [1, 38, 55, 125–141] and the emission color is green. The density of the material is  $\rho = 1.51 \pm 0.03$  g/cm<sup>3</sup> [87] and the molecular mass 459 g/mol (C<sub>27</sub>H<sub>18</sub>N<sub>3</sub>O<sub>3</sub>Al). This data has been used for thickness calibrations with RUTHERFORD-backscattering measurements [87]. The Alq<sub>3</sub> has been purchased at Eastman Kodak and purified by evaporation inside an effusion cell or outside in a special sublimation machine until small crystals were formed. The material purity is a very important factor in these experiments. The reproducibility of the electrical measurements was much better with Alq<sub>3</sub> pulverized from the small crystals (see also section 2.7).

## B.2 NPB

N,N'-bis-{1-naphthyl}-N,N'-diphenyl-1,1'-biphenyl-4,4'-diamine (NPB or  $\alpha$ -NPD) (Fig. B.5) is a “hole transport material”. The glass transition temperature, an indicator of the thermal stability of the device, is 95° C [61, 142] and the melting point is 278° C (according to the material specifications from Eastman Kodak). Fig. B.4 shows the UPS spectra of NPB on ITO (see next section) and the inset gives a close-up of the vacuum cutoff edge for the determination of the ionization potential. The energy of the HOMO relative to FERMI-level of the ITO can be determined from Fig. B.4 and results in  $E_{\text{HOMO}} = 1.3$  eV. This value is in good agreement with the literature value of 1.4 eV [143]. The ionization potential can also be quantified from the

<sup>3</sup> The transmission of the glass (gray curve) is also displayed in Fig. B.3

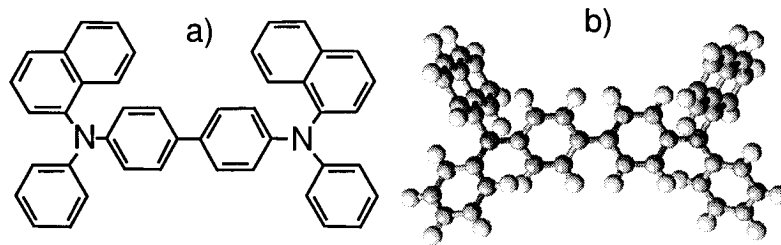


**Figure B.5:** (a) Chemical structure and (b) 3D-visualization of the N,N'-bis-{1-naphthyl}-N,N'-diphenyl-1,1'-biphenyl-4,4'-diamine (NPB or  $\alpha$ -NPD) molecule.

position of the vacuum cut off, the LUMO position and the photon energy. The resulting  $E_{IP} = 5.5$  eV lies within the literature data: 5.2 eV [118] and 5.7 eV [122]. The optical absorption starts at 400 nm (3.1 eV) [144].

## B.3 ITO

The most widely used material for OLED anodes is Indium tin oxide (ITO) because of its availability (also used for liquid crystal displays), high transparency (96% measured at 531nm for the ITO samples of this work) and good electrical conductivity [145–147]. The work function of the ITO samples in this work has been measured by UPS. A UPS spectra is shown in Fig. B.6, the extracted work function value is  $\Phi_{ITO} = 5.2$  eV. From the UPS measurement one can see only a small number of electrons at the FERMI-level, but enough to create a reasonable electrical conduction. The work function value is very sensitive to the pre-treatment and fabrication process [46, 148, 149].

## B.4 Magnesium

The electronic properties of magnesium and their changes by oxidation are described in the section 2.3 and section 2.5 respectively.

## B.5 Magnesium:Silver

A widely used cathode structure in the literature is the Mg:Ag (10:1) alloy with enhanced stability during device operation compared to pure Mg [24, 25, 44, 46, 57, 62, 65, 67–69, 76, 78, 136, 150–159]. There are some doubts regarding the homogeneity of the alloy towards the interface with Alq<sub>3</sub> due to the known interface reaction of Mg [73, 160, 161], which leads to a low sticking coefficient during the evaporation.

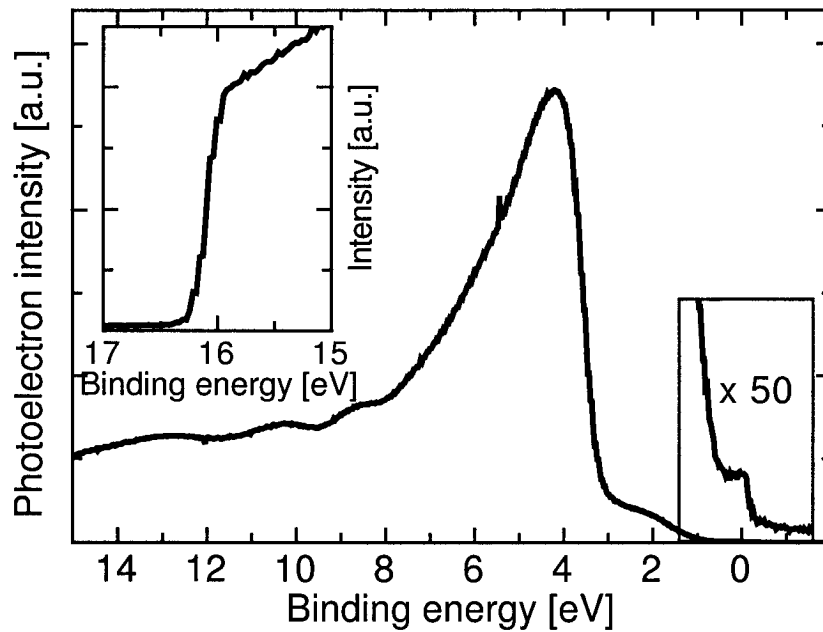


**Figure B.6:** UPS-spectra of ITO. The FERMI-edge is shown in a close up view (50x magnification factor) and the inset gives the position of the vacuum energy cutoff.

A 90 nm thick  $\text{Alq}_3$  film was fabricated on an ITO substrate and a 120 nm Mg:Ag film, with a ratio nearly 10:1, was deposited on top. XPS measurements were performed at 285 eV (carbon 1s signal), 531 eV (oxygen 1s), 368 eV (silver 3d) and 50 eV (magnesium 2p) with alternating sputtering using argon ions to get a depth profile. The sputter speed is different for different materials (here Mg:Ag and  $\text{Alq}_3$ ) and therefore only a qualitative analysis is shown in Fig. B.7. The XPS-signal of the corresponding energy is plotted vs. the number of sputter cycles. From the first diagram the position of the organic layer (the only material with carbon) can be estimated. The beginning of the carbon signal is shown in all diagrams as a gray background. The sample is slightly oxidized<sup>4</sup> on the surface (see the second diagram) and towards the organic interface the silver signal grows and the magnesium signal drops (third and fourth diagram). The calculated ratio of the silver / magnesium signal shows unequivocally that the interface is dominated by silver (the XPS-Signal of silver is about 3 times higher at its maximum compared to the surface value). Hence, the resulting work function at the interface will be dominated by the value of silver ( $\Phi_{\text{Ag}} = 4.6 \text{ eV}$  [114]).

If  $\text{Alq}_3$  is deposited on Mg:Ag films this interface problem will not happen. There is a good reason to doubt the symmetry of Mg:Ag /  $\text{Alq}_3$  / Mg:Ag

<sup>4</sup> The sample has been stored for one day after fabrication in the UHV before the measurement has been performed.

devices regarding the work function value and therefore the electrical properties. Therefore only magnesium was used in this work for devices with symmetrical contacts (see section 2.6 and section 2.7), the electrical symmetry of the Mg contacts on Alq<sub>3</sub> is shown in section 2.7.

It has to be mentioned that with the number of sputter cycles the roughness of the sample increases (especially within the organic layer) and therefore the interface is not visible in the measurement as a sharp transition (based on experiences during this work and visible in Fig. B.7 as large silver and magnesium signal within the organic region).

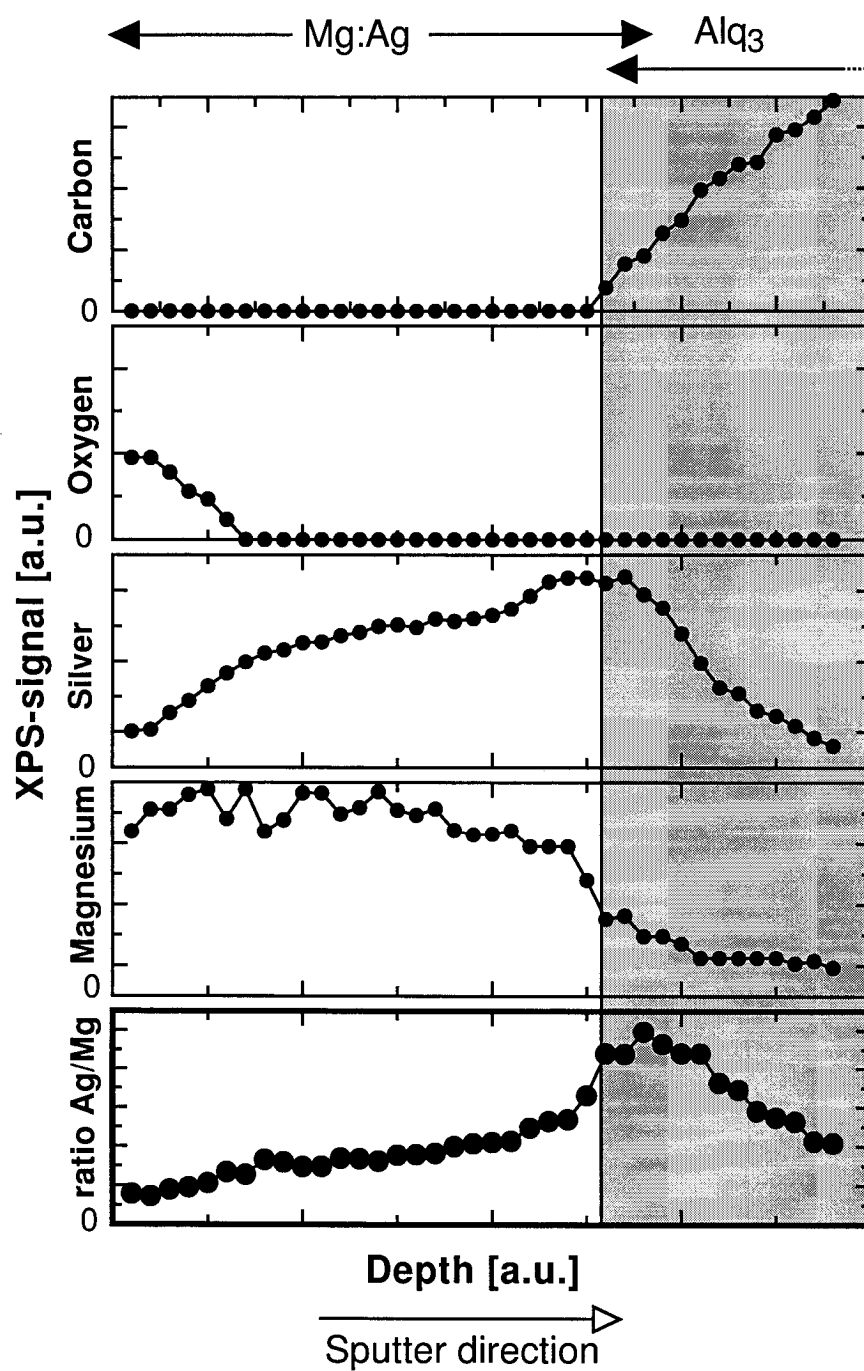


Figure B.7: XPS-signal of C, O, Ag, Mg and the ratio of the Ag / Mg signal plotted vs. the number of sputter cycles of a Mg:Ag / Alq<sub>3</sub> sample. The left side corresponds to the Mg:Ag surface, the gray background shows the measurement within the organic layer.

---

# Bibliography

- [1] C. W. Tang and S. A. VanSlyke  
*Organic electroluminescent diodes*  
Appl. Phys. Lett. **51**(12), 913–915 (1987)
- [2] M. Pope, H. Kallmann, and P. Magnante  
*Electroluminescence in organic crystals*  
J. Chem. Phys. **38**, 2042–2043 (1963)
- [3] W. Helfrich and W. G. Schneider  
*Recombination Radiation in Anthracene Crystals*  
Phys. Rev. Lett. **14**(7), 229–231 (1965)
- [4] C. K. Chiang, C. R. Fincher, Y.W. Park, A. J. Heeger, H. Shirakawa, E. J. Louis, S. C. Gau, and A. G. MacDiarmid  
*Electrical Conductivity in Doped Polyacetylene*  
Phys. Rev. Lett. **39**, 1098 (1997)
- [5] J. H. Burroughes, D. D. C. Bradley, A. R. Brown, R. N. Marks, K. Mackay, R. H. Friend, P. L. Burns, and A. B. Holmes  
*Light-emitting diodes based on conjugated polymers*  
Nature **347**(6293), 539–541 (1990)
- [6] J. H. Schön, Kloc Ch, and B. Batlogg  
*Fractional quantum Hall effect in organic molecular semiconductors*  
Science **288**(5475), 2338–2340 (2000)
- [7] J. H. Schön, C. Kloc, A. Dodabalapur, and B. Batlogg  
*An organic solid state injection laser*  
Science **289**, 599–601 (2000)
- [8] J. H. Schön, A. Dodabalapur, C. Kloc, and B. Batlogg  
*A light-emitting field-effect transistor*  
Science **290**(549), 963–965 (2000)
- [9] J. H. Schön, C. Kloc, and B. Batlogg  
*Superconductivity in molecular crystals induced by charge injection*  
Nature **406**(6797), 702–704 (2000)
- [10] J. H. Schön, A. Dodabalapur, Z. Bao, Kloc Ch, O. Schenker, and B. Batlogg  
*Gate-induced superconductivity in a solution-processed organic polymer film*  
Nature **410**(6825), 189–192 (2001)
- [11] M. Kiy  
*Organisch ins nächste Jahrhundert*  
c't (Heise Verlag) **13**, 43 (1999)
- [12] M. Kiy  
*Molekulares Leuchten - Organische Displays auf dem Vormarsch*  
c't (Heise Verlag) **20**, 110–113 (2000)
- [13] M. Kiy  
*Moleculaire verlichting : de opmars van organische displays*  
c't (Heise Verlag) **12**, 82–86 (2000)

- [14] A. Ioannidis, E. Forsythe, Yongli Gao, M. W. Wu, and E. M. Conwell  
*Current-voltage characteristic of organic light emitting diodes*  
Appl. Phys. Lett. **72**(23), 3038–3040 (1998)
- [15] A. J. Campbell, D. D. C. Bradley, and D. G. Lidzey  
*Space-charge limited conduction with traps in poly(phenylene vinylene) light emitting diodes*  
J. Appl. Phys. **82**(12), 6326–6342 (1997)
- [16] V. I. Arkhipov, E. V. Emelianova, Y. H. Tak, and H. Bässler  
*Charge injection into light-emitting diodes: Theory and experiment*  
J. Appl. Phys. **84**(2), 848 (1998)
- [17] V. I. Arkhipov, U. Wolf, and H. Bässler  
*Current injection from a metal to a disordered hopping system. II. Comparison between analytic theory and simulation*  
Phys. Rev. B **59**(11), 7514–7520 (1999)
- [18] J. Staudigel, M. Stössel, F. Steuber, and J. Simmerer  
*A quantitative numerical model of multilayer vapor-deposited organic light emitting diodes*  
J. Appl. Phys. **86**(7), 3895–3910 (1999)
- [19] U. Wolf and H. Bässler  
*Enhanced electron injection into light-emitting diodes via interfacial tunneling*  
Appl. Phys. Lett. **74**(25), 3848–3850 (1999)
- [20] U. Wolf, V. I. Arkhipov, and H. Bässler  
*Current injection from a metal to a disordered hopping system. I. Monte Carlo simulation*  
Phys. Rev. B **59**(11), 507–7513 (1999)
- [21] J. Yang and J. Shen  
*Effects of discrete trap levels on organic light emitting diodes*  
J. Appl. Phys. **85**(5), 2699 (1999)
- [22] G. Horowitz  
*Organic field-effect transistors*  
Advanced Materials **10**(5), 365–377 (1998)
- [23] G. Malliaras and J. Scott  
*Numerical simulation of the electrical characteristics and the efficiencies of single-layer organic light emitting diodes*  
J. Appl. Phys. **85**(10), 7426 (1999)
- [24] M. A. Baldo and S. R. Forrest  
*Interface-limited injection in amorphous organic semiconductors*  
Phys. Rev. B **64**(8), 085201/1–085201/17 (2001)
- [25] S. Barth, U. Wolf, H. Bässler, P. Müller, H. Riel, H. Vestweber, P. F. Seidler, and W. Riess  
*Current injection from a metal to a disordered hopping system. III. Comparison between experiment and Monte Carlo simulation*  
Phys. Rev. B **60**(12), 8791–8797 (1999)
- [26] I. D. Parker  
*Carrier tunneling and device characteristics in polymer light-emitting diodes*  
J. Appl. Phys. **75**(3), 1656–1666 (1994)

- [27] M. Koehler and I. A. Hümmelgen  
*Temperature dependent tunnelling current at metal/polymer interfaces-potential barrier height determination*  
Appl. Phys. Lett. **70**(24), 3254–3256 (1997)
- [28] Y. Yang and A. J. Heeger  
*Polyaniline as a transparent electrode for polymer light-emitting diodes: lower operating voltage and higher efficiency*  
Appl. Phys. Lett. **64**(10), 1245–1247 (1994)
- [29] M. Matsumura, T. Akai, M. Saito, and T. Kimura  
*Height of the energy barrier existing between cathodes and hydroxyquinoline-aluminum complex of organic electroluminescence devices*  
J. Appl. Phys. **79**(1), 264–268 (1996)
- [30] J. Godlewski and J. Kalinowski  
*Injection-limited currents in insulators*  
Jpn. J. Appl. Phys. **28**(1), 24–38 (1989)
- [31] Several authors  
*Organic electroluminescent materials and devices*  
Gordon and Breach Publishers, 1 edition (1997)
- [32] Murray A. Lampert and Peter Mark  
*Current injection in solids*  
Academic Press, New York and London (1970)
- [33] Murray A. Lampert  
*Simplified Theory of Space-Charge-Limited Currents in an Insulator with Traps*  
Phys. Rev. **103**(6), 1648–1656 (1956)
- [34] Murray A. Lampert  
*Injection Currents in Insulators*  
Proceedings of the IRE **50**(8), 1781–1795 (1962)
- [35] N. F. Mott and R. W. Gurney  
*Electronic Processes in Ionic Crystals*  
Oxford University Press, New York (1940)
- [36] A. Rose  
*Space-Charge-Limited Currents in Solids*  
Phys. Rev. **97**(6), 1538–1544 (1954)
- [37] P. Losio  
*Charge injection and transport in Alq<sub>3</sub>*  
unpublished, (2001)
- [38] A. Dodabalapur, L. J. Rothberg, R. H. Jordan, T. M. Miller, R. E. Slusher, and J. M. Phillips  
*Physics and applications of organic microcavity light emitting diodes*  
J. Appl. Phys. **80**(12), 954–964 (1996)
- [39] G. G. Malliaras and J. C. Scott  
*The roles of injection and mobility in organic light emitting diodes*  
J. Appl. Phys. **83**(10), 5399 (1998)
- [40] Y. Kawabe, G. E. Jabbour, S. E. Shaheen, B. Kippelen, and N. Peyghambarian  
*A model for the current-voltage characteristics and the quantum efficiency of single-layer organic light emitting diodes*  
Appl. Phys. Lett. **71**(10), 1290 (1997)



- [41] A. Boehler, S. Dirr, H-H. Johannes, D. Ammermann, and W. Kowalsky  
*Influence of the process vacuum on the device performance of organic light-emitting diodes*  
Synth. Met. **91**(1-3), 95-97 (1997)
- [42] T. A. Beierlein, W. Brütting, H. Riel, E. I. Haskal, P. Müller, and W. Rieß  
*Kelvin Probe Investigations of Metal Work Functions and Correlation to Device Performance of Organic Light-Emitting Devices*  
IBM Research Report **RZ3143**(93189) (1999)
- [43] I. H. Campbell, D. L. Smith, and J. P. Ferraris  
*Electrical impedance measurements of polymer light-emitting diodes*  
Appl. Phys. Lett. **66**(22), 3030-3032 (1995)
- [44] F. Steuber, J. Staudigel, M. Stössel, J. Simmerer, and A. Winnacker  
*Reduced operating voltage of organic electroluminescent devices by plasma treatment of the indium tin oxide anode*  
Appl. Phys. Lett. **74**(23), 3558 (1999)
- [45] B. Choi, H. Yoon, and H. H. Lee  
*Surface treatment of indium tin oxide by SF6 plasma for organic light-emitting diodes*  
Appl. Phys. Lett. **76**(4), 412 (2000)
- [46] C. C. Wu, C. I. Wu, J. C. Sturm, and A. Kahn  
*Surface modification of indium tin oxide by plasma treatment: An effective method to improve the efficiency, brightness, and reliability of organic light emitting devices*  
Appl. Phys. Lett. **70**(11), 1348 (1997)
- [47] H. Tang, F. Li, and J. Shinar  
*Bright high efficiency blue organic light-emitting diodes with Al<sub>2</sub>O<sub>3</sub>/Al cathodes*  
Appl. Phys. Lett. **71**(18), 2560 (1997)
- [48] Masenelli-B; Tutis-E; Bussac-MN; Zuppiroli-L  
*Numerical model for injection and transport in multilayers OLEDs*  
Synth. Met. **122**(1), 141-144 (2001)
- [49] F. Li, H. Tang, J. Andereg, and J. Shinar  
*Fabrication and electroluminescence of double-layered organic light-emitting diodes with the Al<sub>2</sub>O<sub>3</sub>/Al cathode*  
Appl. Phys. Lett. **70**(10), 1233 (1997)
- [50] P. F. Tian, V. Bulovic, P. E. Burrows, G. Gu, S. R. Forrest, and T. X. Zhou  
*Precise, scalable shadow mask patterning of vacuum-deposited organic light emitting devices*  
J. Vac. Sci. Technol. A **17**(5), 2975 (1999)
- [51] I. H. Campbell, D. L. Smith, C. J. Neef, and J. P. Ferraris  
*Charge transport in polymer light-emitting diodes at high current density*  
Appl. Phys. Lett. **75**(6), 841-843 (1999)
- [52] G. G. Malliaras, J. R. Salem, P. J. Brock, and J. C. Scott  
*Photovoltaic measurement of the built-in potential in organic light emitting diodes and photodiodes*  
J. Appl. Phys. **84**(3), 1583-1587 (1998)
- [53] D. Kolosov, D. S. English, V. Bulovic, P. F. Barbara, S. R. Forrest, and M. E. Thompson

- Direct observation of structural changes in organic light emitting devices during degradation*  
J. Appl. Phys. **90**(7), 3242–3247 (2001)
- [54] B. K. Crone, I. H. Campbell, P. S. Davids, D. L. Smith, C. J. Neef, and J. P. Ferraris  
*Device physics of single layer organic light-emitting diodes*  
J. Appl. Phys. **86**(10), 5767 (1999)
- [55] G. Gu, G. Parthasarathy, P. E. Burrows, P. Tian, I. G. Hill, A. Kahn, and S. R. Forrest  
*Transparent stacked organic light emitting devices. I. Design principles and transparent compound electrodes*  
J. Appl. Phys. **86**(8), 4067 (1999)
- [56] A. Kraft, A. C. Grimsdale, and A. B. Holmes  
*Electroluminescent conjugated polymers - seeing polymers in a new light*  
Angew. Chem. Int. Ed. **37**, 402 (1998)
- [57] P. E. Burrows, V. Bulovic, S. R. Forrest, L. S. Sapochak, D. M. McCarty, and M. E. Thompson  
*Reliability and degradation of organic light emitting devices*  
Appl. Phys. Lett. **65**(23), 2922 (1994)
- [58] J. Shi and C. W. Tang  
*Doped organic electroluminescent devices with improved stability*  
Appl. Phys. Lett. **70**(13), 1665 (1997)
- [59] G. E. Jabbour, Y. Kawabe, S. E. Shaheen, J. F. Wang, M. M. Morrell, B. Kippelen, and N. Peyghambarian  
*Highly efficient and bright organic electroluminescent devices with an aluminum cathode*  
Appl. Phys. Lett. **71**(13), 1762 (1997)
- [60] G. E. Jabbour, B. Kippelen, N. R. Armstrong, and N. Peyghambarian  
*Aluminum based cathode structure for enhanced electron injection in electroluminescent organic devices*  
Appl. Phys. Lett. **73**(9), 1185 (1998)
- [61] S. A. Van Slyke, C. H. Chen, and C. W. Tang  
*Organic electroluminescent devices with improved stability*  
Appl. Phys. Lett. **69**(15), 2160 (1996)
- [62] L. S. Hung, C. W. Tang, and M. G. Mason  
*Enhanced electron injection in organic electroluminescence devices using an Al/LiF electrode*  
Appl. Phys. Lett. **70**(2), 152 (1997)
- [63] L. S. Hung and C. W. Tang  
*Interface engineering in preparation of organic surface-emitting diodes*  
Appl. Phys. Lett. **74**(21), 3209 (1999)
- [64] L. S. Hung, L. S. Liao, C. S. Lee, and S. T. Lee  
*Sputter deposition of cathodes in organic light emitting diodes*  
J. Appl. Phys. **86**(8), 4607 (1999)
- [65] S. T. Lee, Z. Q. Gao, and L. S. Hung  
*Metal diffusion from electrodes in organic light-emitting diodes*  
Appl. Phys. Lett. **75**(10), 1404 (1999)

- [66] E. I. Haskal, A. Curioni, P. F. Seidler, and W. Andreoni  
*Lithium–aluminum contacts for organic light-emitting devices*  
Appl. Phys. Lett. **71**(9), 1151 (1997)
- [67] K. Chondroudis and D. B. Mitzi  
*The use of ionic salt dyes as amorphous, thermally stable emitting layers in organic light-emitting diodes*  
Appl. Phys. Lett. **76**(1), 58–60 (2000)
- [68] M. G. Mason, L. S. Hung, C. W. Tang, S. T. Lee, K. W. Wong, and M. Wang  
*Characterization of treated indium–tin–oxide surfaces used in electroluminescent devices*  
J. Appl. Phys. **86**(3), 1688 (1999)
- [69] S. Barth, P. Müller, H. Riel, P. F. Seidler, W. Rie, H. Vestweber, and H. Bässler  
*Electron mobility in tris(8-hydroxy-quinoline)aluminum thin films determined via transient electroluminescence from single- and multilayer organic light-emitting diodes*  
J. Appl. Phys. **89**(7), 3711–3719 (2001)
- [70] C. Shen, I. G. Hill, and A. Kahn  
*Role of electrode Contamination in electron injection at Mg:Ag/Alq<sub>3</sub> interfaces*  
Adv. Mater. **11**(18), 1523 (1999)
- [71] C. Shen, A. Kahn, and J. Schwartz  
*Chemical and electrical properties of interfaces between magnesium and aluminum and tris-(8-hydroxy quinoline) aluminum*  
J. Appl. Phys. **89**(1), 449–459 (2001)
- [72] Y. Tao, A. Kündig, C. Cai, B. Müller, and P. Günter  
*Inter-diffusion at the Mg / Alq<sub>3</sub> interface: an in-situ XPS study*  
unpublished  
About the growth of Mg on Alq and the better growth with an Ag thin insertion layer.
- [73] A. Rajagopal and A. Kahn  
*Photoemission spectroscopy investigation of magnesium-Alq<sub>3</sub> interfaces*  
J. Appl. Phys. **84**(1), 355–358 (1998)
- [74] M. Probst and R. Haight  
*Diffusion of metals into organic films*  
Appl. Phys. Lett. **70**(11), 1420 (1997)
- [75] H. Aziz, Z. Popovic, S. Xie, A.-M. Hor, N.-X. Hu, C. Tripp, and G. Xu  
*Humidity-induced crystallization of tris(8-hydroxyquinoline) aluminium layers in organic light-emitting devices*  
Appl. Phys. Lett. **72**(7), 756 (1998)
- [76] H. Aziz, Z. Popovic, C. P. Tripp, Nan Xing Hu, Ah Mee Hor, and Gu Xu  
*Degradation processes at the cathode/organic interface in organic light emitting devices with Mg:Ag cathodes*  
Appl. Phys. Lett. **72**(21), 2642–2644 (1998)
- [77] H. Aziz, Z. D. Popovic, N.-X. Hu, A.-M. Hor, and G. Xu  
*Degradation Mechanism of Small Molecule-Based Organic Light-Emitting Devices*  
Science **283**, 1900 (1999)

- [78] Q.T. Le, F. M. Avendano, E. W. Forsythe, Li Yan, Yongli Gao, and C. W. Tang  
*X-ray photoelectron spectroscopy and atomic force microscopy investigation of stability mechanism of tris-(8-hydroxyquinoline) aluminum-based light-emitting devices*  
J. Vac. Sci. Technol. A **17**(4), 2314 (1999)
- [79] M. Fujihira, L.-M. Do, A. Koike, and E.-M. Han  
*Growth of dark spots by interdiffusion across organic layers in organic electroluminescent devices*  
Appl. Phys. Lett. **68**(13), 1787–1789 (1996)
- [80] G. Horowitz, D. Fichou, X. Peng, and P. Delannoy  
*Evidence for a linear low-voltage space-charge-limited current in organic thin films. Film thickness and temperature dependence in alpha-conjugated sexithienyl*  
Journal de Physique **51**(13), 1489–1499 (1990)
- [81] P. Delannoy  
*Dark conductivity, photoconductivity and photovoltaic conversion in organic molecular solids*  
Materials Science **7**(1), 13–21 (1981)
- [82] R. Q. Zhang, X. Y. Hou, and S. T. Lee  
*Theory of magnesium/Alq<sub>3</sub> interaction in organic light emitting devices*  
Appl. Phys. Lett. **74**(11), 1612 (1999)
- [83] M. Kiy, I. Gamboni, U. Suhner, I. Biaggio, and P. Günter  
*Interface dependent electrical properties of organic light emitting devices in ultra high vacuum*  
Synth. Met. **111–112**, 307–310 (2000)
- [84] M. Kiy, I. Biaggio, and P. Günter  
*Photoelectron Spectroscopy on a running Organic Light Emitting Diode*  
Nonlinear Opt. **25**, 461–466 (2001)
- [85] S. A. Flodström, L.-G. Petersson, and S. B. M. Hagström  
*Photoemission study of clean and oxygen-covered aluminum and magnesium*  
Solid State Commun. **19**, 257 (1976)
- [86] R. Ono, P. Losio, I. Biaggio, and Günter  
*Impedance spectroscopy of Alq<sub>3</sub> based organic light emitting diodes in ultra high vacuum*  
Nonlinear Opt. **25**, 479–484 (2001)
- [87] C. H. M. Mareé, R. A. Weller, L. C. Feldman, K. Pakbaz, and H. W. H. Lee  
*Accurate thickness/density measurements of organic light-emitting diodes*  
J. Appl. Phys. **84**(7), 4013 (1998)
- [88] J. H. Schön, Ch. Kloc, R. A. Laudise, and B. Batlogg  
*Surface and bulk mobilities of oligothiophene single crystals*  
Appl. Phys. Lett. **73**(24), 3574–3576 (1998)
- [89] J. H. Schön, Ch. Kloc, R. A. Laudise, and B. Batlogg  
*Electrical properties of single crystals of rigid rodlike conjugated molecules*  
Phys. Rev. B **58**(19), 12952–12957 (1998)
- [90] W. Brütting, S. Berleb, and A. G. Mückl  
*Device physics of organic light-emitting diodes based on molecular materials*  
Org. Electr. **2**, 1–36 (2001)

- [91] I. H. Campbell and D. L. Smith  
*Schottky energy barriers and charge injection in metal/Alq/metal structures*  
Appl. Phys. Lett. **74**(4), 561 (1999)
- [92] M. Stössel, J. Staudigel, F. Steuber, J. Blässing, J. Simmerer, and A. Winnacker  
*Space-charge-limited electron currents in 8-hydroxyquinoline aluminum*  
Appl. Phys. Lett. **76**(1), 115 (2000)
- [93] J. Staudigel, M. Stössel, F. Steuber, J. Blässing, and J. Simmerer  
*Activation energies in organic light emitting diodes comprising ohmic contacts both for electron and hole injection*  
Synth. Met. **111–112**, 69–73 (2000)
- [94] M. Stössel, J. Staudigel, F. Steuber, J. Blässing, J. Simmerer, A. Winnacker, H. Neuner, D. Metzendorf, H-H. Johannes, and W. Kowalsky  
*Electron injection and transport in 8-hydroxyquinoline aluminum*  
Synth. Met. **111–112**, 19–24 (2000)
- [95] W. Brütting, S. Berleb, and A. G. Mückl  
*Space-charge limited conduction with a field and temperature dependent mobility in Alq light-emitting devices*  
Synth. Met. **122**(1), 99–104 (2001)
- [96] H. Heil, J. Steiger, S. Karg, M. Gastel, H. Ortner, H. von Seggern, and M. Stössel  
*Mechanisms of injection enhancement in organic light-emitting diodes through an Al/LiF electrode*  
J. Appl. Phys. **89**(1), 420–424 (2001)
- [97] S. Berleb, A. G. Mückl, W. Brütting, and M. Schwoerer  
*Temperature dependent device characteristics of organic light-emitting devices*  
Synth. Met. **111–112**, 341–344 (2000)
- [98] S. Barth, P. Müller, H. Riel, P. F. Seidler, W. Riess, H. Vestweber, U. Wolf, and H. Bässler  
*Electron injection into an Alq<sub>3</sub> single-layer organic light-emitting diode*  
Synth. Met. **111–112**, 327–330 (2000)
- [99] U. Wolf, S. Barth, and H. Bässler  
*Electrode versus space-charge-limited conduction in organic light-emitting diodes*  
Appl. Phys. Lett. **75**(14), 2035 (1999)
- [100] M. Kiy, I. Gamboni, I. Biaggio, and P. Günter  
*Ultra-high vacuum reveals interface dependent and impurity-gas dependent charge-injection in organic light-emitting diodes*  
SPIE **4105**, 290–298 (2001)
- [101] R. G. Kepler, P. M. Beeson, S. J. Jacobs, R. A. Anderson, M. B. Sinclair, V. S. Valencia, and P. A. Cahill  
*Electron and hole mobility in tris(8-hydroxyquinolinolato-N1,O8) aluminum*  
Appl. Phys. Lett. **66**(26), 3618–3620 (1995)
- [102] B. Chen and S. Liu  
*Measurement of electron/hole mobility in organic/polymeric thin films using modified time-of-flight apparatus*  
Synth. Met. **91**, 169–171 (1997)
- [103] S. Hayashi, T. T. Wang, S. Matsuoka, and S. Saito  
*Electroluminescence in amorphous pyrazoline films under DC fields*  
Molecular Crystals and Liquid Crystals **135**(3–4), 355–364 (1986)

- [104] D. Ma, I. A. Hümmelgen, B. Hu, F. E. Karasz, X. Jing, L. Wang, and F. Wang  
*Determination of electron mobility in a blue-emitting alternating block copolymer by space-charge-limited current measurements*  
Solid State Communications **112**(5), 251–254 (1999)
- [105] M. Kiy, P. Losio, I. Biaggio, M. Koehler, A. Tapponnier, and P. Günter  
*Observation of the Mott-Gurney law in tris(8-hydroxyquinoline)aluminum films*  
Appl. Phys. Lett. **80**(7), 1198–1200 (2002)
- [106] M. Henzler and W. Göpel  
*Oberflächenphysik des Festkörpers*  
B. G. Teubner, Stuttgart, 2. edition (1994)
- [107] Frank Gitmans  
*Growth of LiTaO<sub>3</sub> and LiNbO<sub>3</sub> thin films by molecular beam epitaxy / by Frank Gitmans*  
PhD thesis, Diss. Naturwiss. ETH Zürich, Nr. 11693 (1996)
- [108] Raoul Schlessler  
*Organic electro-optic crystals and thin films : optical characterization and molecular beam*  
PhD thesis, Diss. Naturwiss. ETH Zürich, Nr. 11456 (1996)
- [109] M. Knudsen  
*Die maximale Verdampfungsgeschwindigkeit des Quecksilbers*  
Annalen der Physik **4**(47), 679–708 (1915)
- [110] M. A. Herman and H. Sitter  
*Molecular beam epitaxy*  
Springer (1989)
- [111] E. H. C. Parker (ed.)  
*The Technology and Physics of Molecular Beam Epitaxy*  
Plenum Press, New York (1985)
- [112] W. Hallwachs  
*Über den Einfluss des Lichtes auf electrostatisch geladene Körper*  
Annalen der Physik und Chemie **33**, 301–312 (1888)
- [113] A. Einstein  
*Über einen die Erzeugung und Verwandlung des Lichtes betreffenden heuristischen Gesichtspunkt*  
Annalen der Physik **17**, 132 (1905)
- [114] M. Cardona and L. Ley  
*Photoemission in solids II*  
Springer (1979)
- [115] M. Cardona and L. Ley  
*Photoemission in solids I*  
Springer (1978)
- [116] S. F. Alvarado, L. Rossi, P. Müller, P. F. Seidler, and W. Riess  
*STM-excited electroluminescence and spectroscopy on organic materials for display applications*  
IBM J.Res & Dev. **45**(1), 89–100 (2001)
- [117] S. T. Lee, X. Y. Hou, M. G. Mason, and C. W. Tang  
*Energy level alignment at Alq/metal interfaces*  
Appl. Phys. Lett. **72**(13), 1593 (1998)

- [118] S. T. Lee, Y. M. Wang, X. Y. Hou, S. T. Lee, Y. M. Wang, and X. Y. Hou  
*Interfacial electronic structures in an organic light-emitting diode*  
Appl. Phys. Lett. **74**(5), 670 (1999)
- [119] I. G. Hill, A. J. Makinen, and Z. H. Kafafi  
*Initial stages of metal/organic semiconductor interface formation*  
J. Appl. Phys. **88**(2), 889–895 (2000)
- [120] K. Sugiyama, D. Yoshimura, T. Miyamae, T. Miyazaki, H. Ishii, Y. Ouchi, and K. Seki  
*Electronic structures of organic molecular materials for organic electroluminescent devices studied by ultraviolet photoemission spectroscopy*  
J. Appl. Phys. **83**(9), 4928 (1998)
- [121] R. L. Martin, J. D. Kress, L. H. Campbell, and D. L. Smith  
*Molecular and solid-state properties of tris-(8-hydroxyquinolate)-aluminum*  
Phys. Rev. B **61**(23), 15804–15811 (2000)
- [122] A. Rajagopal, C. I. Wu, and A. Kahn  
*Energy level offset at organic semiconductor heterojunctions*  
J. Appl. Phys. **83**(5), 2649–2655 (1998)
- [123] T. Mori, H. Fujikawa, S. Tokito, and Y. Taga  
*Electronic structure of 8-hydroxyquinoline aluminum/LiF/Al interface for organic electroluminescent device studied by ultraviolet photoelectron spectroscopy*  
Appl. Phys. Lett. **73**(19), 2763 (1998)
- [124] A. Schmidt, M. L. Anderson, and N. R. Armstrong  
*Electronic states of vapor deposited electron and hole transport agents and luminescent materials for light-emitting diodes*  
J. Appl. Phys. **78**(9), 5619–5625 (1995)
- [125] I. Sokolik, R. Priestley, A. D. Walser, R. Dorsinville, and C. W. Tang  
*Bimolecular reactions of singlet excitons in tris(8-hydroxyquinoline) aluminum*  
Appl. Phys. Lett. **69**(27), 4168–4170 (1996)
- [126] C. Giebeler, H. Antoniadis, D. D. C. Bradley, and Y. Shirota  
*Influence of the hole transport layer on the performance of organic light-emitting diodes*  
J. Appl. Phys. **85**(1), 608 (1999)
- [127] S. E. Shaheen, B. Kippelen, N. Peyghambarian, J.-F. Wang, J. D. Anderson, E. A. Mash, P. A. Lee, N. R. Armstrong, and Y. Kawabe  
*Energy and charge transfer in organic light-emitting diodes: A soluble quinacridone study*  
J. Appl. Phys. **85**(11), 7939 (1999)
- [128] W. Stampor, J. Kalinowski, P. Di Marco, and V. Fattori  
*Electric field effect on luminescence efficiency in 8-hydroxyquinoline aluminum (Alq<sub>3</sub>) thin films*  
Appl. Phys. Lett. **70**(15), 1935 (1997)
- [129] J. Kido and Y. Iizumi  
*Fabrication of highly efficient organic electroluminescent devices*  
Appl. Phys. Lett. **73**(19), 2721 (1998)
- [130] P. F. Tian, P. E. Burrows, and S. R. Forrest  
*Photolithographic patterning of vacuum-deposited organic light emitting devices*  
Appl. Phys. Lett. **71**(22), 3197 (1997)

- [131] J. Kalinowski, P. Di Marco, V. Fattori, L. Giulietti, and M. Cocchi  
*Voltage-induced evolution of emission spectra in organic light-emitting diodes*  
J. Appl. Phys. **83**(8), 4242 (1998)
- [132] J. Kalinowski, P. D. Marco, M. Cocci, V. Fattori, N. Camaioni, and J. Duff  
*Voltage-tunable-color multilayer organic light emitting diode*  
Appl. Phys. Lett. **68**(17), 2317 (1999)
- [133] T. A. Hopkins, K. Meerholz, S. Shaheen, M. L. Anderson, A. Schmidt, B. Kippelen, A. B. Padias, H. K. Hall, N. Peyghambarian, and N. R. Armstrong  
*Substituted Aluminum and Zinc Quinolates with Blue-Shifted Absorbance/Luminescence Bands: Synthesis and Spectroscopic, Photoluminescence, and Electroluminescence Characterization*  
Chem. Mater. **8**, 344 (1996)
- [134] G. Gu, G. Parthasarathy, P. Tian, P. E. Burrows, and S. R. Forrest  
*Transparent stacked organic light emitting devices. II. Device performance and applications to displays*  
J. Appl. Phys. **86**(8), 4076 (1999)
- [135] G. Gu, G. Parthasarathy, and S. R. Forrest  
*A metal-free full color stacked organic light-emitting device*  
Appl. Phys. Lett. **74**(2), 305 (1999)
- [136] G. Gu, V. Bulovic, P. E. Burrows, S. R. Forrest, and M. E. Thompson  
*Transparent organic light emitting devices*  
Appl. Phys. Lett. **68**(19), 2606 (1996)
- [137] S. R. Forrest, P. E. Burrows, and M. E. Thompson  
*Organic emitters promise a new generation of displays*  
Laser Focus World **2**, 99 (1995)
- [138] A. Dodabalapur  
*Organic light emitting diodes*  
SOLID STATE COMMUNICATIONS **102**(2-3), 59-267 (1997)
- [139] G. M. Credo and S. K. Buratto  
*Near-field fluorescence microscopy of tris-8-hydroxyquinoline aluminum films*  
Adv. Mater. **12**(3), 183 (2000)
- [140] M. A. Baldo, D. F. O'Brien, M. E. Thompson, and S. R. Forrest  
*Excitonic singlet-triplet ratio in a semiconducting organic thin film*  
Phys. Rev. B **60**(20), 14422 (1999)
- [141] A. Bacher, I. Bleyl, C. H. Erdelen, D. Haarer, W. Paulus, and H.-W. Schmidt  
*Low molecular weight and polymeric triphenylenes as hole transport materials in organic two-layer LEDs*  
Adv. Mater. **9**(13), 1997 (1997)
- [142] H. Murata, C. D. Merritt, H. Inada, Y. Shirota, and Z. H. Kafafi  
*Molecular organic light-emitting diodes with temperature-independent quantum efficiency and improved thermal durability*  
Appl. Phys. Lett. **75**(21), 3252 (1999)
- [143] E. W. Forsythe, V.-E. Choong, T. Q. Le, and Yongli Gao  
*Interface analysis of naphthyl-substituted benzidine derivative and tris-8-(hydroxyquinoline) aluminum using ultraviolet and x-ray photoemission spectroscopy*  
J. Vac. Sci. Technol. A **17**(6), 3429 (1999)



- [144] H. Mattoussi, H. Murata, C. D. Merrit, Y. Iizumi, J. Kido, and Z. H. Kafafi  
*Photoluminescence quantum yield of pure and molecular doped organic solid films*  
J. Appl. Phys. **86**(5), 2642 (1999)
- [145] S. A. Knickerbocker and A. K. Kulkarni  
*Estimation and verification of the optical properties of indium tin oxide based on the energy band diagram*  
J. Vac. Sci. Technol. A **14**(3), 757 (1996)
- [146] R. B. H. Tahar, T. Ban, Y. Ohya, and Y. Takahasi  
*Tin doped indium oxide thin films: Electrical properties*  
J. Appl. Phys. **83**(5), 2631 (1998)
- [147] A. K. Kulkarni and S. A. Knickerbocker  
*Estimation and verification of the electrical properties of indium tin oxide based on the energy band diagram*  
J. Vac. Sci. Technol. A **14**(3), 1709 (1996)
- [148] J. S. Kim, M. Granström, R. H. Friend, N. Johansson, W. R. Salaneck, R. Daik, W. J. Feast, and F. Cacialli  
*Indium-tin oxide treatments for single- and double-layer polymeric light-emitting diodes: The relation between the anode physical, chemical, and morphological properties and the device performance*  
J. Appl. Phys. **84**(12), 6859 (1998)
- [149] D. J. Milliron, I. G. Hill, C. Shen, A. Kahn, and J. Schwartz  
*Surface oxidation activates indium tin oxide for hole injection*  
J. Appl. Phys. **87**(1), 572–576 (2000)
- [150] H. Suzuki  
*Fabrication of electron injecting Mg:Ag alloy electrodes for organic light emitting diodes with radio frequency magnetron deposition*  
Appl. Phys. Lett. **69**(11), 1611 (1996)
- [151] Jonda Ch, A. B. R. Mayer, and W. Grothe  
*Determination of the barrier heights for electron injection in organic light emitting devices*  
J. Appl. Phys. **85**(9), 6884–6888 (1999)
- [152] M. Matsumura and Y. Jinde  
*Analysis of current–voltage characteristics of organic light emitting diodes having a LiF/Al cathode and an Al–hydroxyquinoline/diamine junction*  
Appl. Phys. Lett. **73**(20), 2872 (1998)
- [153] G. Gu, P. E. Burrows, S. Venkatesh, S. R. Forrest, and M. E. Thompson  
*Vacuum-deposited, nonpolymeric flexible organic light-emitting devices*  
Opt. Lett. **22**, 172 (1997)
- [154] M. A. Baldo, V. G. Kozlov, P. E. Burrows, S. R. Forrest, V. S. Ban, B. Koene, and M. E. Thompson  
*Low pressure organic vapor phase deposition of small molecular weight organic light emitting device structures*  
Appl. Phys. Lett. **71**(21), 3033 (1997)
- [155] P. E. Burrows, S. R. Forrest, S. P. Sibley, and M. E. Thompson  
*Color-tunable organic light-emitting devices*  
Appl. Phys. Lett. **69**(20), 2959 (1996)

- 
- [156] H. Kim, A. Piqué, J. S. Horwitz, H. Mattoussi, H. Murata, Z. H. Kafafi, and D. B. Chrisey  
*Indium tin oxide thin films for organic light-emitting devices*  
Appl. Phys. Lett. **74**(23), 3444 (1999)
- [157] M. Matsumura, A. Ito, and Y. Miyamae  
*Accumulation of positive charges in organic light-emitting diodes with a double-layer structure*  
Appl. Phys. Lett. **75**(8), 1042 (1999)
- [158] M. Uchida, C. Adachi, T. Koyama, and Y. Taniguchi  
*Charge carrier trapping effect by luminescent dopant molecules in single-layer organic light emitting diodes*  
J. Appl. Phys. **86**(3), 1680 (1999)
- [159] F. Röhlfing, Toshiki Yamada, and T. Tsutsui  
*Electroabsorption spectroscopy on tris-(8-hydroxyquinoline) aluminum-based light emitting diodes*  
J. Appl. Phys. **86**(9), 4978 (1999)
- [160] A. Curioni and W. Andreoni  
*The organic-cathode interface in Alq(3)-based OLEDs: New insights from ab-initio molecular dynamics*  
Synth. Met. **111–112**(0), 299–391 (2000)
- [161] A. Curioni and W. Andreoni  
*Metal-Alq<sub>3</sub> Complexes: The Nature of the Chemical Bonding*  
J. Am. Chem. Soc. **121**, 8216 (1999)

Seite Leer /  
Blank leaf

# Publications related to this work

## In reviewed journals

- M. Kiy, I. Biaggio, M. Koehler and P. Günter, "Conditions for ohmic electron injection at the Mg/Alq<sub>3</sub> interface", *Applied Physics Letters* Vol. 80(23), page 4366-4368 (2002)
- M. Kiy, P. Losio, I. Biaggio, M. Koehler, A. Tapponnier, and P. Günter, "Observation of the Mott-Gurney law in tris (8-hydroxyquinoline) aluminum films", *Applied Physics Letters* Vol. 80(7), page 1198-1200 (2002)
- M. Kiy, I. Gamboni, I. Biaggio, P. Günter, "Ultra-high vacuum reveals interface dependent and impurity-gas dependent charge-injection in organic light-emitting diodes", *Proceedings of Int. Soc. Opt. Eng. (SPIE) Volume 4105: Organic Light-Emitting Materials and Devices IV*, page 290-298 (2001)
- M. Kiy, I. Gamboni, U. Suhner, I. Biaggio, and P. Günter, "Interface dependent electrical properties of organic light emitting devices in ultra high vacuum", *Synthetic Metals*, Vol. 111-112(0), page 307-310, (2000)
- M. Kiy, I. Biaggio, and P. Günter, "Photoelectron Spectroscopy on a running Organic Light Emitting Diode", *Nonlinear Optics (Gordon+Breach)*, Vol. 25, page 461-466 (2001)
- R. Ono, M. Kiy, I. Biaggio, P. Günter, "Impurity Gas Dependent Charge Injection Properties at the Electrode-Organic Interface in Organic Light Emitting Diodes", *Materials Science and Engineering B*, 85(2-3), page 144-148, (2001)
- R. Ono, M. Kiy, I. Biaggio, P. Günter, "Electrical properties of Organic Light Emitting Diodes (OLEDs) studied by Impedance Spectroscopy in Ultra High Vacuum", *Proceedings of Int. Soc. Opt. Eng. (SPIE) Volume 4105: Organic Light-Emitting Materials and Devices IV*, page 299-306 (2001)
- A. Tapponnier, I. Biaggio, M. Kiy, R. Ono, Günter, "Transient photocurrent investigation of charge transport in electroluminescent organic thin films", *Nonlinear Optics*, Vol. 25, page 497-501 (2001)

## Book chapters

- C. Cai, M. Bösch, C. Bosshard, B. Müller, Y. Tao, A. Kündig, J. Weckesser, J. V. Barth, L. Bürgi, O. Jeandupeux, M. Kiy, I. Biaggio, I. Liakatas, K. Kern, and P. Günter, "Self-Assembly Growth of Organic Thin Films and Nanostructures by Molecular Beam Deposition.", "Anisotropic Organic Materials. Approaches to Polar Order. Opportunities for Organic Chemists at the Frontier of the Multidiscipline of Optical Science and Engineering for the 21st Century". Eds. R. Glaser, P. Kaszynski, ACS Symp. Ser., 2000.

## Conference contributions (poster and talks)

- **M. Kiy**, A. Tapponnier, I. Biaggio and P. Günter,  
*“Injection and Charge Transport in OLEDs under Influence of Impurity Gases and in UHV”*,  
Poster at the 244. Heraeus-Seminar: “Organic Electronics: Physics, Materials, and Devices” in Bad Honnef (Germany) November 2000
- **M. Kiy**, I. Gamboni, I. Biaggio, and P. Günter,  
*“Ultra-high vacuum reveals interface dependent and impurity dependent charge-injection in OLEDs”*,  
Poster at the SPIEs 45th Annual Meeting in San Diego (California, USA), August 2000
- R. Ono, **M. Kiy**, I. Biaggio, and P. Günter,  
*“Electrical properties of organic light-emitting diodes studied by impedance spectroscopy in ultra-high vacuum”*, Poster at the SPIEs 45th Annual Meeting in San Diego (California, USA), August 2000
- R. Ono, **M. Kiy**, I. Biaggio, and P. Günter,  
*“Impurity gas dependent charge injection properties at the electrode-organic interface in organic light emitting diodes”*,  
Poster at the IUMRS 6th international conference (asia) in Hongkong (HK) July 2000
- **M. Kiy**  
*“Charge injection properties in organic light-emitting devices at various impurity levels: From ultra-high vacuum to air”*,  
Talk at the E-MRS - IUMRS - ICEM conference in Strasbourg (France) May 2000
- A. Tapponnier, R. Ono, **M. Kiy**, I. Biaggio, and P. Günter,  
*“Impedance and photoconductivity spectroscopy of organic light-emitting diodes”*,  
Poster at the E-MRS - IUMRS - ICEM conference in Strasbourg (France) May 2000
- **M. Kiy**, I. Biaggio, P. Günter,  
*“Ultra high vacuum reveals interface-dependent charge-injection properties of organic light emitting diodes, and the effect of exposure to impurity gases”*,  
Poster at the ICONO5 conference in Davos (CH) March 2000
- C. Cai, **M. Kiy**, A. Tapponnier, R. Ono, I. Biaggio, Ch. Bosshard and P. Günter,  
*“Nonlinear optical thin films based on strong head-to-tail hydrogen bonding grown by oblique incidence molecular beam deposition”*,  
Poster at the ICONO5 conference in Davos (CH) March 2000
- R. Ono, P. Losio, **M. Kiy**, A. Tapponnier, I. Gamboni, I. Biaggio, and P. Günter,  
*“Impedance spectroscopy of Alq<sub>3</sub> based- organic light emitting diodes measured in ultra-high vacuum and air”*,  
Poster at the ICONO5 conference in Davos (CH) March 2000
- **M. Kiy**, I. Gamboni, U. Suhner, G. Conradin, I. Biaggio, and P. Günter,  
*“Interface dependent electrical properties of organic light emitting devices in ultra high vacuum”*,  
Poster at the ICEL2 conference in Sheffield (UK) May 1999
- C. Cai, **M. Kiy**, Y. Tao, I. Biaggio, and P. Günter,  
*“A new type of hole-transport material based on biothiophene stilbene”*,  
Poster at the MRS Fall Meeting Symposium R “Organic Electronic and Photonic Materials and Devices”, November 1998 in Boston (USA)

## Other OLED publications - not related to this work

The author wants to mention that he published 2 articles in the german popular computer journal "c't" (Heise Verlag) with an overview of the state of the art of organic display technology. One article has been translated and appeared in the dutch "c't" (F&L Publishing Group B.V).

- **Michael Kiy**  
"Molekulares Leuchten - Organische Displays auf dem Vormarsch"  
(<http://www.heise.de/kiosk/archiv/ct/00/20/110/>),  
c't 20/2000, page 110, Heise Verlag (<http://www.heise.de>)
- **Michael Kiy**,  
"Moleculaire verlichting : de opmars van organische displays" (dutch translation of the german article above, <http://www.fnl.nl/ct-nl/archief2000/ct2000-12/index.htm>),  
Dutch c't 12/2000, page 82, F&L Publishing Group B.V. (<http://www.fnl.nl>)
- **Michael Kiy**,  
"Organisch ins nächste Jahrhundert - Polymer-Displays auf dem Weg zum Massenmarkt" (<http://www.heise.de/kiosk/archiv/ct/99/13/043/>),  
c't 13/1999, page 43, Heise Verlag (<http://www.heise.de>)

# Acknowledgements

I wish to express my gratitude to all those who contributed to the completion of this work:

- Prof. Dr. P. Günter for giving me the chance to work in the Nonlinear Optics Laboratory on such an interesting topic with an challenging vacuum machine and for giving me research freedom.
- Prof. Dr. B. Batlogg for accepting to be the co-examiner of this thesis.
- PD Dr. I. Biaggio for being an excellent supervisor of my research work, for careful reading and commenting on the manuscript, the very helpful discussions and for his valuable advice in moments of despair.
- I. Gamboni for her technical support in the first half of this work.
- A. Tapponnier for the companionship in the lab.
- E. Delvigne for the funny year with interesting discussions and table tennis matches.
- Dr. Marlus Koehler for his excellent explanations of complicated theories.
- Dr. Ali Rashid for the purification of  $\text{Alq}_3$ , the careful reading and corrections of the manuscript and the american atmosphere.
- P. Losio for his outstanding semester and diploma work and his contribution to this thesis.
- Dr. Cudney for carefully reading the manuscript.
- Dr. M. Abplanalp for his fantastic thesis template and extensions of the literature database on which this work is based, AFM measurements and nice discussions as well.
- Dr. Y. Tao for sharing his knowledge.
- H. Wüest and E. Hausamann, for the excellent technical support.
- The rest of the Nonlinear Optics Laboratory for the nice working atmosphere and interesting discussions in the coffee room.

- H. Scherrer and his team for depositing the gold contacts and vacuum support.
- M. Doebeli for the Rutherford-Backscattering measurements.
- U. Suhner for his excellent semester work and G. Conradin for his diploma work.
- The ETH for the financial support.
- The L<sup>A</sup>T<sub>E</sub>X programmers which developed a 100% stable, powerful and free text processing system (I still have all my hairs).
- My parents for the opportunity to study and their support.
- Marianne for her love, care and support.



# Curriculum Vitae

## Personal data

Name	Kiy
First names	Michael
Date of birth	6.7.1972
Nationality	German
Birthplace	Wurzen (Germany)

## Education

1978–1982	Elementary school in Conakry (Rep. of Guinea), Grimma (Germany)
1982–1987	Secondary school in Grimma, Königs Wusterhausen (Germany)
1987–1991	Extended School in math. - scient. direction, Leipzig (Germany)
1993–1998	Study of physics at the Technical University Braunschweig (Germany)
1998	Graduation as "Diplom Physiker" (Master of Science) in experimental physics with thesis on "Ultraviolet photoelectron spectroscopy on magnetic materials"
1998–2002	Ph.D. student at the Nonlinear Optics Laboratory of Prof. Günter in the Institute of Quantum Electronics at the Swiss Federal Institute of Technology (ETH Zürich)

Zürich, May 2002

Michael Kiy